Planification de trajectoires et commande d'une classe de systèmes mécaniques plats et liouvilliens

Balint Kiss

▶ **To cite this version:**

Balint Kiss. Planification de trajectoires et commande d'une classe de systèmes mécaniques plats et liouvilliens. Automatique / Robotique. École Nationale Supérieure des Mines de Paris, 2001. Français. NNT : . pastel-00838938

HAL Id: pastel-00838938

https://pastel.hal.science/pastel-00838938

Submitted on 26 Jun 2013

THÈSE

présentée à

L'ÉCOLE NATIONALE SUPÉRIEURE DES MINES DE PARIS

par

Bálint KISS

pour obtenir le titre de

DOCTEUR DE L'ÉCOLE DES MINES DE PARIS

Spécialité

MATHÉMATIQUES ET AUTOMATIQUE

Sujet de la thèse

PLANIFICATION DE TRAJECTOIRES ET COMMANDE D'UNE CLASSE DE SYSTÈMES MÉCANIQUES PLATS ET LIOUVILLIENS

soutenue le 23 avril 2001 devant le jury composé de

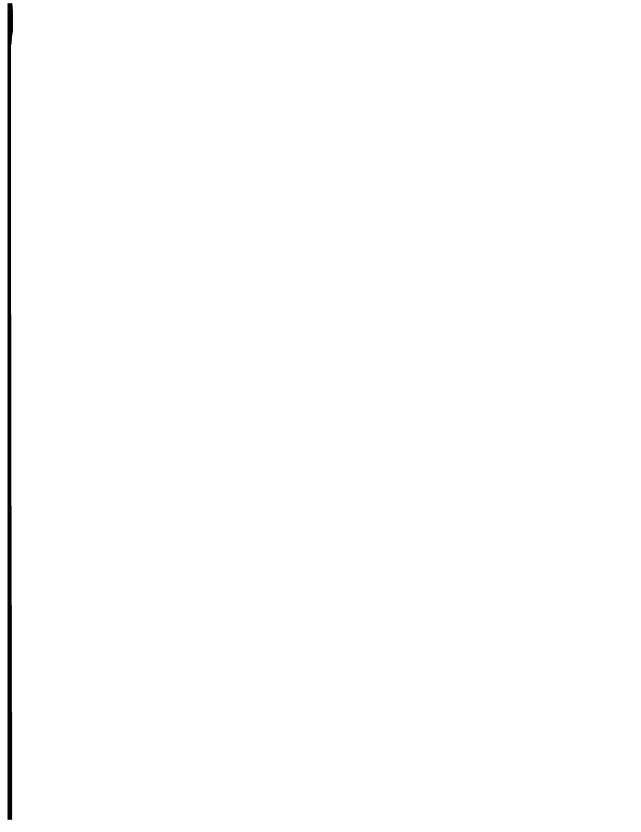| MM.	Michel FLIESS	Président
	Michel de MATHELIN	Rapporteur
	Rodolphe SÉPULCHRE	Rapporteur
	Péter ARATÓ	Examinateur
	Jean LÉVINE	Examinateur
	Romeo ORTEGA	Examinateur

Remerciements

Cette thèse a été effectuée en co-tutelle entre l'École des Mines de Paris et l'Université des Sciences Techniques et Économiques de Budapest sous les directions de MM. Jean Lévine et Béla Lantos. Je me permets donc de diviser les remerciements en deux parties et d'exprimer ma gratitude aux personnes concernées dans leurs langues respectives.

Je tiens à remercier M. Jean Lévine, mon directeur de thèse à l'École des Mines de Paris qui a su diriger et motiver mon travail tout au long de la thèse. Sa rigueur et sa maîtrise scientifiques m'ont permis de beaucoup apprendre.

Je tiens à remercier également M. Michel Fliess pour avoir accepté de présider mon jury de thèse ainsi que MM. Michel de Mathelin et Rodolphe Sépulchre pour leur travail de rapporteur qui a permis d'améliorer considérablement le manuscrit. Je remercie également M. Romeo Ortega pour participer au jury en tant qu'examinateur.

Je dois exprimer ma sincère gratitude à M. Philippe Müllhaupt pour la fructueuse collaboration sur le sujet de la commande des grues. Je tiens à remercier M. Walter Rumsey pour la réalisation précise de la maquette de la grue.

Je suis également reconnaissant à tous les permanents du Centre Automatique et Systèmes pour leur accueil chaleureux au sein du laboratoire.

Mes séjours en France ont été financés par une bourse du Ministère des Affaires Étrangers dont je suis reconnaissant. J'ai également apprécié le travail des administrations concernées qui a permis le bon déroulement de mes séjours en France.

Köszönetnyilvánítás

Introduction

Cette thèse porte sur les problèmes de planification de trajectoire et de commande de deux classes de systèmes mécaniques : mains de robots et engins de levage.

Les mains de robots sont utilisées pour saisir et manipuler divers objets. La dextérité des mains de robots est la conséquence de la richesse des déplacements relatifs aux contacts entre l'objet et les doigts. On considère ici un modèle de contact ponctuel, permettant des roulements sans glissement entre les surfaces. La condition de roulement sans glissement fait intervenir des contraintes cinématiques qui ne sont pas intégrables en général. Par conséquent, les mains de robots appartiennent à la classe des systèmes mécaniques *non-holonomes*.

Les grues (ainsi que divers autres engins de levage) comprennent un ensemble de câbles et de poulies, portés par une structure mécanique, servant à soulever et à déplacer de lourdes charges. Comme le déplacement de la charge n'est pas actionné directement par un moteur mais par le câble qui y est attaché, un comportement oscillant mal amorti caractérise ces mécanismes. Ainsi, les grues appartiennent à la classe des systèmes mécaniques *sous-actionnés*.

Le contrôle de ces systèmes nécessite d'abord le choix d'une trajectoire de référence réalisant l'objectif fixé par l'utilisateur. C'est ce qu'on appelle le problème de planification de trajectoire. Dans le cas des mains de robots, l'objectif consiste à atteindre une orientation et une position désirée de l'objet. Dans le cas des grues, on veut transporter la charge à une position d'équilibre donnée, aussi vite que possible et en évitant les oscillations à l'arrivée.

Un deuxième aspect consiste à suivre la trajectoire de référence en présence des perturbations et des incertitudes du modèle

Dans le cas des mains de robots, une littérature très riche est disponible dans divers domaines : modélisation [12, 13, 28, 48, 49], planification de trajectoires utilisant des approximations quasi-statiques [11, 63], planification de trajectoires pour le modèle cinématique non-holonome utilisant des entrées sinusoïdales ou constantes par morceaux [39, 53, 24] et stabilisation de l'objet par bouclage [12, 55].

La *contribution* de la thèse concerne la solution du problème de la planification de trajectoires, utilisant la notion de *platitude* et de *système Liouvillien*. Une classification des structures mains-objets est présentée avec des algorithmes de planification de trajectoires spécifiques à chaque cas étudié.

Concernant les grues et les engins de levage, une grande partie de la littérature utilise des approches linéaires [8, 26, 59, 66] ou des approches de commande optimale [47, 67]. Plusieurs méthodes sont proposées dans [23, 27, 57] pour diminuer les oscillations créées par les perturbations extérieures. Les auteurs de [7, 14] utilisent des techniques énergétiques en exploitant le

fait qu'une grue peut être identifiée à un pendule si on fixe la longueur du câble vertical relié à la charge.

Nous considérons d'abord une méthode de modélisation générale pour une classe étendue d'engins de levage. comprenant en particulier les modèles des ponts roulants et de la grue de la marine américaine. Nous montrons que chaque élément de la classe est différentiellement plat et. utilisant les même algorithmes de planification de trajectoires que pour les mains de robots. on peut construire des trajectoires correspondant à des déplacements rapides de la charge sans oscillations à l'arrivée.

Finalement, nous considérons le problème de suivi qui consiste à stabiliser les trajectoires de références calculées précédemment en n'utilisant que des mesures des positions angulaires des moteurs et en ne disposant pas en particulier des mesures sur la position de la charge et les angles entre les câbles. Nous montrons d'abord que toutes les positions d'équilibre peuvent être globalement stabilisées par un bouclage PD sur les variables mesurées dans le cas des grues étudiées. Pour la grue de la marine américaine. les simulations montrent. en outre. que l'utilisation du même bouclage PD en remplaçant la référence d'équilibre par la trajectoire de référence calculé précédemment. permet de suivre cette trajectoire en améliorant les performances du bouclage PD globalement stable.

Le manuscrit est divisé en deux parties   la première est dédiée aux mains de robots (chapitre 2) et la deuxième aux engins de levage (chapitre 3). Les perspectives et des problèmes ouverts qui peuvent être les sujets de futures recherches sont résumés dans la conclusion. Une annexe récapitulant les notions de bases de la mécanique analytique utilisées dans la thèse se trouve à la fin du manuscrit.

Comme la thèse a été effectuée en co-tutelle à l'École Nationale Supérieure des Mines de Paris et à l'Université des Sciences Techniques et Économiques de Budapest (Hongrie), le manuscrit est rédigé en anglais (une traduction des conclusions en français suit le chapitre correspondant en anglais).

Parties de la thèse ont été publiées dans [30, 31, 32, 33, 34, 36, 37, 38, 35].

Contents

Chapter 1

Introduction

This work studies the motion planning and control problems related to two classes of mechanical systems: robotic hands and cranes.

Robotic hands are used to grasp and manipulate objects. Their dexterity follows from the richness of the relative displacements of the fingers and the object in contact, hence the importance of a good understanding of these relative motions. Here, we consider the case of one-point rolling contacts without slipping between the surfaces which give rise to kinematic constraints in the model. Since these constraints are not integrable in general, hand-object systems belong to the larger class of *nonholonomic* mechanical systems.

Cranes (or more generally, weight handling equipments) comprise a hoisting apparatus supported by a mechanical structure allowing to carry heavy weights. Since the load is not directly actuated, but displaced via a rope attached to it, these devices belong to the larger class of *underactuated* mechanical systems and present poorly damped and undesired oscillatory behaviour.

The control of these mechanical systems requires first the choice of a reference trajectory realizing the desired control objective. For robotic hands, the desired objective is to bring the grasped object into a prescribed position and orientation. For cranes, one wishes to carry the load as fast as possible to a desired equilibrium along a trajectory which avoids the obstacles in the working space. Moreover, undesirable oscillations have to be damped at the final equilibrium.

A second aspect concerns the tracking of the reference trajectory despite of external disturbances and model uncertainties.

As far as robotic hands are concerned, a huge literature is available on various aspects: modelling [12, 13, 28, 48, 49], motion planning by quasi-static methods [11, 63], motion planning with piecewise constant or sinusoidal inputs for non-holonomic models [39, 53, 24], and feedback stabilization of grasp [12, 55].

Our contribution here concerns solutions of the motion planning problem using flatness and Liouvillian systems. A classification of hand-object structures according to these properties is presented and specific motion planning algorithms are obtained in each case. We do not consider in this work the feedback tracking aspects.

Concerning cranes and weight handling equipments, most of the literature refers to linear and adaptive techniques [8, 26, 59, 66] and optimal control [47, 67]. Various anti-sway algorithms are proposed in [23, 27, 57]. Some papers exploit the fact that, if the vertical rope length is fixed, a crane can be identified to a pendulum and saturation control or energy-based techniques can be adapted [7, 14].

Here, we first consider the modelling of a quite general class of weight handling equipments, including the overhead crane and three-dimensional models of cantilever, and US Navy cranes. We prove that all the models of this class are flat and, using the same algorithms as for the robotic hands, we construct reference trajectories corresponding to fast displacements of the load without oscillations at the final point.

Finally, we consider the tracking problem where we want to stabilize the previous reference trajectories using only motor position measurements, and in particular, without information on the load position and the rope angles. We first prove that every equilibrium position can be globally stabilized by a measurement feedback PD controller in the case of all studied cranes. For the US Navy crane, simulations show that replacing the equilibrium reference by the previously derived reference trajectory in the PD controller, the closed loop system is able to satisfactorily track this trajectory, even improving the globally stable controller.

The manuscript is divided into two parts — the robotic part (Chapter 2) and the crane part (Chapter 3). Some open problems and perspectives for future research are presented in a concluding chapter. An appendix on basics in analytical mechanics is provided at the end of the thesis.

Parts of this thesis have been published in [30, 31, 32, 33, 34, 36, 37, 38, 35].

Chapter 2

Robotic manipulation with permanent rolling contacts

We study the motion planning problem (MPP) or, roughly speaking, the open-loop trajectory design of robotic hands manipulating objects via one-point rolling contacts without slipping. In such systems all fingers' degrees of freedom are actuated as opposed to the object's ones. The control objective is to change the orientation, position and grasp of the manipulated object

The modelling of hand-object structures (HOS) and the kinematics of contact in the context of dextrous manipulation is treated in details in the robotics literature (see e.g. [13, 48, 49, 52], and [44, 45] including controllability aspects). An exhaustive review of static grasping methods is presented in [61].

The kinematics of the model includes constraints due to the rolling without slipping assumptions which are linear w.r.t. the time derivatives of the configuration variables of the system and have the form [21, 56]:

$$A(q) \cdot \dot{q} = 0 \qquad (2.1)$$

where q is the vector of the configuration variables (see also Appendix A).

Motion planning algorithms which can be applied to a large class of dextrous manipulation problems are reported in [11, 63] using quasi-static approximations. These algorithms involve optimization in order to find contact forces, with constant velocity, based on Peshkin's minimum power principle [58].

Due to the constraints of rolling without slipping, general three-dimensional HOSs are non-holonomic. The underlying MPP can be solved without quasi-static approximations by methods reported in [39, 53] using piecewise constant or sinusoidal inputs. An explicit solution in this framework is provided for the case of two parallel planar fingers with a symmetric object including non-pivoting constraints by [45]. An extension of the method of [39] when fingers are allowed to break contact with the object (i.e when the configuration space is stratified) can be found in [24].

Our approach uses the notions of (differential) flatness [17, 18, 20, 22, 46] and Liouvillian systems. The latter notion was defined in an algebraic context in [10] and extended [62] in a slightly different way than the one we propose here.

Note that, though flatness can be also exploited for feedback design purposes, the feedback design and tracking aspects are not dealt with in this chapter. For the sake of completeness, let us mention some contributions concerning feedback control of object manipulation: [13] for the rigid body case, [3, 9] with soft fingers and with uncertainties on the Jacobian matrices, and the learning control scheme proposed in [55] with unknown inertia parameters of the object.

Coming back to motion planning, the flatness property allows an easy parameterization of all feasible trajectories of the system which does not require integration of differential equations, and does not restrict to quasi-static approximations. More precisely, the definition of flatness directly implies the existence of a so-called flat output, of the same dimension as the input, such that there is a one-to-one mapping between sufficiently smooth trajectories of the flat output and feasible trajectories of the system, including the inputs, making the integration of the system dynamics useless. Thus, the motion planning can be done in the flat output space using elementary interpolation methods. The Liouvillian property according to the viewpoint we adopt here is slightly weaker. Roughly speaking, we say that a system is Liouvillian if there exists an output of the same dimension as the input such that all the system variables can be expressed as functions of this output, a finite number of its derivatives, and a finite number of functions of its integrals. The output in this case is called a partially flat output, and the additional functions of the output integrals are referred to as integral variables. Thus, the flatness based approach to motion planning can be extended up to the computation of a finite number of integrals of functions of time which is still simpler than integrating the system differential equations.

We prove that the dynamic model of planar HOSs are flat as a consequence of the constraints holonomy. Here the inputs are the joint torques of the fingers and combinations of the contact forces. In the three-dimensional case the rolling without slipping condition gives rise to nonholonomic constraints. As is, nonholonomy does not exclude flatness (see for instance the examples of the car with n-trailers or of the rolling hoop, or penny, in [46]), but in our case the kinematic equations form a Liouvillian system.

According to the dimension, the number of fingers, and the model type (i.e. dynamic or kinematic) we show that the HOSs can be classified as summarized in Table 2.1

hand structure	no. of fingers	holonomy	flatness	Liouvillian
2D	> 1	yes	yes	
3D	1	no	yes	
3D	> 1	no	?	yes
3D + symmetry	> 2	no	?	yes

Table 2.1:   Classification of HOSs

Parts of this chapter are published in [31, 33, 34]

2.1 Modelling

We study robotic hands comprising small size manipulators with open kinematic chain, equipped in general with three or four joints. By anthropomorphic analogy, such a small manipulator is called a finger. The modelling of a robotic hand linked to a robot arm as the one developed at the Budapest University of Technology and Economics [41] is not studied here.

The model presented in this section covers all the cases dealt with in this Chapter and inspired from earlier works [13, 12, 28]. A schematic representation of a robotic hand with a grasped object is given in Figure 2.1. We assume that the fingers are numbered from 1 to m
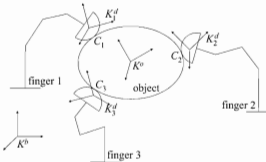
Figure 2.1. Robotic hand with the manipulated object ($m = 3$)

where m is the total number of the fingers of the hand.

Let us start with an enumeration of (classical) assumptions.

A1. All segments of the hand and the manipulated object are rigid bodies (see Definition 12 in Appendix A).

A2. Only the last segments of the fingers can be in contact with the manipulated object

A3. Surfaces may roll on each other without slipping.

A4. Contacts are permanently maintained.

A5. The surface of the manipulated object is strictly convex everywhere. (This implies that the radii of curvature are everywhere finite.)

A6. The surfaces of the fingers are convex everywhere.

Remark 1. *The rigid body assumption* **A1** *excludes both the penetration of the bodies in contact in each other and the case of soft contacts, namely non-vanishing contact surfaces due to deformations.*

Remark 2. *Assumptions* **A5** *and* **A6** *allow to eliminate the case of multiple contact points between the manipulated object and the fingers, thus making the contact point globally unique.*

By abuse of vocabulary, the manipulated object will be simply referred to as object in the sequel.

2.1.1   Geometry and kinematics

In this section we derive the contact condition equations based on Assumptions **A1**-**A6**. The contact conditions are of two kinds: geometric, expressing constraints on positions, and kinematic, expressing constraints on velocities. Moreover, the relations defining the geometry of the fingers are needed. Thus, we first express the geometric constraints and then the kinematic ones, and finally the relations with the joint coordinates.

Geometry of the contact

The inertial reference frame is denoted by K^h. We denote by K^o the frame fixed to the manipulated object at its center of mass given by the point O, and by K_i^d the frame[1] fixed to an arbitrary point D_i of the last segment of finger i, with $i = 1, 2, \ldots, m$. Let us denote by p^o (resp. p_i^d) the coordinates of the point O (resp. D_i), expressed in the basis of K^h.

Let us denote by the matrix $\Omega(\phi^o)$ (resp. $\Omega(\phi_i^d)$), the orientation of the frame K^o (resp. K_i^d) w.r.t. frame K^h where $\phi^o, \phi_i^d \in \mathbb{R}^3$. (See Appendix A for the definition and for a short discussion on the properties of such matrices.) Define the pair

$$(p_i^r, \Omega(\phi^r)) = (\Omega(\phi_i^d)^T(p^o - p_i^d), \Omega(\phi_i^d)^T\Omega(\phi^o)) \qquad (2.2)$$

where p_i^r (resp. $\Omega(\phi^r)$) gives the relative position (resp. relative orientation) of the object w.r.t finger i. (Note that such pairs define homogenous transformation matrices frequently used in robotics.) It is clear from Equation (2.2) that vector p_i^r is expressed in the frame K_i^d.

Consider the contact between finger i and the object (see Figure 2.2). The contact point between the manipulated object and finger i is denoted by C_i.
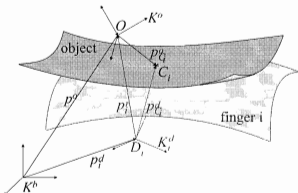

Figure 2.2: Contact between finger i and the object

The vector $p_{C_i}^o$ (resp. $p_{C_i}^d$) denotes the position of the contact point C_i, expressed in the basis of the frame K^o (resp. K_i^d). Using Equation (2.2), these vectors are connected by the

---

[1]The notation K^{d_i} would be more consequent, but we preferred to avoid double subscripts for readability's sake.

equation

$$p_i^r + \Omega(\phi_i^r)p_{C_i}^o - p_{C_i}^d = 0. \tag{2.3}$$

Let c^o and c_i^d define the boundaries of the object and finger i (see Appendix A. Definition 12). If C_i is the contact point between the object and finger i we have

$$c^o(p_{C_i}^o) = 0 \tag{2.4}$$

$$c_i^d(p_{C_i}^d) = 0. \tag{2.5}$$

Denote by Dc the derivative of a function[2] c (i.e. the function $\mathbb{R}^3 \rightarrow L(\mathbb{R}^3, \mathbb{R})$). It has the local form

$$Dc = \begin{bmatrix} \dfrac{\partial c}{\partial x} & \dfrac{\partial c}{\partial y} & \dfrac{\partial c}{\partial z} \end{bmatrix}$$

The right null-space (or kernel) of $Dc_i^d(p_{C_i}^d)$ (i.e. $\{v \in \mathbb{R}^3 \quad Dc_i^d(p_{C_i}^d) \cdot v = 0\}$) defines the tangent plane to the surface of finger i at the contact point C_i. Thus the transpose of $Dc_i^d(p_{C_i}^d)$ gives the direction of the outward normal vector of the surface (expressed in the frame fixed to the finger). The local uniqueness of the contact point reads

$$\frac{Dc_i^d(p_{C_i}^d)}{\| Dc_i^d(p_{C_i}^d) \|} = -\frac{Dc^o(p_{C_i}^o)\Omega(\phi^r)^T}{\| Dc^o(p_{C_i}^o) \|}. \tag{2.6}$$

Geometrically, this equation expresses the fact that the tangent planes of the surfaces in contact coincide at the contact point, or equivalently, that the normal vectors are colinear with opposite direction. Note that, according to the convexity assumptions **A5** and **A6**. Equation (2.6) implies that the surfaces in contact just touch but don't penetrate in each other. Therefore (2.6) is also referred to as the non-penetration constraint.

Kinematics of contact

Let us introduce the vectors $\{w_{1,C_i}^d, w_{2,C_i}^d\}$ spanning $\ker Dc_i^d(p_{C_i}^d)$, the common tangent plane at the contact point (see Figure 2.3). The vectors are expressed in the basis of K_i^d. The kinematic part of the model gives constraints of type (2.1). depending on the time derivatives of already introduced variables.

The velocity state of the object w.r.t. finger i is given by the pair $(v_i^r, [\omega_i^r \times])$ (see also Appendix A):

$$v_i^r = \dot{p}_i^r \qquad [\omega_i^r \times] = \frac{d\Omega(\phi_i^r)}{dt}\Omega(\phi_i^r)^T = \begin{bmatrix} 0 & -\omega_{iz}^r & \omega_{iy}^r \\ \omega_{iz}^r & 0 & -\omega_{ix}^r \\ -\omega_{iy}^r & \omega_{ix}^r & 0 \end{bmatrix}$$

This allows to calculate the relative velocity at the contact point C_i (see Equation (A.5)):

$$v_{C_i}^r = v_i^r + [\omega_i^r \times]\Omega(\phi_i^r)p_{C_i}^o \tag{2.7}$$

---

[2]This notation comes from [1]
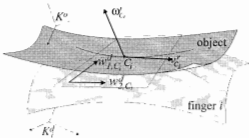
Figure 2.3: Rolling without slipping of surfaces

Since the contact is permanently maintained by Assumption **A4**, the geometric constraints of
the previous section restrict the relative velocity in the common tangent plane of the surfaces
in contact, i.e. $v_{C_i}^r \in \text{span}\{w_{1,C_i}^d, w_{2,C_i}^d\}$. Hence the rolling without slipping constraints read

$$(w_{j,C_i}^d)^T v_{C_i}^r = 0, \qquad j = 1, 2. \tag{2.8}$$

Observe that these constraints are indeed linear w.r.t. the velocities and thus have the same
form as (2.1).

Geometry of the fingers

As it has been already mentioned, the robotic hand is a set of m small manipulators with open
kinematic chains (see Figure 2.4). Their modelling follows the standards of the robotics liter-
ature [40, 48, 52]. The segments of the fingers are connected via one-degree-of-freedom joints.

Figure 2.4: The open kinematic chain of a finger of the robotic hand

These joints can be rotational or translational according to the possible relative displacement
of the connected segments. Because of the openness of the kinematic chain, the joints of each
finger can be enumerated from 1 to a_i where a_i is the number of joints of finger i. The joint
coordinate of the articulation j ($j = 1, \dots, a_i$) of the finger i ($i = 1, \dots, m$) is denoted by q_{ij}.
Hence the vector $q_i = [q_{i1}, \dots, q_{ia_i}]^T$ contains the joint coordinates of finger i.

If the jth joint of finger i is rotational, then $q_{ij} \in \mathbb{R}/2\pi\mathbb{Z}$. if it is translational. then $q_{ij} \in \mathbb{R}$. therefore the configuration manifold of each finger is a Cartesian product of the sets $\mathbb{R}/2\pi\mathbb{Z}$ and $\mathbb{R}$.

The direct geometry of finger i allow to express the position p_i^d and the orientation $\Omega(\phi_i^d)$ of the frame K_i^d as functions of the vector of joint coordinates q_i of finger i.

For. denote by $\mathcal{F}_i$ the list with elements $\mathbb{R}/2\pi\mathbb{Z}$ and $\mathbb{R}$ such that the nth element of $\mathcal{F}_i$ is $\mathbb{R}$ (resp. $\mathbb{R}/2\pi\mathbb{Z}$) if the nth joint of finger i is translational (resp. rotational). The notation $\mathcal{F}_i$ will also be used to denote the Cartesian product of the elements of the list, taken in the order imposed by the list.

Hence the direct geometry function of finger i is defined by:

$$d_i . \mathcal{F}_i \to \mathbb{R}^3 \times SO(3), \qquad d_i(q_i) = (p_i^d, \Omega(\phi_i^d)). \tag{2.9}$$

The function d_i sums up the geometry of finger i and its explicit form can be obtained once the Denavit-Hartenberg parameters of finger i are known. (Roughly speaking. these Denavit-Hartenberg parameters define the homogeneous transformation between K^b and K_i^d.)

Borrowing again some notations from the robotics literature, the derivative of the direct geometry function d_i is defined by

$$J_i(.) = Dd_i(.) \in L(\mathcal{F}_i, \mathbb{R}^3 \times SO(3)). \tag{2.10}$$

and will be referred to as the jacobian of finger i. Since the orientation of the frame relative to the fingertip in $SO(3)$ is locally described by three rotation angles (see Appendix A). the local expression of the jacobian of the finger i is a matrix with six rows and a_i columns. A configuration q_i of finger i is said to be singular if

$$\dim \mathrm{Im} Dd_i(q_i) < \min \left\{ \dim q_i, \dim \left(\mathbb{R}^3 \times SO(3) \right) \right\} = \min \{a_i, 6\}$$

where $\mathrm{Im} Dd_i(q_i)$ stands for the image of the linear map $Dd_i(q_i)$ under $\mathcal{F}_i$.

Inventory of variables and constraints

To make an inventory of the variables and constraints introduced to describe the geometry and the kinematics of a HOS. we summarized them in Tables 2.2 and 2.3. Recall that m gives the number of fingers and a_i gives the number of joints of the finger i with $i = 1$. . m. All entries are valid in the case of three-dimensional configurations. (The two-dimensional case is addressed in Section 2.1.6 where the entries of both tables are updated accordingly.)

By Table 2.2. the configuration manifold M of the HOS is defined as

$$M = \mathcal{F}_1 \times \quad \times \mathcal{F}_m \times SE(3) \times \underbrace{SE(3) \times \quad \times SE(3)}_{2m} \times \underbrace{\mathbb{R}^3 \times \quad \times \mathbb{R}^3}_{m} \underbrace{\mathbb{R}^3 \times \quad \times \mathbb{R}^3}_{m},$$

where $SE = \mathbb{R}^3 \times SO(3)$ is the special Euclidean group. In accordance with Table 2.2. the vector of local coordinates of a point in the configuration manifold M reads

$$(q_1, \quad . q_m, p^o, \phi^o, p_1^d, \phi_1^d, \quad . p_m^d, \phi_m^d, p_1^c, \phi_1^c, \quad . p_m^c, \phi_m^c, p_{C_1}^o, \quad . p_{C_m}^o, p_{C_1}^d, \quad . p_{C_m}^d).$$

variables	description	$\sharp$
q_i, $i = 1, \ldots, m$	joint coordinates	$\sum_{k=1}^{m} a_k$
p^o, ϕ^o	position & orientation of the object	6
p_i^d, ϕ_i^d, $i = 1, \ldots, m$	positions & orientations of the fingertips	6m
p_i^r, ϕ_i^r, $i = 1, \ldots, m$	relative positions & orientations	6m
$p_{C_i}^o$, $i = 1, \ldots, m$	contact points on the object's surface	3m
$p_{C_i}^d$, $i = 1, \ldots, m$	contact points on the fingers' surface	3m

Table 2.2:   Variables

constraint	type	number of equations per finger
(2.2)	geometric	6
(2.3)	geometric	3
(2.4)-(2.5)	geometric	2
(2.6)	geometric	2
(2.9)	geometric	6
(2.8)	kinematic	2

Table 2.3:   Constraints

The geometric constraints of Table 2.3 define a sub-manifold of M, denoted by M_A. The kinematic constraints of rolling without slipping, given by Equation (2.8) define a codistribution of M_A. The corresponding annihilating distribution contains the admissible displacement directions of the HOS in the tangent space of M_A.

Remark 3. *If the robotic hand has only one finger and the Assumptions **A1-A6** are satisfied, then the kinematic constraints (2.8) of rolling without slipping are always nonholonomic (see Appendix A, Definition 14 for the notion of holonomy). However, in the case of more than one finger, the kinematic constraints are not fully nonholonomic in general.*

2.1.2   Pivoting and autonomous motions of the object

The kinematic constraints (2.8) given in the previous section are obtained from Assumption **A3** and eliminated sliding motions between the object and the fingers. In this section we study motions of the object which may be undesirable, but have been not eliminated by Assumption **A3**. These motions are the pivoting [45, 54] and autonomous motions of the object.

Recall that (2.8) determines the admissible directions in the tangent space of the manifold M_A, defined by the geometry of the HOS. By analyzing the directions corresponding to pivoting and autonomous motions in the tangent space of M_A, further kinematic constraints can be added to the kinematic model in order to eliminate these directions. The corresponding constraints are also of type (2.1).

Considering the object, pivoting (or spinning) motions correspond to rotations around an axis passing through a surface point and normal to the corresponding tangent plane.

Definition 1 (pivoting around a surface point). *Consider an object with the frame K^o fixed to it, an inertial reference frame K^b and a surface point C of the object. Let $(p^o, \Omega(o^o)) \in (\mathbb{R}^3 \times SO(3))$ give the position and the orientation of the object w.r.t. K^b. A vector $(v^o, \omega^o) \in \mathbb{R}^6$ $(v^o, \omega^o) \neq (0, 0)$ is said to be a pivoting motion of the object if*

   1. the velocity of the point C vanishes in the frame K^b i.e. $v_C = 0$.

   2. the tangent plane of the object at the point C remains unchanged.

Definition 2 (pivoting around multiple surface points). *Consider an object with the frame K^o fixed to it, an inertial reference frame K^b and a set of surface points $\{C_1, \ldots C_m\}$ of the object. Let $(p^o, \Omega(o^o)) \in (\mathbb{R}^3 \times SO(3))$ give the position and the orientation of the object w.r.t. K^b. A vector $(v^o, \omega^o) \in \mathbb{R}^6$, $(v^o, \omega^o) \neq (0, 0)$ is said to be a pivoting motion around the points $\{C_1, \ldots C_m\}$ if (v^o, ω^o) is a pivoting motion around each C_i, $i = 1, \ldots, m$ in the sense of the Definition 1.*

These definitions imply that $\omega^o \neq 0$ for any pivoting motions. The following statements can be easily proven.

Proposition 1. *Consider an object. For any point C of its surface, there is a unique direction in $\mathbb{R}^6$ corresponding to a pivoting motion of the object around the point C*

Proof. Denote by n_C^b the unit normal of the object surface at the point C, expressed in the basis of K^b. By Definition 1, the tangent plane at the point C to the object surface has to remain unchanged, hence ω^o must be parallel with n_C^b, i.e. $\omega^o = \lambda n_C^b$. ($\lambda \in \mathbb{R}, \lambda \neq 0$). By (A.5), the velocity of the point C is given by

$$v_C = v^o + [\omega^o \times] \Omega(o^o) p_C^o \qquad (2.11)$$

which must vanish by Definition 1. Using that $[a \times] b = -[b \times] a$, and isolating v^o we get

$$v^o = [\Omega(o^o) p_C^o \times] \omega^o = \lambda [\Omega(o^o) p_C^o \times] n_C^b.$$

Thus the unique direction in $\mathbb{R}^6$ corresponding to pivoting around the point C is given by $\left([\Omega(o^o) p_C^o \times] n_C^b, n_C^b\right)$. □

Proposition 2. *Consider an object and two different points of its surface: C_1 and C_2. The necessary and sufficient condition for the existence of a direction in $\mathbb{R}^6$ corresponding to a pivoting motion around C_1 and C_2 are*

   1 the surface normals $n_{C_1}^b$ and $n_{C_2}^b$ are colinear.

   2. $[n_{C_1}^b \times] \Omega(o^o) p_{C_1}^o = [n_{C_2}^b \times] \Omega(o^o) p_{C_2}^o$.

Proof. Since ω^o must be parallel both with $n_{C_1}^b$ and $n_{C_2}^b$, $\omega^o \neq 0$ implies that $n_{C_1}^b$ and $n_{C_2}^b$ are colinear. Hence $\omega^o = \lambda n_{C_1}^b$, and by Definition 2, the velocity vector v^o and the scalar λ have to satisfy the following equation obtained from (2.11)

$$0 = \begin{bmatrix} I & [n_{C_1}^b \times]\Omega(\phi^o)p_{C_1}^b \\ I & [n_{C_1}^b \times]\Omega(\phi^o)p_{C_2}^b \end{bmatrix} \begin{bmatrix} v^o \\ \lambda \end{bmatrix} \qquad (2.12)$$

where I is the identity matrix of suitable dimensions. This equation has a nonzero solution if and only if

$$[n_{C_1}^b \times]\Omega(\phi^o)p_{C_1}^o = [n_{C_1}^b \times]\Omega(\phi^o)p_{C_2}^o.$$

Then we have the relation

$$v^o = -\lambda[n_{C_1}^b \times]\Omega(\phi^o)p_{C_1}^o$$

giving a unique direction in $\mathbb{R}^6$ corresponding to a pivoting motion around both points. Observe that the second condition can be rearranged to get

$$[n_{C_1}^b \times]\Omega(\phi^o)(p_{C_1}^o - p_{C_2}^o) = 0$$

which is equivalent to the colinearity of the normal vectors with the vector connecting the surface points C_1 and C_2. □

Corollary 1. *Consider a strictly convex object. For a set of three different surface points* $\{C_1, C_2, C_3\}$, *there is no direction in $\mathbb{R}^6$ corresponding to a pivoting motion around all contact points.*

Proof. Suppose that (v^o, ω^o) is a possible pivoting motion around all the three surface points, hence the conditions of Proposition 2 must be satisfied for any pair of surface points in $\{C_1, C_2, C_3\}$. This implies that $n_{C_1}^b \| n_{C_2}^b$ and $n_{C_1}^b \| n_{C_3}^b$, thus all the three surface normals must be colinear. But this is excluded by the strict convexity assumption, thus $\omega^o = 0$, a contradiction. □

Corollary 2. *Consider a strictly convex object. For all set comprising different surface points:* $\{C_i : i = 1, 2, \dots, j\}, j > 3$, *there is no pivoting motion in $\mathbb{R}^6$ around all points of the set*

Proof. Consequence of Corollary 1 □

Remark 4. *Since the object is everywhere strictly convex by Assumption* **A5**, *the set of surface points satisfying the conditions of Proposition 2 has Lebesgue measure 0 in the set of all pairs of points of the object surface.*

Remark 5. *In the case of multiple surface points, the non-existence of a pivoting motion around all surface points does not exclude the possibility of pivoting around one of the surface points.*

Remark 6. *Corollaries 1 and 2 have the following consequence. For all HOSs satisfying Assumptions* **A1-A6** *with at least three fingers, any change of orientation implies pivoting around at least one contact point. Thus the elimination of pivoting motions around each contact point would block the orientation of the object.*

In the literature one calls rolling without slipping and spinning the relative motion of two surfaces such that pivoting motions are eliminated in addition to the rolling without slipping constraints (2.8).

We use Definition 2 to obtain the constraint that eliminates spinning motions. For. recall the relation giving the coordinates of the contact point C_i in the basis of the inertial reference frame K^b and the definition of the outward unit normal vector:

$$p_{C_i}^b = p^o + \Omega(\phi^o)p_{C_i}^o, \qquad n_{C_i}^b = \Omega(\phi^o)\frac{Dc^o(p_{C_i}^o)^T}{\|Dc^o(p_{C_i}^o)\|}.$$

Definition 2 asserts that $\dot{p}_{C_i}^b = 0$ and $\dot{n}_{C_i}^b = 0$ during pivoting motions for all contact points C_i ($i = 1, \dots, m$) on the surface and note that the second condition is equivalent to $\|Dc^o(p_{C_i}^o)\|\dot{n}_{C_i}^b = 0$ since the contacts point are fixed on the surface. Calculating these time derivatives gives

$$\begin{bmatrix} \dot{p}_{C_1}^b \\ \|Dc^o(p_{C_1}^o)\|\dot{n}_{C_1}^b \\ \vdots \\ \dot{p}_{C_m}^b \\ \|Dc^o(p_{C_m}^o)\|\dot{n}_{C_m}^b \end{bmatrix} = \begin{bmatrix} I \cdot \dot{p}^o + \frac{d\Omega(\phi^o)}{dt}\Omega(\phi^o)^T\Omega(\phi^o)p_{C_1}^o \\ \frac{d\Omega(\phi^o)}{dt}\Omega(\phi^o)^T\Omega(\phi^o)Dc^o(p_{C_1}^o)^T \\ \vdots \\ I \cdot \dot{p}^o + \frac{d\Omega(\phi^o)}{dt}\Omega(\phi^o)^T\Omega(\phi^o)p_{C_m}^o \\ \frac{d\Omega(\phi^o)}{dt}\Omega(\phi^o)^T\Omega(\phi^o)Dc^o(p_{C_m}^o)^T \end{bmatrix}$$

Using that $[\omega^o \times] = \frac{d\Omega(\phi^o)}{dt}\Omega(\phi^o)^T$ and the anti-symmetry of the cross product we get

$$\begin{bmatrix} \dot{p}_{C_1}^b \\ \|Dc^o(p_{C_1}^o)\|\dot{n}_{C_1}^b \\ \vdots \\ \dot{p}_{C_m}^b \\ \|Dc^o(p_{C_m}^o)\|\dot{n}_{C_m}^b \end{bmatrix} = \begin{bmatrix} I & -[\Omega(\phi^o)p_{C_1}^o \times] \\ 0 & -[\Omega(\phi^o)Dc^o(p_{C_1}^o)^T \times] \\ \vdots & \vdots \\ I & -[\Omega(\phi^o)p_{C_m}^o \times] \\ 0 & -[\Omega(\phi^o)Dc^o(p_{C_m}^o)^T \times] \end{bmatrix} \begin{bmatrix} \dot{p}^o \\ \omega^o \end{bmatrix} \stackrel{\text{def}}{=} \eta \begin{bmatrix} \dot{p}^o \\ \omega^o \end{bmatrix} \tag{2.13}$$

defining the linear map η.

According to Definition 2, the right null-space of η gives precisely the directions in $\mathbb{R}^6$ corresponding to pivoting motions. Corollaries 1-2 assert that this null-space contains only the null vector for all positions and orientations $(p^o, \Omega(\phi^o))$ of the object if $m \geq 3$. If $m = 2$, the null-space contains a non-null vector for a set of contact point pairs of measure 0 and has always a unique non-null component if $m = 1$.

Denote by w_3 ($w_3 \in \mathbb{R}^6$) the vector spanning the null-space of η. Then the non-spinning constraint reads

$$w_3^T \begin{bmatrix} v^o \\ \omega^o \end{bmatrix} = 0. \tag{2.14}$$

The notion of the pivoting motion has been defined without need to consider the geometry of the fingers. Hence, all pivoting motions around all contact points leave both the contact points and the joint coordinates of all fingers unchanged. Note that in the case of most robotic hands, the joint coordinates may be considered as the controlled variables which implies that pivoting motions can neither be generated nor eliminated through the control variables. One may ask if there exists other kinds of motions which cannot be controlled through the joint coordinates.

Thus we are naturally driven to consider a more general notion of autonomous motions of the HOS defined as follows.

Definition 3 (autonomous motions). *Consider an object in contact with m fingers. A direction in TM_A corresponds to an autonomous motion if it satisfies the kinematic constraints of rolling without slipping (Equation (2.8)) and has no component in $\frac{\partial}{\partial q_{\iota}}$ with $j = 1, \ldots, a_\iota$ (a_ι is the number of joints of finger i), and $\iota = 1, \ldots, m$, (m being the number of fingers).*

Clearly, an autonomous motion is such that the joint coordinates of the fingers do not change. Pivoting motions of the object around all the m contact points are also autonomous motions but pivoting around j contact points $j = 1, \ldots, m-1$ do not belong to this class. This is because pivoting around multiple contact points doesn't exclude the motion of the joints of the remaining fingers.

Let us turn back our attention to the inventory of the variables (Table 2.2) and the constraints (Table 2.3). We have $18m + 6 + \sum_{k=1}^{m} a_k$ variables, and, by adding the non-spinning kinematic constraint (2.14) to the constraints of Table 2.3, $(19 + 2)m + \delta(1 - m)$ constraints. (The function δ is defined such that δ vanishes everywhere but at 0 where it equals to 1.)

2.1.3   Examples

The following four simple examples illustrate the modelling procedure of the geometry and the kinematics. Their simplicity allows easy elimination and hence an immediate choice of the variables determining the local chart on M_A. The modelling is based on Section 2.1.1 and thus follows a systematic procedure. The existence of pivoting motions around all contact points is also investigated for each example.

Example 1 (ball on the plane). The object is a ball with radius R and the last segment of the unique finger is a plane, parallel to the xy-plane of the reference frame K^b. (The index i is omitted since the setup has a unique finger.) The finger has three degrees of freedom, all translational along the three coordinate axes of K^b ($\mathcal{F} = \{\mathbb{R}, \mathbb{R}, \mathbb{R}\}$). The setup is illustrated in Figure 2.5. The axes of the frame fixed to the fingertip are parallel with those of K^b. The RPY angles (see also Appendix A) are chosen to describe locally the orientation of the ball. The corresponding orientation matrix reads

$$\Omega(\phi^o) = \begin{bmatrix} \cos\varphi\cos\theta & \cos\varphi\sin\theta\sin\psi - \sin\varphi\cos\psi & \cos\varphi\sin\theta\cos\psi + \sin\varphi\sin\psi \\ \sin\varphi\cos\theta & \sin\varphi\sin\theta\sin\psi + \cos\varphi\cos\psi & \sin\varphi\sin\theta\cos\psi - \cos\varphi\sin\psi \\ -\sin\theta & \cos\theta\sin\psi & \cos\theta\cos\psi \end{bmatrix}$$

$$(2.15)$$

where $\phi^o = (\varphi, \theta, \psi)$.
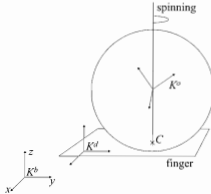
Figure 2.5: Ball rolling on the plane

The surface equations (2.4)-(2.5) (satisfied by the coordinates of the contact point $p_C^o = (x_C^o, y_C^o, z_C^o)$ and by $p_C^d = (x_C^d, y_C^d, z_C^d)$, respectively) read

$$(x_C^o)^2 + (y_C^o)^2 + (z_C^o)^2 - R^2 = 0 \qquad z_C^o = 0.$$

The derivative Dc^o of c^o is given by

$$Dc^o(p_C^o) = [2x_C^o \quad 2y_C^o \quad 2z_C^o] = 2(p_C^o)^T \qquad (2.16)$$

Similarly,

$$Dc^d(p_C^d) = [0 \quad 0 \quad 1]$$

Since all joints are translational, the direct geometry of the finger (2.9) reads

$$q = \begin{bmatrix} q_1 \\ q_2 \\ q_3 \end{bmatrix} = p^d \begin{bmatrix} 1 & 0 & 0 \\ 0 & 1 & 0 \\ 0 & 0 & 1 \end{bmatrix} = \Omega(\phi^d),$$

hence $\Omega(\phi^r) = \Omega(\phi^d)^T \Omega(\phi^o) = \Omega(\phi^o)$. Since $\|Dc^o(p_C^o)\| = 2R$, Constraint (2.6) for the tangent planes reads:

$$\frac{1}{R}(p_C^o)^T \Omega(\phi^o)^T = [0 \quad 0 \quad -1] \qquad (2.17)$$

Using the fact that $[\omega^r \times] = \frac{d}{dt}\Omega(\phi^r) \cdot \Omega(\phi^r)^T$ (see Appendix A), the relative angular velocity of the ball w.r.t. the finger (i.e. w.r.t. the inertial reference frame K^b too) reads

$$\omega^r = \omega^o = \begin{bmatrix} -\dot{\theta}\sin\varphi + \psi\cos\varphi\cos\theta \\ \dot{\theta}\cos\varphi + \dot{\psi}\sin\varphi\cos\theta \\ \dot{\varphi} - \dot{\psi}\sin\theta \end{bmatrix} \qquad (2.18)$$

allowing to calculate v_C^r. the relative velocity at the contact point:

$$v_C^r = \dot{p}^o + [\omega^r \times]\Omega(\phi^r)p_C^o - \dot{p}^d \tag{2.19}$$

To simplify this expression. note that by (2.3):

$$p^r = p_C^d - \Omega(\phi^r)p_C^o = \begin{bmatrix} x_C^d \\ y_C^d \\ R \end{bmatrix}$$

Hence, using (2.17) and replacing in (2.19), one gets

$$v_C^r = \begin{bmatrix} -R\dot{\theta}\cos\varphi - Rw\sin\varphi\cos\theta + \dot{x}_C^d \\ -R\dot{\theta}\sin\varphi + R\dot{\psi}\cos\varphi\cos\theta + \dot{y}_C^d \\ 0 \end{bmatrix}$$

Since the tangent plane at the contact point C is spanned by the vectors $w_{1,C}^d = (1.0.0)^T$ and $w_{2,C}^d = (0.1.0)^T$ the rolling without sliding constraints (2.8) have the form

$$- R\dot{\theta}\cos\varphi - Rw\sin\varphi\cos\theta + \dot{x}_C^d = 0 \tag{2.20}$$
$$- R\dot{\theta}\sin\varphi + R\dot{\psi}\cos\varphi\cos\theta + \dot{y}_C^d = 0. \tag{2.21}$$

The linear map η in Equation (2.13) has the matrix

$$\eta = \begin{bmatrix} I & \begin{bmatrix} 0 & -R & 0 \\ R & 0 & 0 \\ 0 & 0 & 0 \end{bmatrix} \\ 0 & \begin{bmatrix} 0 & -2R & 0 \\ 2R & 0 & 0 \\ 0 & 0 & 0 \end{bmatrix} \end{bmatrix}$$

It is easy to see that $w_3 = (0.0.0.0.0.1)^T$ spans the null-space of η and gives the following constraint of non-spinning:

$$w_z^r = \dot{\varphi} - w\sin\theta = 0. \tag{2.22}$$

Observe that Equations (2.20)-(2.22) involve only the variables $\phi^o = (\varphi, \theta, w)$. x_C^d and y_C^d. Using Tables 2.2 and 2.3. the dimension of M_A equals to dim $M_A = 27 - 19 = 8$. Thus a possible choice of the local coordinates of the manifold M_A is given by $q_A = (\varphi, \theta, w, x_C^d, y_C^d, q)$.

Lemma 1. *The codistribution* Π_1 *spanned by the one-forms obtained from (2.20)-(2.21). namely*

$$\varpi_1 = dx_C^d - R(\cos\varphi d\theta + \sin\varphi\cos\theta dw)$$
$$\varpi_2 = dy_C^d - R(\sin\varphi d\theta - \cos\varphi\cos\theta d\psi)$$

is fully nonholonomic. Moreover, the codistribution Π_2 *obtained by adding the non-pivoting constraint (2.22)*

$$\varpi_3 = d\varphi - \sin\theta d\psi.$$

to ϖ_1 *and* ϖ_2 *is also fully nonholonomic.*

Proof. For both cases, the same geometric constraints are used to eliminate variables, hence the kinematic constraints must be satisfied on an eight-dimensional manifold determined by x_C^d, y_C^d, q, and $\phi^o = (\varphi, \theta, \psi)$. The one-forms ϖ_1, ϖ_2, and ϖ_3 are linearly independent because of the components in dx_C^d, dy_C^d, and $d\varphi$. Let us calculate first the derived flags (see Definition 13) associated to the codistributions $\Pi_1 = I_1^0 = \operatorname{span}\{\varpi_1, \varpi_2\}$ and $\Pi_2 = I_2^0 = \operatorname{span}\{\varpi_1, \varpi_2, \varpi_3\}$. After some lengthy but elementary calculations, the dimensions of the codistributions in the derived flag are $\{2, 0\}$ (resp. $\{3, 2, 0\}$) for I_1^0 (resp. I_2^0). Since the dimension of the last codistribution of the derived flag is 0 in both cases, the lemma follows from Definition 14. □

The kinematics corresponding to q being trivial, we are interested in driftless systems associated to the kinematic constraints (2.20)-(2.22) which evolve on a submanifold of M_A' of M_A, given by the variables $\phi^o = (\varphi, \theta, \psi)$, x_C^d and y_C^d.

Two driftless systems will be associated to the kinematic constraints (2.20)-(2.21) and (2.22) using Definition 15. The driftless system whose vector fields annihilate the one-forms given by the constraints (2.20)-(2.21) is referred to as the spinning case whereas the driftless system whose vector fields annihilate all the three other one-forms is referred to as the non-spinning case. The linearly independent vector fields

$$g_1 = \frac{1}{R} \begin{bmatrix} \sin\varphi \tan\theta \\ \cos\varphi \\ \frac{\sin\varphi}{\cos\theta} \\ R \\ 0 \end{bmatrix} \qquad g_2 = \frac{1}{R} \begin{bmatrix} -\cos\varphi \tan\theta \\ \sin\varphi \\ -\frac{\cos\varphi}{\cos\theta} \\ 0 \\ R \end{bmatrix} \qquad g_3 = \begin{bmatrix} 1 \\ 0 \\ 0 \\ 0 \\ 0 \end{bmatrix} \qquad (2.23)$$

gives the driftless system for the spinning case. For the non-spinning case, the vector fields of the associated driftless system are only g_1 and g_2. The generalized velocities associated to these vector fields are $u_1 = \dot{x}_C^d$, $u_2 = \dot{y}_C^d$ and $u_3 = \omega_z^o = \dot{\varphi} - \dot{\psi}\sin\theta$. Note that the non-spinning constraint (2.22) eliminates precisely u_3 equaling it identically to zero. ∎

Example 2 (ball between two parallel planes). This example, illustrated in Figure 2.6 (together with the preceding one) is popular in the robotics literature and in the literature of the non-holonomic systems in general [5, 45, 54]. Finger 1 has the same properties as the finger in the preceding example. Finger 2, parallel with the first one, has a unique translational joint along the z axis of K^b. The same modelling processus is followed as in the preceding example. The surface equations are

$$\left(x_{C_i}^o\right)^2 + \left(y_{C_i}^o\right)^2 + \left(z_{C_i}^o\right)^2 - R^2 = 0 \qquad z_{C_1}^d = 0 \qquad -z_{C_2}^d = 0 \qquad (2.24)$$

and their derivatives read

$$Dc^o(p_{C_i}^o) = 2(p_{C_i}^o)^T \qquad Dc_i^d(p_{C_i}^d) = \begin{bmatrix} 0 & 0 & (-1)^{i-1} \end{bmatrix} \qquad \iota = 1, 2. \qquad (2.25)$$

The direct geometry of the fingers read

$$\begin{bmatrix} q_{11} \\ q_{12} \\ q_{13} \end{bmatrix} = p_1^d \qquad I = \Omega(\phi_1^d) \qquad \begin{bmatrix} r_{21} \\ r_{22} \\ q_{21} \end{bmatrix} = p_2^d \qquad I = \Omega(\phi_2^d),$$
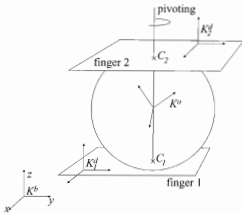
Figure 2.6: Ball between two parallel planes

hence $\Omega(\phi_1^d) = \Omega(\phi_2^d) = \Omega(\sigma^o)$. The parameters r_{21} and r_{22} are geometric constants of the hand. Using the fact that $\|Dc^o(p_{C_1}^o)\| = 2R$, the non-penetration constraint (2.6) results

$$\frac{1}{R}(p_{C_i}^o)^T \Omega(\sigma^o)^T = \begin{bmatrix} 0 & 0 & (-1)^i \end{bmatrix} \qquad i = 1, 2. \tag{2.26}$$

The relative angular velocity ω^r of the ball w.r.t. both fingers is already given by Equation (2.18) of the preceding example, and since $\omega_i^d = 0$ for $i = 1, 2$ we have $\omega_1^r = \omega_2^r = \omega^r$. For finger 1, the kinematic constraints (2.8) are the same as in the preceding example:

$$- R\dot{\theta}\cos\varphi - Rv\sin\varphi\cos\theta + \dot{x}_{C_1}^d = 0 \tag{2.27}$$

$$- R\dot{\theta}\sin\varphi + R\dot{\psi}\cos\varphi\cos\theta + \dot{y}_{C_1}^d = 0. \tag{2.28}$$

The relative velocity at the contact point C_2 reads

$$v_{C_2}^r = \dot{p}_2^r + [\omega_2^r \times]\Omega(\phi_2^i)p_{C_2}^o = \dot{p}_2^r + [\omega_2^r \times]\begin{bmatrix} 0 \\ 0 \\ R \end{bmatrix} \tag{2.29}$$

Using (2.3) together with (2.26), we have

$$p_2^r = p_{C_2}^d - \Omega(\phi_2^d)p_{C_2}^o = \begin{bmatrix} x_{C_2}^d \\ y_{C_2}^d \\ 0 \end{bmatrix} - \begin{bmatrix} 0 \\ 0 \\ R \end{bmatrix}$$

Differentiating this expression w.r.t. the time and reporting in (2.29) we get

$$v_{C_2}^r = \begin{bmatrix} R\dot{\theta}\cos\varphi + Rv\sin\varphi\cos\theta + \dot{x}_{C_2}^d \\ R\dot{\theta}\sin\varphi - R\dot{\psi}\cos\varphi\cos\theta + \dot{y}_{C_2}^d \\ 0 \end{bmatrix}$$

Since $w^d_{1,C_2} = (1, 0, 0)^T$ and $w^d_{2,C_2} = (0, 1, 0)^T$ the kinematic constraints (2.8) read

$$R\dot\theta\cos\varphi + Rv\sin\varphi\cos\theta + \dot x^d_{C_2} = 0 \tag{2.30}$$

$$R\dot\theta\sin\varphi - Rv\cos\varphi\cos\theta + \dot y^d_{C_2} = 0. \tag{2.31}$$

The kinematic constraints (2.27)-(2.28) and (2.30)-(2.31) are not fully nonholonomic because some of them are integrable. In fact, summing up (2.27) with (2.30) and (2.28) with (2.31) we obtain

$$\dot x^d_{C_2} + \dot x^d_{C_1} = 0 \qquad \dot y^d_{C_2} + \dot y^d_{C_1} = 0$$

which can be integrated as

$$x^d_{C_2} + x^d_{C_1} = x^d_{C_1}(0) + x^d_{C_2}(0) \qquad y^d_{C_2} + y^d_{C_1} = y^d_{C_1}(0) + y^d_{C_2}(0). \tag{2.32}$$

These integrated kinematic constraints can be used to eliminate $x^d_{C_2}$ and $y^d_{C_2}$, as functions of $x^d_{C_1}$ and $y^d_{C_1}$. Then, using again Tables 2.2 and 2.3 together with the two additionally obtained geometric constraints (2.32), which can be also used to eliminate variables, the dimension of M_A can be calculated as $\dim M_A = 46 - 38 - 2 = 6$. Hence the local coordinates of a point of M_A can be given by the variables $q_A = (\varphi, \theta, \psi, x^d_{C_1}, y^d_{C_1}, q_{21})$

The remaining two nonholonomic kinematic equations on M_A are similar to those obtained in the preceding example:

$$-R\dot\theta\cos\varphi - Rv\sin\varphi\cos\theta + \dot x^d_{C_1} = 0 \tag{2.33}$$

$$-R\dot\theta\sin\varphi + Rv\cos\varphi\cos\theta + \dot y^d_{C_1} = 0. \tag{2.34}$$

To add the non-pivoting constraint we determine the linear map η first:

$$\eta = \begin{bmatrix} I & \begin{bmatrix} 0 & -R & 0 \\ R & 0 & 0 \\ 0 & 0 & 0 \end{bmatrix} \\ 0 & \begin{bmatrix} 0 & -2R & 0 \\ 2R & 0 & 0 \\ 0 & 0 & 0 \end{bmatrix} \\ I & \begin{bmatrix} 0 & R & 0 \\ R & 0 & 0 \\ 0 & 0 & 0 \end{bmatrix} \\ 0 & \begin{bmatrix} 0 & 2R & 0 \\ -2R & 0 & 0 \\ 0 & 0 & 0 \end{bmatrix} \end{bmatrix}$$

The null-space of this matrix is again given by $w^d = (0, 0, 0, 0, 0, 1)^T$ hence one obtains the same non-spinning constraint (2.22) as in the preceding example. Since the kinematic constraints are similar to those obtained in Example 1, Lemma 1 remains valid for this example.

The kinematic constraints do not include all the variables of M_A (i.e. the variable q_{21} is not involved). Thus the associated driftless systems evolve again on a five-dimensional submanifold of M_A and defined by the vector fields (2.23) of Example 1

The driftless system for the spinning case is given by

$$\dot{q}_A = g_1 u_1 + g_2 u_2 + g_3 u_3,$$

whereas the driftless system associated to the non-spinning case reads

$$\dot{q}_A = g_1 u_1 + g_2 u_2,$$

with $u_1 = \dot{x}_C^d$, $u_2 = \dot{y}_C^d$ and $u_3 = \omega_z^o = \dot{\varphi} - \psi \sin\theta$.   ■

Example 3 (ball between two oblique planes). The setup (see Figure 2.7) is the same as in the preceding example, but the two planes representing the fingers are no longer parallel but oblique with an angle remaining constant during the manipulation.
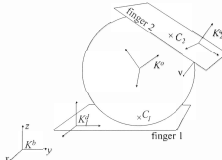
Figure 2.7: Ball between two oblique planes

The surface equations are already given by (2.24) in the preceding example together with their derivatives (2.25). The translational degree of freedom of finger 2 is parallel to the unit normal $v = (x_v^b, y_v^b, z_v^b)^T$ of the plane of the finger. We suppose that v is such that $(x_v^b)^2 + (y_v^b)^2 \neq 0$ (note that $(x_v^b)^2 + (y_v^b)^2 = 0$ would give the setup studied in Example 2). The direct geometry of the fingers reads

$$
\begin{bmatrix} q_{11} \\ q_{12} \\ q_{13} \end{bmatrix} = p_1^d \qquad I = \Omega(\phi_1^d) \qquad r_2 + q_{21} \cdot v = p_2^d
$$

$$
\begin{bmatrix} \dfrac{y_v^b}{\sqrt{(x_v^b)^2+(y_v^b)^2}} & \dfrac{x_v^b z_v^b}{\sqrt{(x_v^b)^2+(y_v^b)^2}} & -x_v^b \\ \dfrac{x_v^b}{\sqrt{(x_v^b)^2+(y_v^b)^2}} & \dfrac{y_v^b z_v^b}{\sqrt{(x_v^b)^2+(y_v^b)^2}} & -y_v^b \\ 0 & -\sqrt{(x_v^b)^2+(y_v^b)^2} & -z_v^b \end{bmatrix} = \Omega(\phi_2^d). \quad (2.35)
$$

Constraint (2.6) for the second finger gives

$$\frac{1}{2R}Dc^o(p_{C_2}^o)\Omega(\phi_2^r)^T = \frac{1}{R}(p_{C_3}^o)^T\Omega(\phi^o)^T\Omega(\phi_2^d) = -Dc_2^d(p_{C_2}^d) = \begin{bmatrix} 0 & 0 & 1 \end{bmatrix}$$

Multiplying both sides by $R\Omega(\phi_2^d)^T$ and taking the transpose, we get

$$\Omega(\phi^o)p_{C_2}^o = -Rv \tag{2.36}$$

which relation can be also read form Figure 2.7

The kinematic constraints at the contact between the object and finger 1 are already given by Equations (2.27) and (2.28) (we simplify for readability's sake):

$$\dot{x}_{C_1}^d - R\omega_y^o = 0 \tag{2.37}$$

$$\dot{x}_{C_1}^d + R\omega_x^o = 0. \tag{2.38}$$

The relative velocity at the contact point C_2 is obtained using (2.3), (2.7), and that $\frac{d\Omega(\phi_2^r)}{dt} = 0$:

$$v_{C_2}^r = \Omega(\phi_2^d)^T(\dot{p}^o - \dot{p}_2^d) + \frac{d\Omega(\phi_2^r)}{dt}\Omega(\phi_2^r)^T\Omega(\phi_2^d)p_{C_2}^o = \Omega(\phi_2^d)^T(\dot{p}^o - \dot{p}_2^d) +$$

$$\Omega(\phi_2^d)^T\frac{d\Omega(\phi^o)}{dt}\Omega(\phi^o)^T\Omega(\phi_2^d)\Omega(\phi_2^d)^T\Omega(\phi^o)p_{C_2}^o = \Omega(\phi_2^d)^T\left[(\dot{p}^o - \dot{p}_2^d) + [\omega^o\times]\Omega(\phi^o)p_{C_2}^o\right]$$

The vectors w_{1,C_2}^d and w_{2,C_2}^d spanning the tangent plane are expressed in the frame fixed to the finger by convention:

$$w_{1,C_2}^d = (1,0,0)^T \qquad w_{2,C_2}^d = (0,1,0)^T$$

Since, by the direct geometry of the finger 2 (2.35) we have

$$\Omega(\phi_2^d)^T\tilde{p}_2^d = \dot{q}_{21}\Omega(\phi_2^d)^Tv = \begin{bmatrix} 0 \\ 0 \\ -\dot{q}_{21} \end{bmatrix}$$

the kinematic constraints corresponding to (2.8) for finger 2 read:

$$-\dot{p}_y^o y_v + \dot{p}_z^o z_v^b + R\omega_x^o x_v^b z_v^b + R\omega_y^o y_v^b z_v^b - R\omega_z^o((x_v^b)^2 + (y_v^b)^2) = 0 \tag{2.39}$$

$$\dot{p}_x^o x_v^b z_v^b + \dot{p}_y^o y_v^b z_v^b + \dot{p}_z^o((x_v^b)^2 + (y_v^b)^2) + R\omega_y^o y_v^b - R\omega_y^o x_v^b = 0. \tag{2.40}$$

There is non-spinning constraint, since the null-space of η contains only the null vector. Observe that the last constraint (2.40), combined with Equations (2.37) and (2.38) gives

$$\dot{p}_x^o x_v^b z_v^b + \dot{p}_y^o y_v^b z_v^b + \dot{p}_z^o((x_v^b)^2 + (y_v^b)^2) - \dot{y}_{C_1}^d y_v^b - \dot{x}_{C_1}^d x_v^b = 0$$

which can be integrated to obtain

$$p_x^o x_v^b z_v^b + p_y^o y_v^b z_v^b + p_z^o((x_v^b)^2 + (y_v^b)^2) - y_{C_1}^d y_v^b - x_{C_1}^d x_v^b$$
$$= p_x^o(0)x_v^b z_v^b + p_y^o(0)y_v^b z_v^b + p_z^o(0)((x_v^b)^2 + (y_v^b)^2) - y_{C_1}^d(0)y_v^b - x_{C_1}^d(0)x_v^b, \tag{2.41}$$

eliminating one of the kinematic constraint. Thus we are left (using again the Tables 2.2 and 2.3 to count variables and constraints) with a manifold M_A of dimension dim $M_A = 46 - 38 - 1 = 7$ with $q_a = \varphi, \theta, \psi, p_x^o, p_y^o, p_z^o, y_{C_1}^d$ and the kinematics is given by the equations (2.38) and (2.39) (2.40). ∎
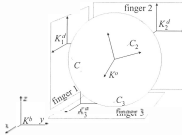
Figure 2.8: The ball between three planes

Example 4 (ball between three perpendicular planes). The setup is illustrated in Figure 2.8. The fingers are again tangent planes to a ball of radius R, parallel to the three respective Cartesian planes of the inertial reference frame, defined by $y^b = 0$, $x^b = 0$ and $z^b = 0$. All joints are translational and their displacements are restricted along the corresponding directions.

The frames fixed to the planes have the same orientations as the base frame. The positions of their origins are denoted by $p_i^d = (x_i^d, y_i^d, z_i^d)^T$ $i = 1, 2, 3$. The origin of the sphere and its orientation is given by $p^o = (x^o, y^o, z^o)^T$ and $\phi^o = (\varphi, \theta, \psi)$ (RPY angles) as in the previous examples. The surface equations are given as

$$\left(x_{C_1}^o\right)^2 + \left(y_{C_1}^o\right)^2 + \left(z_{C_1}^o\right)^2 - R^2 = 0 \qquad y_{C_2}^d = 0 \qquad x_{C_2}^d = 0 \qquad z_{C_3}^d = 0$$

and their derivatives read

$$Dc^o(p_{C_1}^o) = 2\left(p_{C_1}^o\right)^T \quad Dc_1^d(p_{C_1}^d) = (0, 1, 0) \quad Dc_2^d(p_{C_2}^d) = (1, 0, 0) \quad Dc_3^d(p_{C_3}^d) = (0, 0, 1).$$

The direct geometry of the fingers are given by

$$q_i = p_i^d \qquad l = \Omega(\phi_i^d) \qquad i = 1, 2, 3,$$

hence $\Omega(\phi_i^r) = \Omega(\phi^o)$.

Since $\|Dc^o(p_{C_i}^o)\| = 2R$ for $i = 1, 2, 3$. Constraint (2.6) for the tangent planes gives

$$\Omega(\phi^o)p_{C_1}^d = -Re_2 \qquad \Omega(\phi^o)p_{C_2}^d = -Re_1 \qquad \Omega(\phi^o)p_{C_3}^d = -Re_3.$$

with $e_1 = (1, 0, 0)^T$ $e_2 = (0, 1, 0)^T$ and $e_3 = (0, 0, 1)^T$ Thus the geometric constraints corresponding to (2.3):

$$p_{C_i}^d = (p^o - p_i^d) + \Omega(\phi^o)p_{C_i}^o, \qquad i = 1, 2, 3.$$

can be simplified by the use of the above expressions. Isolating the coordinates of the origin of the frame fixed to the object one obtains

$$
\begin{aligned}
x^o &= x_1^d + x_{C_1}^o & x^o &= x_2^d + R & x^o &= x_3^d + x_{C_3}^o \\
y^o &= y_1^d + R & y^o &= y_2^d + y_{C_2}^o & y^o &= y_3^d + y_{C_3}^o \\
z^o &= z_1^d + z_{C_1}^o & z^o &= z_2^d + z_{C_2}^o & z^o &= z_3^d + R.
\end{aligned}
\qquad (2.42)
$$

The relative velocity at the contact point C_i reads

$$v_{C_i}^c = [\omega^o \times]\Omega(\phi^o)p_{C_i}^o + \dot{p}^o - \dot{p}_i^d = 0 \qquad i = 1, 2, 3.$$

The vectors spanning the tangent planes of the fingers are $w_{1,C_1}^d = w_{1,C_3}^d = e_1$, $w_{2,C_2}^d = w_{1,C_2}^d = e_2$, and $w_{2,C_1}^d = w_{2,C_3}^d = e_3$. Reporting this in the expression (2.8) of the kinematic constraint and using the fact (see (A.4)) that

$$[\omega^o \times] = \begin{bmatrix} 0 & \omega_z^o & \omega_y^o \\ \omega_z^o & 0 & -\omega_x^o \\ -\omega_y^o & \omega_x^o & 0 \end{bmatrix}$$

we get

$$\begin{array}{lll} R\omega_x^o + \dot{x}^o - \dot{x}_1^d = 0 & -R\omega_x^o + \dot{y}^o - \dot{y}_2^d = 0 & -R\omega_y^o + \dot{x}^o - \dot{x}_3^d = 0 \\ -R\omega_z^o + \dot{z}^o - \dot{z}_1^d = 0 & R\omega_y^o + \dot{z}^o - \dot{z}_2^d = 0 & R\omega_x^o + \dot{y}^o - \dot{y}_3^d = 0. \end{array}$$

These kinematic constraints are not fully nonholonomic. For, observe that eliminating $R\omega_x^o$ one gets

$$-\dot{z}^o + \dot{z}_1^d = \dot{y}^o - \dot{y}_3^d. \tag{2.43}$$

Differentiating the geometric constraints $z^o = z_1^d + z_{C_1}^d$ and $y^o = y_3^d + y_{C_3}^d$ obtained in (2.42), and reporting them in (2.43) we get $\dot{z}_{C_1}^d = -\dot{y}_{C_3}^d$ which can be integrated as $z_{C_1}^d - z_{C_1}^d(0) = -y_{C_3}^d + y_{C_3}^d(0)$. One may get similar relations by eliminating ω_y^o and ω_z^o. This gives three integrated constraints:

$$\begin{array}{l} z_{C_1}^d - z_{C_1}^d(0) = -y_{C_3}^d + y_{C_3}^d(0) \\ z_{C_2}^d - z_{C_1}^d(0) = -x_{C_3}^d + x_{C_3}^d(0) \\ x_{C_1}^d - x_{C_1}^d(0) = -y_{C_2}^d + y_{C_2}^d(0) \end{array} \tag{2.44}$$

where $x_{C_1}^d(0)$, $x_{C_2}^d(0)$, $y_{C_2}^d(0)$, $y_{C_3}^d(0)$, $z_{C_1}^d(0)$ and $z_{C_3}^d(0)$ are initial conditions. Using these expressions together with the geometric constraints (2.42) and the expression of ω^o in the RPY representation (2.18), the remaining kinematic constraints read:

$$R \begin{bmatrix} 1 & 0 & -\sin\theta \\ 0 & \cos\varphi & \sin\varphi\cos\theta \\ 0 & \sin\varphi & -\cos\varphi\cos\theta \end{bmatrix} \begin{bmatrix} \dot{\varphi} \\ \dot{\theta} \\ \dot{\psi} \end{bmatrix} + \begin{bmatrix} \dot{x}_{C_1}^d \\ \dot{z}_{C_1}^d \\ \dot{z}_{C_3}^d \end{bmatrix} = 0. \tag{2.45}$$

Since the hand has three fingers, the conditions of Corollary 1 are satisfied. Hence, there are no spinning motions to eliminate by additional kinematic constraint.

Tables 2.2 and 2.3 show that the geometric constraints and the integrated kinematic ones (2.44) allow to eliminate 60 variables out of 69. Hence, the dimension of M_A equals to dim $M_A = 9$, $q_A = \varphi, \theta, \psi, x_{C_1}^d, z_{C_2}^d, z_{C_1}^d, q_{12}, q_{21}, q_{33}$.

Lemma 2. *The codistribution* Π, *spanned by the one-forms obtained from the constraints* (2.45), *namely:*

$$
\begin{aligned}
\varpi_1 &= R d\varphi - R\sin\theta d\psi + dx_{C_1}^{\mathcal{A}} \\
\varpi_2 &= R\cos\varphi d\theta + R\sin\varphi\cos\theta d\psi + dz_{C_2}^{\mathcal{A}} \\
\varpi_3 &= R\sin\varphi d\theta - R\cos\varphi\cos\theta d\psi + dz_{C_1}^{\mathcal{A}}
\end{aligned}
\qquad (2.46)
$$

is fully nonholonomic.

Proof. After the elimination of variables using the geometric and the integrated kinematic constraints, the remaining kinematic constraints (2.45) must be satisfied on the nine-dimensional manifold $M_{\mathcal{A}}$. The one-forms ϖ_1, ϖ_2, and ϖ_3 are linearly independent because of their components in $dy_{C_1}^{\mathcal{A}}$, $dz_{C_1}^{\mathcal{A}}$, and $dz_{C_2}^{\mathcal{A}}$. The dimensions of the codistributions in the derived flag of $\Pi = I^0 = \mathrm{span}\{\varpi_1, \varpi_2, \varpi_3\}$ is $\{3, 0\}$. Since the dimension of the last codistribution in the derived flag is 0, the claim follows from Definition 14. $\qquad\square$

The kinematic constraints (2.45) involve only the first six variables of $q_{\mathcal{A}}$. Observe that the last three coordinates q_{12}, q_{21}, q_{33} in $q_{\mathcal{A}}$ determine the position of the ball, since we have (using the geometric constraints (2.42) and the direct geometry of the fingers)

$$
x^o = q_{21} + R \qquad\qquad y^o = q_{12} + R \qquad\qquad z^o = q_{33} + R.
$$

In fact, due to the translational joints of the fingers, the translational motions of the ball are decoupled from the kinematics (2.45) which determines the orientation of the ball.

Therefore, the associated driftless system is calculated on a submanifold $M_{\mathcal{A}}'$ of $M_{\mathcal{A}}$, given by the variables $\varphi, \theta, \psi, x_{C_1}^{\mathcal{A}}, z_{C_2}^{\mathcal{A}}, z_{C_1}^{\mathcal{A}}$, involved in the kinematic constraints. The vector fields annihilating the codistribution spanned by the one-forms (2.46) on the manifold $M_{\mathcal{A}}'$ are

$$
g_1 = \frac{1}{R}\begin{bmatrix} -1 \\ 0 \\ 0 \\ R \\ 0 \\ 0 \end{bmatrix}
\qquad
g_2 = \frac{1}{R}\begin{bmatrix} -\sin\varphi\tan\theta \\ -\cos\varphi \\ -\dfrac{\sin\varphi}{\cos\theta} \\ 0 \\ R \\ 0 \end{bmatrix}
\qquad
g_3 = \frac{1}{R}\begin{bmatrix} \cos\varphi\tan\theta \\ -\sin\varphi \\ \dfrac{\cos\varphi}{\cos\theta} \\ 0 \\ 0 \\ R \end{bmatrix}
$$

giving the driftless system

$$
\begin{bmatrix} \dot\varphi & \dot\theta & \dot\psi & \dot x_{C_1}^{\mathcal{A}} & \dot z_{C_2}^{\mathcal{A}} & \dot z_{C_1}^{\mathcal{A}} \end{bmatrix}^T = g_1 u_1 + g_2 u_2 + g_3 u_3
\qquad (2.47)
$$

where the inputs are $u_1 = \dot x_{C_1}^{\mathcal{A}}$, $u_2 = \dot z_{C_2}^{\mathcal{A}}$ and $u_3 = \dot z_{C_1}^{\mathcal{A}}$.

Note that by Lemma 2, this system is locally commandable (i.e. the involutive closure of the distribution spanned by g_1, g_2 and g_3 has dimension 6 which equals to the dimension of $M_{\mathcal{A}}'$). $\qquad\blacksquare$

2.1.4 Dynamics

The notations introduced in Section 2.1.1 are reused.

The dynamic equations are obtained separately for each finger and the object. These equations are connected by means of the contact forces. The contact force applied by the finger $\imath$ to the object is denoted by the vector $f_\imath \in \mathbb{R}^3$ such that its coordinates are expressed in the inertial reference frame K^b.

For the fingers, contact forces are transformed to exterior torques in the joint space (see Figure 2.9).
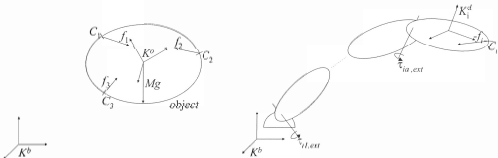
Figure 2.9: Contact forces

Let us introduce the inertial parameters given by Table 2.4 (recall that $q_\imath$ is the vector of joint coordinates of the finger $\imath$). The dynamics of the object are given by the Newton-Euler

notation	definition
$H_\imath(q_\imath)$	inertia matrix of the finger $\imath$
Θ	inertia matrix of the object
M	mass of the object

Table 2.4: Inertia parameters

equations

$$M\ddot{p}^o = Mg + \sum_{i=1}^{m} f_i \qquad (2.48)$$

$$\Theta\dot{\omega}^o = \sum_{i=1}^{m} \left(\Omega(\phi^o) p_{C_i}^o \times f_i \right) - \omega^o \times \Theta\omega^o \qquad (2.49)$$

where $g = (0, 0, -9.81)^T$ is the vector of gravity acceleration. The dynamics of the fingers are

obtained using the Lagrangian [40, 52] of the corresponding manipulators:

$$H_i(q_i)\ddot{q}_i + h_i(q_i, \dot{q}_i) = \tau_i - \tau_{i,ext} \qquad i = 1, \quad . m \qquad (2.50)$$

where h_i contains the gravitational and quadratic terms w.r.t. the joint velocities.

The torques delivered by the motors at the joints are considered as the input variables of the HOS. The vector of these joint torques of the finger i is denoted by τ_i. As mentioned above, contact forces are transformed into exterior joint torques, denoted by the vector $\tau_{i,ext}$ for the finger i.

In order to precise the relation between the contact force f_i and the vector of exterior torques $\tau_{i,ext}$, we determine first the equivalent wrench (force and moment taken together) corresponding to the contact force at the origin of the frame K_i^d, fixed to the last segment of the finger i.

This transformation is linear for any fixed finger configuration and contact point and given by the relation

$$\tau_{i,ext} = J_i^T G^T f_i \qquad (2.51)$$

where J^T is the transposed jacobian of the finger i (defined by (2.10)) and the matrix G^T reads

$$G_i^T = \begin{bmatrix} -I \\ -[\Omega(\phi_i^d)p_{C_i}^d \times] \end{bmatrix}$$

The contact is said to be non-singular if the matrix $J_i^T G_i^T$ can be inverted. This allows to eliminate the contact forces f_i and the exterior torques $\tau_{i,ext}$ and to report Equations (2.50) and (2.51) in the dynamics of the object resulting

$$M\ddot{p}^o = Mg + \sum_{i=1}^{3}(J_i^T G_i^T)^{-1}[\tau_i - H_i\ddot{q}_i - h_i(q_i, \dot{q}_i)]$$

$$\Theta\dot{\omega}^o = \sum_{i=1}^{3}\{\Omega(\phi_i^d)p_{C_i}^o \times (J_i^T G_i^T)^{-1}[\tau_i - H_i\ddot{q}_i - h_i(q_i, \dot{q}_i)]\} - \omega^o \times \Theta\omega^o$$

Remark 7 *In the case of redundant fingers (i.e. such that the number of joints exceeds three) the pseudo-inverse of $J_i^T G_i^T$ should be used.*

2.1.5   Inequality constraints

The contact forces applied to the object by the fingers must oriented inwards the object. This requirement is expressed by the inequality

$$Dc^o(p_{C_i}^o)f_i < 0. \qquad (2.52)$$

Since we suppose permanent *rolling* contacts (i.e. there is no slip, see Assumption **A4**), the forces must also remain inside the so called friction cone. Supposing Coulomb friction model,

the volume of this friction cone is determined by the friction coefficient μ and the corresponding constraint reads:

$$\frac{\|f_{it}\|}{\|f_{in}\|} < \mu$$

where f_{in} (resp. f_{it}) give the normal (resp. tangent) component of the contact force between the finger $\imath$ and the object

Other inequality constraint may also be present in order to describe the limits of the hand's working space and to avoid collisions between the fingers. These constraints are not addressed here and will be relaxed in the sequel.

2.1.6 Planar hand-object structures

Assumptions **A1**-**A6** remain unchanged for planar HOSs. However, important simplifications can be made w.r.t. the general three-dimensional case. We proceed the same way as for the modelling of three-dimensional HOSs, namely we start with the equations defining the geometry and the kinematics and then we continue with the dynamics.

Recall that the frames fixed to the $\imath$-th finger and to the object are K_i^d and K^o and we denote by the vector $p_i^r \in \mathbb{R}^2$ and by the angle $\phi_i^r \in \mathbb{S}$ their relative position and orientation. Recall also that the coordinates of the contact point $p_{C_i}^j = [x_{C_i}^j, y_{C_i}^j]^T$ $j \in \{o, d\}$ are expressed in the frame K^o and K_i^d, respectively.

Since ϕ^o and ϕ_i^r are scalar, all orientation matrices have the form

$$\Omega(\phi) = \begin{bmatrix} \cos\phi & -\sin\phi \\ \sin\phi & \cos\phi \end{bmatrix} \qquad \phi \in \{\phi^o, \phi_i^r\}.$$

and we simply have $\omega^o = \dot{\phi}^o$ and $\omega_i^r = \dot{\phi}_i^r$ In particular, the relative position and orientation of the object and finger $\imath$, corresponding to (2.2), is defined as

$$(p_i^r, \phi_i^r) = (\Omega(\phi_i^d)^T(p^o - p_i^d), \phi^o - \phi_i^d). \tag{2.53}$$

Observe that the geometry of the contact between the object and the $\imath$th finger is defined by the constraints

$$c_i^d(p_{C_i}^d) = 0 \tag{2.54}$$

$$c^o(p_{C_i}^o) = 0 \tag{2.55}$$

$$p_{C_i}^o - p_i^r - \Omega(\phi_i^r)p_{C_i}^d = 0 \tag{2.56}$$

$$\det\begin{pmatrix} Dc_i^d(p_{C_i}^d) \\ Dc^o(p_{C_i}^o) \cdot \Omega(\phi_i^r)^T \end{pmatrix} = 0. \tag{2.57}$$

corresponding to the equations (2.4), (2.5), (2.3) and (2.6), respectively. These constraints depend exclusively on the variables $(p_{C_i}^o, p_{C_i}^d, p_i^r, \phi_i^r)$, describing the relative situation of the object and finger $\imath$.

Since $\ker Dc_i^{\mathcal{A}}(p_{C_i}^{\mathcal{A}})$ is one-dimensional, it is spanned by

$$w_{C_i}^{\mathcal{A}} = \begin{bmatrix} 0 & -1 \\ 1 & 0 \end{bmatrix} Dc_i^{\mathcal{A}}(p_{C_i}^{\mathcal{A}})^T$$

Taking into account the fact that the relative velocity of the object and the finger i at the contact point is

$$v_{C_i}^r = \dot{p}_i^r + [\dot{\phi}_i^r \times]\left(p_{C_i}^r - p_i^r\right)$$

the kinematic constraint corresponding to (2.8) reads

$$(w_{C_i}^{\mathcal{A}})^T \left(\dot{p}_i^r + [\dot{\phi}_i^r \times]\left(p_{C_i}^r - p_i^r\right)\right) = 0 \qquad (2.58)$$

where

$$[\dot{\phi}_i^r \times] = \begin{bmatrix} 0 & -\dot{\phi}_i^r \\ \dot{\phi}_i^r & 0 \end{bmatrix}$$

To define the geometry of finger i, recall that $\mathcal{F}_i$ gives the set in which the vector q_i gets its values. The definition of the direct geometry function d_i of finger i in the plane is similar to (2.9) but with a different range space:

$$d_i : \mathcal{F}_i \to \mathbb{R}^2 \times \mathbb{R}/2\pi\mathbb{Z}, \qquad d_i(q_i) = (p_i^{\mathcal{A}}, \phi_i^{\mathcal{A}}). \qquad (2.59)$$

We can now give the inventory of the variables and constraints defining the geometry and the kinematics of planar HOSs, similarly to Tables 2.2 and 2.3 referring to the general three-dimensional case.

variables	description	#
q_i, $i = 1, \quad , m$	joint coordinates	$\sum_{k=1}^m a_k$
p^o, ϕ^o	position & orientation of the object	3
$p_i^{\mathcal{A}}, \phi_i^{\mathcal{A}}$, $i = 1, \quad , m$	positions & orientations of the fingertips	$3m$
p_i^r, ϕ_i^r, $i = 1, \quad , m$	relative positions & orientations	$3m$
$p_{C_i}^o$, $i = 1, \quad , m$	contact points on the object surface	$2m$
$p_{C_i}^{\mathcal{A}}$, $i = 1, \quad , m$	contact points on the fingers' surface	$2m$

Table 2.5: Variables in two dimensions

Remark 8. *It is shown later (see Proposition 3 in Section 2.2) that the kinematic constraint is always integrable in the planar case.*

The dynamical equations of the object and the fingers for the two-dimensional case read

$$mp^o = f_g + \sum_{i=1}^m f_i \qquad (2.60)$$

$$\Theta\dot{\phi}^o = \sum_{i=1}^m \Omega(\phi^o)p_{C_i}^o \times f_i \qquad (2.61)$$

$$H_i(q_i)\ddot{q}_i + h_i(q_i, \dot{q}_i) = \tau_i \quad J_i^T G_i^T \quad f_i. \qquad (2.62)$$

constraint	type	number of equation per finger
(2.53)	geometric	3
(2.56)	geometric	2
(2.54)-(2.55)	geometric	2
(2.57)	geometric	1
(2.59)	geometric	3
(2.58)	kinematic	1

Table 2.6: Constraints in two dimensions

The following example illustrates the modelling of a planar HOS.

Example 5. Consider the HOS given in Figure 2.10. The hand has two fingers with prismatic (translational) joints and fingertips of radius r_i, $i = 1, 2$. The manipulated object is a disc of radius R. The position of the object is given by the coordinates x^o and y^o of the point O and its orientation is determined by the angle ϕ^o
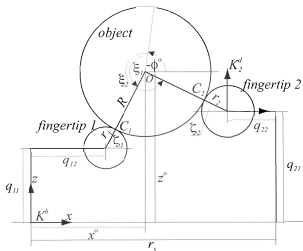

Figure 2.10: Planar HOS.

The geometric constraints (2.54)-(2.57) read

$$(x_{C_i}^d)^2 + (y_{C_i}^d)^2 - r_i^2 = 0 \qquad (2.63)$$

$$(x_{C_i}^o)^2 + (y_{C_i}^o)^2 - R^2 = 0 \qquad (2.64)$$

$$\begin{bmatrix} q_{i2} \\ q_{i1} \end{bmatrix} - \begin{bmatrix} x^o - x_{C_i}^d \\ y^o - y_{C_i}^d \end{bmatrix} - \begin{bmatrix} \cos\phi^o & -\sin\phi^o \\ \sin\phi^o & \cos\phi^o \end{bmatrix} \begin{bmatrix} x_{C_i}^o \\ y_{C_i}^o \end{bmatrix} = 0 \qquad (2.65)$$

$$\det \begin{bmatrix} x_{C_i}^d & y_{C_i}^d \\ x_{C_i}^o \cos\phi^o - y_{C_i}^o \sin\phi^o & x_{C_i}^o \sin\phi^o + y_{C_i}^o \cos\phi^o \end{bmatrix} = 0. \qquad (2.66)$$

for $i = 1, 2$. The kinematic constraint (2.58) reads

$$\begin{bmatrix} -y_{C_i}^d & x_{C_i}^d \end{bmatrix} \left(\begin{bmatrix} \dot{x}^o - \dot{q}_{i2} \\ \dot{y}^o - \dot{q}_{i1} \end{bmatrix} + [\dot{\phi}^o \times] \begin{bmatrix} x_{C_i}^o - x^o + q_{i2} \\ y_{C_i}^o - y^o + q_{i1} \end{bmatrix} \right) = 0. \qquad (2.67)$$

The dynamic equations of the object are given by (2.60)-(2.61), while the dynamics of the finger i, corresponding to (2.62) reads

$$\begin{bmatrix} m_{i1} + m_{i2} & 0 \\ 0 & m_{i2} \end{bmatrix} \begin{bmatrix} \ddot{q}_{i1} \\ \ddot{q}_{i2} \end{bmatrix} + \begin{bmatrix} -(m_{i1} + m_{i2})g \\ 0 \end{bmatrix} = \begin{bmatrix} \tau_{i1} \\ \tau_{i2} \end{bmatrix} - \begin{bmatrix} f_{i,y} \\ (-1)^{i-1} f_{i,x} \end{bmatrix} \qquad (2.68)$$

where m_{ij} gives the mass of the jth segment of finger i. ∎

2.1.7 Hand-object structures with special morphology

Consider a robotic hand with 3 fingers, each with 5 joints. Suppose that the following properties are satisfied (see Figure 2.11).

1 The last segments of the fingers are spheres such that they can be rotated around two independent symmetry axes. These rotations correspond to the joints 4 and 5.

2. For each finger, the joint coordinates corresponding to the joints number 4 and 5 are cyclic coordinates [65]:

$$\frac{\partial \mathcal{L}_i}{\partial q_{i4}} = \frac{\partial \mathcal{L}_i}{\partial q_{i5}} = 0 \qquad i = 1, \quad , 3$$

where $\mathcal{L}_i$ is the Lagrangian of the ith finger).

3. The orientation of the last joint axis does not depend on q_{i4} ($i = 1, \quad , 3$).

Remark 9. *The last condition corresponds to special mechanical devices, roughly speaking, similar to the ones used for trackballs and for the mechanical integrator presented in [56, Chapter 1]. The results concerning such hand structures can be easily extended to higher number fingers and joints. We have restricted ourselves to the simplest case for readability's sake.*
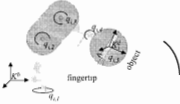
Figure 2.11. Finger with symmetries satisfying the conditions

Remark 10. *Let us give a mechanical consequence of the above conditions. Admitting that the last segments of the fingers have all radius r (these radii may be different for the general case), one can virtually enlarge the volume of the convex object by constructing a new surface which is at distance r from the original on the direction of the corresponding finger. It is easy to see that the centers of the last segments are always on this enlarged surface as far as the contact is maintained. Let this point of the enlarged surface be denoted by C_i for the finger i and let $t_i^b = \overline{C_i C_i}$. (Notice that the direction of t_i^b is normal to both surfaces at C_i and $\bar{C}_i$.) Denote the linear (resp. angular) velocity of the last segment (i.e. the sphere) of the finger i by $v_{4,5}^d$ (resp. $\omega_{4,5}^d$). Then the rolling without slipping constraint at the real contact point C_i reads*

$$v_{C_i}^d = v_{4,5}^d + [\omega_{4,5}^d \times] t_i^b - \left(\dot{p}^o + [\omega^o \times] \Omega(\phi^o) p_{C_i}^o\right) = 0.$$

Since the linear velocity $v_{4,5}^d$ gives the velocity of $\bar{C}_i$ which is also a point of the enlarged surface, the relative velocity at $\bar{C}_i$ gives

$$v_{\bar{C}_i}^d = v_{4,5}^d - \left(\dot{p}^o + [\omega^o \times] \left(\Omega(\phi^o) p_{C_i}^o - t_i^b\right)\right) = \left[(\omega^o - \omega_{4,5}^d) \times\right] t_i^b$$

which is different from zero as far as $\omega^o - \omega_{4,5}^d \neq 0$. Therefore, the origin of the last segment (i.e. that of the sphere) slides on the enlarged surface of the object. The equality $\omega^o - \omega_{4,5}^d = 0$ corresponds to pure relative rotations at the point $\bar{C}_i$ of the object and the finger i.

The modelling of HOSs including a robotic hand satisfying Conditions 1-3 follows the general procedure presented at the beginning of this section.

Example 6. Consider the HOS depicted in Figure 2.12. The manipulated object is a sphere of radius R. The coordinates of the origin of the frame K^o, fixed to the sphere are (x^o, y^o, z^o) and its orientation is represented by the RPY angles $\phi^o = (\varphi, \theta, \psi)$. The vectors $(d_{xi}, d_{yi}, d_{zi})^t$ $(i = 1, 2, 3)$ give the coordinates of the finger base points in the frames K^b. The frames K_i^d are fixed to the centers of the last segments of the fingers. The geometric constraints (2.4)-(2.5) are given by

$$(x_{C_i}^o)^2 + (y_{C_i}^o)^2 + (z_{C_i}^o)^2 - R^2 = 0 \qquad (x_{C_i}^d)^2 + (y_{C_i}^d)^2 + (z_{C_i}^d)^2 - r^2 = 0 \quad i = 1, 2, 3. \quad (2.69)$$

with derivatives

$$Dc^o(p_{C_i}^o) = 2\left(p_{C_i}^o\right)^T \qquad Dc_i^d(p_{C_i}^d) = 2\left(p_{C_i}^d\right)^T$$
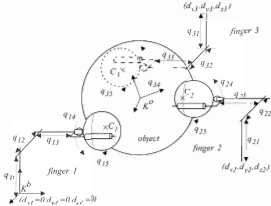
Figure 2.12:   HOS in three dimensions

Since $\|Dc^o(p_{C_1}^o)\| = 2R$ and $\|Dc_i^d(p_{C_1}^d)\| = 2r$, Constraint (2.6) reads

$$p_{C_i}^d = -\frac{r}{R}\Omega(\phi_i^r)p_{C_1}^o.$$

Reporting this in (2.3), and multiplying both sides from left by $\Omega(\phi_i^d)$ we get

$$\begin{bmatrix} q_{i3} + d_{xi} \\ q_{i2} + d_{yi} \\ q_{i1} + d_{zi} \end{bmatrix} - p^o - \left(1 + \frac{r}{R}\right)\Omega(\phi^o)p_{C_1}^o = 0. \tag{2.70}$$

The relative velocity is now expressed in K^b This is simply obtained if Equation (2.7) is multiplied from left by $\Omega(\phi_i^d)$:

$$v_{C_i}^r = \dot{p}^o + [\omega^o \times]\Omega(\phi^o)p_{C_1}^o - \begin{bmatrix} \dot{q}_{i3} \\ \dot{q}_{i2} \\ \dot{q}_{i1} \end{bmatrix} - \begin{bmatrix} 0 & 0 & \dot{q}_{i5} \\ 0 & 0 & -\dot{q}_{i4} \\ -\dot{q}_{i5} & \dot{q}_{i4} & 0 \end{bmatrix}\left(\Omega(\phi^o)p_{C_1}^o + p^o - \begin{bmatrix} q_{i3} + d_{xi} \\ q_{i2} + d_{yi} \\ q_{i1} + d_{zi} \end{bmatrix}\right)$$

The vectors spanning the tangent plane at the contact point are $w_{1,C_i}^d = [-z_{C_i}^d, 0, x_{C_i}^d]^T$ and $w_{2,C_i}^d = [-y_{C_i}^d, x_{C_i}^d, 0]^T$ Finally, since the structure of the inertia matrices are not specified neither for the fingers nor for the object, the dynamic equations of the object and the fingers are given in their general form by (2.48)-(2.49) and by (2.50).   ∎

2.2   Holonomy, flatness and Liouvillian properties

The notion of holonomy is defined in Appendix A. The definitions of (differential) flatness and Liouvillian systems are recalled here. Note that the rth order time derivative of a function $f(t)$ of time is denoted by $f^{(r)}(t) = \frac{d^r f(t)}{dt^r}$.

Definition 4 (flatness). *The system*

$$\dot{x} = f(x, u) \tag{2.71}$$

with $x \in \mathbb{R}^n$ and $u \in \mathbb{R}^m$ is differentially flat if one can find a set of variables, called flat output,

$$y = h(x, u, \dot{u}, \ddot{u}, \quad , u^{(r)}), \qquad y \in \mathbb{R}^m \tag{2.72}$$

with r finite integer, such that

$$\begin{aligned} x &= \alpha(y, \dot{y}, \ddot{y}, \quad , y^{(q)}) \\ u &= \beta(y, \dot{y}, \ddot{y}, \quad , y^{(q+1)}) \end{aligned} \tag{2.73}$$

with q a finite integer, and such that the system equations

$$\frac{d\alpha}{dt}(y, \dot{y}, \ddot{y}, \quad , y^{(q+1)}) = f(\alpha(y, \dot{y}, \ddot{y}, \quad , y^{(q)}), \beta(y, \dot{y}, \ddot{y}, \quad , y^{(q+1)}))$$

are identically satisfied.

The weaker notion of Liouvillian systems is defined in [10] using differential algebra. We adopt here a slightly different definition.

Definition 5 (Liouvillian system). *The system (2.71) is said to be Liouvillian if there exists a set of variables defined as (2.72), and a finite number of variables $\xi_1, \quad , \xi_p$ given by*

$$\xi_i^{(\mu_i)} = \gamma_i(y, \dot{y}, \quad , y^{(q+1)}) \quad i = 1, \quad , p \tag{2.74}$$

such that

$$\begin{aligned} x &= \alpha(y, \dot{y}, \ddot{y}, \quad , y^{(q)}, \bar{\xi}_1^{\mu_1 - 1}, \quad , \bar{\xi}_p^{\mu_p - 1}) \\ u &= \beta(y, \dot{y}, \ddot{y}, \quad , y^{(q+1)}, \bar{\xi}_1^{\mu_1 - 1}, \quad , \bar{\xi}_p^{\mu_p - 1}), \end{aligned} \tag{2.75}$$

with $\bar{\xi}_i^{\mu_i - 1} = (\xi_i, \dot{\xi}_i, \quad , \xi_i^{(\mu_i - 1)})$, and such that α and β identically satisfy the system equations:

$$\frac{d\alpha}{dt} = f(\alpha, \beta). \tag{2.76}$$

We refer to y as a partially flat output and to $\xi, i = 1, \quad , p$ as integral variables.

Let us insist on the fact that the differential equations (2.74), satisfied by the integral variables ξ_i, only depend on the partially flat output y. Therefore, once we choose a smooth trajectory $t \to y(t)$, the RHS[3] of (2.74) becomes a function of t only, which justifies the fact that ξ_i are called integral variables. The remaining part of this section is devoted to the study of these properties in the case of HOSs. General results are obtained for the planar case and for HOSs with symmetries, whose models were presented in Sections 2.1.6 and 2.1.7, respectively. The rest of the results deal with the examples treated in Sections 2.1.3. The solutions for the MPP of HOSs, presented in Section 2.3, are based on the propositions of this section.

---

[3]Right Hand Side

2.2.1   Holonomy and flatness of planar structures

It can be shown that all planar configurations are holonomic. We also show that such configurations are differentially flat with more than one fingers as long as each finger has at least two joints.

Proposition 3. *In the planar case, the kinematic constraints between every finger and the object are holonomic. Consequently, planar HOSs, with an arbitrary number of fingers, are holonomic.*

Proof. It is enough to show that the constraints are holonomic for a single finger in contact with the object, hence the subscript i corresponding to the finger's index is omitted in the proof.

Note that the configuration manifold describing the relative situation of the object and a finger in contact, parameterized by the variables $(p_{C_i}^o, p_{C_i}^A, p_i^r, \phi_i^r)$ and observe that the constraints (2.54)-(2.58) depend only on these variables.

The one-forms corresponding to the geometric and kinematic constraints read

$$\varpi_1 = d(c^A(p_C^A)) = 0 \tag{2.77}$$

$$\varpi_2 = d(c^o(p_C^o)) = 0 \tag{2.78}$$

$$\begin{bmatrix} \varpi_3 \\ \varpi_4 \end{bmatrix} = d\left(p_C^o - p^r \cdot \Omega(\phi^r) p_C^o\right) = 0 \tag{2.79}$$

$$\varpi_5 = d\left(\det \begin{pmatrix} Dc^A(p_C^A) \\ Dc^o(p_C^o) \cdot \Omega(\phi^r)^T \end{pmatrix}\right) = 0 \tag{2.80}$$

$$\varpi_6 = (w_{C_i}^A)^T \left(dp^r + [d\phi^r \times](p_C^o - p^r)\right) = 0 \tag{2.81}$$

where (2.77)-(2.80) are the exterior derivatives of the constraints (2.54)-(2.57). The one-form ϖ_6 comes from the constraint corresponding to the vanishing relative velocity of the surfaces (curves) in contact at the contact point (see Equation (2.58)). These 6 one-forms span a codistribution. Their independence can be checked by lengthy calculations that are omitted here. Nevertheless, this property is easily interpreted in geometric terms by the fact that the independence of the first five equations is a consequence of the opposite convexities of the boundaries of the object and the finger with uniqueness of the contact point and thus the coincidence of the common tangents. Moreover, the last equation is the only one involving the covectors dp^r, $d\phi^r$ without dependence on dp_C^A, dp_C^o. Since the six one-forms are independent on a manifold of dimension 7, the system is always locally integrable which proves holonomy.   □

Proposition 4. *Planar HOSs with at least two fingers, each having at least two joints, are differentially flat.*

Proof. Let m denote the number of fingers ($m \geq 2$) and a_i ($i = 1, \ldots, m$, $a_i \geq 2$) the number of joints of finger i. We thus have $\sum_{i=1}^m a_i$ independent inputs. We claim that a flat output is given by the following $3 + \sum_{i=1}^m a_i - 2m$ variables: p^o ϕ^o $q_{i3}, \ldots q_{i,a_i}$ ($i = 1, \ldots, m$) and by

$$y_i = g_i(f_1, \ldots f_m) \qquad i = 1, \ldots 2m - 3,$$

with g_i arbitrary but fixed combinations of the contact forces. Let us denote by Y the corresponding $\sum_{i=1}^{m} a_i$ dimensional vector:

$$Y = (p^o, \phi^o, q_{1,3}, \quad , q_{1,a_1}, \quad , q_{m,3}, \quad , q_{m,a_m}, y_1, \quad , y_{2m-3}).$$

Consider the finger i and the object. Using Proposition 3, the kinematic equation can be integrated to get rid of $\dot{p}_i^r$ and $\dot{\phi}_i^r$ and (2.54)-(2.58) become a set of six algebraic independent equations depending on seven variables. Therefore, the coordinates of the contact point and the position and orientation of the finger i can be all locally calculated as functions of the relative orientation ϕ_i^r.

Denoting by ϕ_i^d, p_i^d the orientation and position of the frame fixed to the finger, the absolute position and orientation of all the fingers $i = 1, \quad , m$ are given by

$$d_i(q_i) = (p^o - \Omega(\phi_i^d)p_i^r, \phi^o - \phi_i^r) \qquad i = 1, \quad , m, \qquad (2.82)$$

using (2.53) and the direct geometry of the fingers, defined by (2.59). We thus have $3m$ independent equations with the $3 + \sum_{i=1}^{m} a_i + m$ variables: $\phi^o \quad p^o \quad q_{i1}, \quad , q_{i,a_i}, \phi_1^r, \quad , \phi_m^r,$ $(i = 1, \quad , m)$. Note that the inequality $3 + \sum_{i=1}^{m} a_i + m \geq 3 + 3m$ is always satisfied, since $a_i \geq 2$ $(i = 1, \quad , m)$.

This shows that the knowledge of ϕ^o and p^o, the orientation and position of the object, together with $q_{i3}, \quad , q_{i,a_i}$, allows to calculate ϕ_i^r, q_{i1}, q_{i2} for $i = 1, \quad , m$, using Equation (2.82). At this point it is shown that all variables of the kinematics (see Table 2.5) are obtained as functions of the variables in Y.

The dynamic equations of the object (2.60)-(2.61) together with $y_i \in Y$ $(i = 1, \quad 2m - 3)$ gives the contact forces f_i $(i = 1, \quad , m)$ as functions of $Y, \dot{Y}$ and $\ddot{Y}$.

The contact forces and $Y, \dot{Y}, \ddot{Y}$ allow then to calculate the vectors of joint torques of the fingers $\tau_i, (i = 1, \quad , m)$ using (2.62).

Since we have shown that all system variables can be expressed as functions of Y and its derivatives we have proved that Y is a flat output and the system is flat. $\qquad \square$

2.2.2 Flatness study of the kinematics (examples 1 and 2)

We wish to conclude about the (differential) flatness property of the kinematics studied in Examples 1 and 2. For both examples we distinguish two cases. Fist, we study the model allowing pivoting motions, then the constraints eliminating such motions are added to the kinematics.

Kinematics with pivoting motions

This is the case of Examples 1 and 2 without considering the non-pivoting constraints (2.22), same for both examples. Introduce the matrix $\mathbf{A}$ and the vector X defined by

$$\mathbf{A} = \begin{bmatrix} 0 & R\cos\varphi & R\sin\varphi\cos\theta & -1 & 0 \\ 0 & R\sin\varphi & -R\cos\varphi\cos\theta & 0 & -1 \end{bmatrix} \qquad X = \begin{bmatrix} \varphi, \theta, \psi, x_C^d, y_C^d \end{bmatrix}^T \qquad (2.83)$$

where, for Example 2, we identify x_C^d and y_C^d with $x_{C_1}^d$ and $y_{C_1}^d$ (the coordinates of the contact point on the first finger). Hence kinematic constraints (2.20)-(2.21) (resp. (2.27)-(2.28)) of Example 1 (resp. Example 2) read

$$\mathbf{A}\dot{X} = 0. \qquad (2.84)$$

The following driftless system was associated to Equation (2.84) using the vector fields defined by (2.23):

$$
\begin{aligned}
\dot{\varphi} &= \frac{u_1}{R}\sin\varphi\tan\theta - \frac{u_2}{R}\cos\varphi\tan\theta + u_3 \\
\dot{\theta} &= \frac{u_1}{R}\cos\varphi + \frac{u_2}{R}\sin\varphi \\
w &= \frac{u_1}{R}\frac{\sin\varphi}{\cos\theta} - \frac{u_2}{R}\frac{\cos\varphi}{\cos\theta} \\
\dot{x}_C^d &= u_1 \\
\dot{y}_C^d &= u_2,
\end{aligned}
\qquad (2.85)
$$

Recall that the vector fields multiplied by the generalized velocity inputs u_1, u_2 and u_3 an nihilates the codistribution spanned by the rows of the matrix $\mathbf{A}$, defined by (2.83). (These vector fields are already calculated in Example 1.) Recall also that the velocity u_3 corresponds precisely to the angular velocity of spinning, i.e. $u_3 = \dot{\varphi} - \dot{\psi}\sin\theta = \omega_s^o$

Proposition 5. *The kinematics given by (2.84) (or the driftless system (2.85) with three inputs: $u_1 = \dot{x}_C^d$, $u_2 = \dot{y}_C^d$, $u_3 = \omega_s^o$) is differentially flat. The flat output Y is given by*

$$
Y = \begin{bmatrix} \varphi \\ \theta \\ \zeta \end{bmatrix}
$$

with

$$
\zeta = \begin{bmatrix} \dot{\varphi}\sin\varphi\cos\theta + \dot{\theta}\cos\varphi\sin\theta \\ -\dot{\varphi}\cos\varphi\cos\theta + \dot{\theta}\sin\varphi\sin\theta \end{bmatrix}^T \mathbf{A}X \qquad (2.86)
$$

Proof. Introduce the variables y_1 and y_2 as

$$
\begin{bmatrix} y_1 \\ y_2 \end{bmatrix} = \mathbf{A}X \qquad (2.87)
$$

Note that y_1, y_2 and ζ are functions of the system variables (2.84) including the inputs $u_1 = \dot{x}_C^d$, $u_2 = \dot{y}_C^d$, $u_3 = \omega_s^o$.

Differentiating ζ, using (2.86) and (2.87), one obtains

$$
ay_1 + by_2 = \dot{\zeta} + \dot{\theta}\dot{\varphi}^2\cos\theta \qquad (2.88)
$$

with

$$
\begin{aligned}
a &= \ddot{\varphi}\sin\varphi\cos\theta + (\dot{\varphi}^2 + \dot{\theta}^2)\cos\varphi\cos\theta - 2\dot{\varphi}\dot{\theta}\sin\varphi\sin\theta + \ddot{\theta}\cos\varphi\sin\theta \\
b &= -\ddot{\varphi}\cos\varphi\cos\theta + (\dot{\varphi}^2 + \dot{\theta}^2)\sin\varphi\cos\theta + 2\dot{\varphi}\dot{\theta}\cos\varphi\sin\theta + \ddot{\theta}\sin\varphi\sin\theta
\end{aligned}
$$

Observe now that (2.88) together with (2.86) constitutes a linear system w.r.t. to the variables y_1 and y_2

$$\begin{bmatrix} \dot{\varphi} \sin\varphi \cos\theta + \dot{\theta} \cos\varphi \sin\theta & -\dot{\varphi} \cos\varphi \cos\theta + \dot{\theta} \sin\varphi \sin\theta \\ a & b \end{bmatrix} \begin{bmatrix} y_1 \\ y_2 \end{bmatrix} = \begin{bmatrix} \zeta \\ \dot{\zeta} + \theta \dot{\varphi}^2 \cos\theta \end{bmatrix}$$

hence y_1 and y_2 are obtained as functions of ζ, $\dot{\zeta}$, θ, $\dot{\theta}$, $\ddot{\theta}$, φ, $\dot{\varphi}$, and $\ddot{\varphi}$.

In order to obtain ψ as function of ζ, φ, θ and their successive time derivatives, we differentiate Equation (2.87) with (2.84):

$$\begin{bmatrix} \dot{y}_1 \\ \dot{y}_2 \end{bmatrix} = \frac{d}{dt}(\mathbf{A}X) = \left(\frac{d}{dt}\mathbf{A}\right)X = R\begin{bmatrix} -\theta\dot{\varphi}\sin\varphi + \psi\left(\dot{\varphi}\cos\varphi\cos\theta - \dot{\theta}\sin\varphi\sin\theta\right) \\ \theta\dot{\varphi}\cos\varphi + \psi\left(\dot{\varphi}\sin\varphi\cos\theta + \dot{\theta}\cos\varphi\sin\theta\right) \end{bmatrix}$$

thus yielding ψ:

$$\psi = \frac{\dfrac{\dot{y}_1}{R} + \theta\dot{\varphi}\sin\varphi}{\dot{\varphi}\cos\varphi\cos\theta - \dot{\theta}\sin\varphi\sin\theta} = \frac{\dfrac{\dot{y}_2}{R} - \theta\dot{\varphi}\cos\varphi}{\dot{\varphi}\sin\varphi\cos\theta + \dot{\theta}\cos\varphi\sin\theta}. \tag{2.89}$$

Since we have already shown that y_1 and y_2 are functions of Y and its derivatives, the same holds for ψ.

Finally, by (2.87), we have

$$x_C^d = y_1 - R(\theta\cos\varphi + \psi\sin\varphi\cos\theta)$$
$$y_C^d = y_2 - R(\theta\sin\varphi - \psi\cos\varphi\cos\theta)$$

proving that x_C^d and y_C^d are also functions of Y and its time derivatives. Since $u_1 = \dot{x}_C^d$, $u_2 = \dot{y}_C^d$, $u_3 = \omega_s^d = \dot{\varphi} - \dot{\psi}\sin\theta$, the inputs are also functions of Y and derivatives which achieves the proof. □

Remark 11. *The third component ζ of Y appears quite involved and its physical interpretation is far from obvious. It has been obtained by integration techniques which are not reported here and its expression explicitly contains the input variables which is not usual. A simpler flat output is not known at present. Notice that the flatness property of the driftless system (2.84) with three inputs results also from a theorem of [46].*

Case with eliminated spinning motions

The introduction of the non-pivoting constraint (2.22) (same for Examples 1 and 2) that eliminates spinning motions results a different kinematics. Let us define the matrix $\mathbf{A}'$ as

$$\mathbf{A}' = \begin{bmatrix} & \mathbf{A} & \\ 1 & 0 & -\sin\theta & 0 & 0 \end{bmatrix}$$

The kinematics of this system reads

$$\mathbf{A}' \cdot \dot{X} = 0 \qquad (2.90)$$

where $\mathbf{A}$ and X have been already defined by (2.83). Using a result of [46] the non-flatness of the kinematics (2.90) can be shown.

For completeness, the following theorem of [46] is recalled.

Theorem 1. *Let the codistribution Π be spanned by $n-2$ independent one-forms on a manifold M of dimension n. The associated driftless system is feedback linearizable at every point of an open and dense subset if and only if the derived flag of $\Pi = I^0$ satisfies*

$$\dim I^k = n - 2 - k \qquad k = 0, \quad , n-2$$

The one-forms spanning the codistribution defining the kinematics can be read from the rows of the matrix $\mathbf{A}'$

$$\varpi_1 = \cos\varphi d\theta + \sin\varphi \cos\theta d\psi - dx_C^A$$
$$\varpi_2 = \sin\varphi d\theta - \cos\varphi \cos\theta d\psi - dy_C^A$$
$$\varpi_3 = d\varphi - \sin\theta d\psi,$$

giving the codistribution

$$\Pi = \mathrm{span}\,\{\varpi_1, \varpi_2, \varpi_3\}$$

on a five-dimensional manifold, hence the number of inputs of the associated driftless system is two. Observe that the one-forms ϖ_1, ϖ_2, and ϖ_3 are linearly independent everywhere since $\varpi_1 \wedge \varpi_2 \wedge \varpi_3$ has a constant nonzero component in $dx_C^A \wedge dy_C^A \wedge d\varphi$. This allows to apply Theorem 1.

Proposition 6. *The kinematics defined by Π is not differentially flat.*

Proof. Applying Theorem 1, the necessary and sufficient condition of flatness reads

$$\dim I^1 = 2 \qquad \dim I^2 = 1 \qquad \dim I^3 = 0$$

where I^1, I^2 and I^3 are the codistributions in the derived flag of $\Pi = I^0$. Since ϖ_1, ϖ_2, and ϖ_3 are independent one-forms it is enough to consider their exterior derivatives

$$d\varpi_1 = -\sin\varphi d\varphi \wedge d\theta + \cos\theta \cos\varphi d\varphi \wedge d\psi - \sin\theta \sin\varphi d\theta \wedge d\psi$$
$$d\varpi_2 = \cos\varphi d\varphi \wedge d\theta + \cos\theta \sin\varphi d\varphi \wedge d\psi + \sin\theta \cos\varphi d\theta \wedge d\psi$$
$$d\varpi_3 = -\cos\theta d\theta \wedge d\psi.$$

and observe which ones can be obtained as exterior products having the form $\eta_1 \wedge \eta_2$ with $\eta_1 \in \Lambda^1(M)$, and $\eta_2 \in I^0$ Note that all exterior products having the form $\varpi \wedge \varpi_i$ ($\varpi \in \Lambda^1(M)$, $i = 1, 2$) have a component in $\wedge dx_C^A$ or/and in $\wedge dy_C^A$. Since $d\varpi_i$, $i = 1, 2, 3$ have

component nor in $\wedge\, dx_C^d$, neither in $\wedge\, dy_C^d$, this implies that $d\varpi_3 \neq \varpi \wedge \varpi_\imath$ ($\varpi \in \Lambda^1(M)$, $\imath = 1, 2, \jmath = 1, 2, 3$). It remains to examine the exterior products $\varpi \wedge \varpi_3$. Since

$$(\sin\varphi d\theta - \cos\varphi\cos\theta d\psi) \wedge \varpi_3 = d\varpi_1$$
$$(-\cos\varphi d\theta - \sin\varphi\cos\theta d\psi) \wedge \varpi_3 = d\varpi_2,$$

one gets that $I^1 = \mathrm{span}\,\{\varpi_1, \varpi_2\}$, so $\dim I^1 = 2$.

The preceding discussion has shown that $d\varpi_\imath \neq \varpi \wedge \varpi_\imath$ ($\varpi \in \Lambda^1(M)$, $\imath = 1, 2$). Hence $d\varpi_\imath \neq 0 \bmod I^1$ $\imath = 1, 2$, thus $\dim I^2 = 0 \neq 1$ which shows that the necessary and sufficient condition of Theorem 1 is not satisfied and the proposition follows. $\qquad\square$

2.2.3 Liouvillian kinematics

Let us show that all driftless systems obtained in the examples of Section 2.1.3 which are not flat are indeed Liouvillian.

Proposition 7 *The driftless system*

$$\dot\varphi = \frac{u_1}{R}\sin\varphi\tan\theta - \frac{u_2}{R}\cos\varphi\tan\theta$$
$$\dot\theta = \frac{u_1}{R}\cos\varphi + \frac{u_2}{R}\sin\varphi$$
$$\dot\psi = \frac{u_1\sin\varphi}{R\cos\theta} - \frac{u_2\cos\varphi}{R\cos\theta} \qquad\qquad (2.91)$$
$$\dot x_C^d = u_1$$
$$\dot y_C^d = u_2,$$

(obtained in Example 1 and 2 with the non-pivoting constraint (2.22) included in the model and proven to be not flat by Proposition 6) is Liouvillian with $Y = (\varphi, \theta)$ as partially flat output and x_C^d, y_C^d, ψ as integral variables.

Proof. By the first two equations of (2.91), the inputs u_1 and u_2 can be calculated from the trajectory of Y and $\dot Y$

$$\begin{bmatrix} u_1 \\ u_2 \end{bmatrix} = \frac{1}{\tan\theta}\begin{bmatrix} \sin(\varphi)\tan(\theta) & -\cos(\varphi)\tan(\theta) \\ \cos(\varphi) & \sin(\varphi) \end{bmatrix}\begin{bmatrix} \dot\varphi \\ \dot\theta \end{bmatrix} \qquad\qquad (2.92)$$

Hence, the variables x_C^d, y_C^d and ψ can be obtained from

$$\dot\psi = \frac{u_1\sin\varphi}{R\cos\theta} - \frac{u_2\cos\varphi}{R\cos\theta}$$
$$\dot x_C^d = u_1$$
$$\dot y_C^d = u_2.$$

by simple integrals provided that their initial conditions are known which proves that Y is a partially flat output *and that x_C^d, y_C^d, ψ are integral variables.* The system is thus proven to be Liouvillian. $\qquad\square$

Proposition 8. *The driftless system*

$$\dot{\varphi} = -\frac{u_1}{R} - \frac{u_2}{R}\sin\varphi\tan\theta + \frac{u_3}{R}\cos\varphi\tan\theta$$

$$\dot{\theta} = -\frac{u_2}{R}\cos\varphi - \frac{u_3}{R}\sin\varphi$$

$$\dot{\psi} = -\frac{u_2\sin\varphi}{R\cos\theta} + \frac{u_3\cos\varphi}{R\cos\theta}$$

$$\dot{x}_{C_1}^d = u_1$$

$$\dot{z}_{C_2}^d = u_2$$

$$\dot{z}_{C_3}^d = u_3$$

(obtained in Example 4 as the associated driftless system to (2.45)) is Liouvillian with $Y = (\varphi, \theta, \psi)$ as partially flat output and $x_{C_1}^d$, $z_{C_2}^d$, and $z_{C_3}^d$ as integral variables.

Proof. The inputs are obtained as functions of Y and $\dot{Y}$

$$\begin{bmatrix} u_1 \\ u_2 \\ u_3 \end{bmatrix} = R \begin{bmatrix} -1 & 0 & \sin\theta \\ 0 & -\cos\varphi & \cdot\sin\varphi\cos\theta \\ 0 & -\sin\varphi & \cos\varphi\cos\theta \end{bmatrix} \begin{bmatrix} \dot{\varphi} \\ \dot{\theta} \\ \dot{\psi} \end{bmatrix}$$

and the integral variables are obtained as integrals of the inputs. □

2.2.4 Liouvillian dynamics of hand-object structures with special morphology

Proposition 9. *Consider a HOS such that Conditions 1-3 of Section 2.1.7 hold true with three fingers, five degrees of freedom each. This system is Liouvillian and admits a partially flat output*

$$Y = (p^o, \phi^o, x_{C_1}^o, y_{C_1}^o, y_1, y_2, y_3),$$

position and orientation of the object and coordinates of the contact points on the object boundary, with three combinations of the contact forces: $y_i = g_i(f_1, f_2, f_3)$, $i = 1, 2, 3$. Moreover, q_{i4}, q_{i5}, $i = 1, 2, 3$, the last two joint coordinates of the fingers are integral variables.

Proof. Without loss of generality, we may assume that each fingertip has radius r

Fix the frame K_i^d to the fingertip of the ith finger with its origin at the center of the sphere. Hence the vector p_i^d giving the origin of K_i^d depends on the joint coordinates q_{i1}, ..., q_{i3} and doesn't depend on the last joint coordinates q_{i4} and q_{i5}. Thus the direct geometry (2.9) is given by

$$\begin{aligned} p_i^d &= p_i^d(q_{i1}, q_{i2}, q_{i3}) \\ \Omega(\phi_i^d) &= \Omega(q_{i1}, q_{i2}, q_{i3}, q_{i4}, q_{i5}) \end{aligned} \tag{2.93}$$

Moreover, due to Condition 3, the angular velocity of the finger ω_i^d doesn't depend on q_{i4} and q_{i5} (it depends on q_{i1}, , q_{i3} and $\dot{q}_{i1}$, , $\dot{q}_{i5}$):

$$\omega_i^d = \omega_i^d(q_{i1}, q_{i2}, q_{i3}, \dot{q}_{i1}, \dot{q}_{i2}, \dot{q}_{i3}, \dot{q}_{i4}, \dot{q}_{i5}) \tag{2.94}$$

Thus the geometric constraints of the unique contact point between the object and the ith finger (2.6) and the kinematic condition of rolling without slipping (2.8) can be formulated without the variables q_{i4}, q_{i5}, and $p_{C_i}^{\mathcal{E}}$.

The geometric constraint (2.3) expressed in the inertial reference frame K^b reads

$$p^o - p_i^d + \Omega(\phi^o)p_{C_i}^o - \Omega(\phi_i^d)p_{C_i}^d. \tag{2.95}$$

But, due to Condition 1,

$$\Omega(\phi_i^d)p_{C_i}^d = -r\frac{Dc^o(p_{C_i}^o)^T}{\|Dc^o(p_{C_i}^o)\|},$$

hence (2.95) becomes

$$p_i^d - p^o - \Omega(\phi^o)\left(p_{C_i}^o + r\frac{Dc^o(p_{C_i}^o)^T}{\|Dc^o(p_{C_i}^o)\|}\right) = 0. \tag{2.96}$$

We make use of Equation (2.4).

$$c^o(p_{C_i}^o) = 0. \tag{2.97}$$

Similarly to the vectors w_{1,C_i}^d and w_{2,C_i}^d, let us denote by w_{1,C_i}^o and w_{2,C_i}^o the vectors spanning ker $Dc^o(p_{C_i}^o)$, i.e. the tangent plane to the object at the contact point.

The relative velocity at the contact point between the ith finger and the object is expressed in the basis of K^b:

$$v_{C_i}^r = v_{C_i}^o - v_{C_i}^d = \dot{p}^o + [\omega^o\times]\Omega(\phi^o)p_{C_i}^o - \dot{p}_i^d - [\omega_i^d\times]\left(\Omega(\phi^o)p_{C_i}^o + p^o - p_i^d\right) \tag{2.98}$$

thus the kinematic constraints are given by

$$w_{1,C_i}^T v_{C_i}^r = 0 \qquad w_{2,C_i}^T v_{C_i}^r = 0. \tag{2.99}$$

Let us prove that $z_{C_i}^o$, p_i^d, q_{i1}, q_{i2}, q_{i3}, $\dot{q}_{i4}$, $\dot{q}_{i5}$ can be expressed as functions of $Y, \dot{Y}$.

First, by (2.97) and by the implicit function theorem, one can express $z_{C_i}^o$ as $z_{C_i}^o = Z_{C_i}^o(x_{C_i}^o, y_{C_i}^o)$, $i = 1, 2, 3$. Then, replacing $z_{C_i}^o$ in (2.96), p_i^d can be obtained as function of Y. The first (vectorial) equation of (2.93) can be locally solved for q_{i1}, q_{i2}, q_{i3}, giving these three variables as functions of Y.

Since the kernel of Dc_i^o is a function of Y, the same holds true for w_{1,C_i}^o, w_{2,C_i}^o. Moreover, by Equation (2.94), ω_i^d depends on $Y, \dot{Y}$ and $\dot{q}_{i5}$. Using (2.98), Equation (2.99) reads

$$-W\bar{\Omega}\omega_i^d = W\left(\dot{p}^o + [\omega^o\times]\Omega(\phi^o)p_{C_i}^o - \dot{p}_i^d\right) \tag{2.100}$$

with $W = (w_{1,C_i}^o, w_{2,C_i}^o)^T$ of rank 2. $\bar{\Omega}$ the rank 2 cross product matrix:

$$\bar{\Omega} = [t \times] = \begin{bmatrix} 0 & -t_z & t_y \\ t_z & 0 & -t_x \\ -t_y & t_x & 0 \end{bmatrix} \quad \text{with} \quad t = \begin{bmatrix} t_x \\ t_y \\ t_z \end{bmatrix} = \Omega(\phi^o)p_{C_i}^o + p^o - p_i^d \neq 0.$$

Equation (2.100) can be locally solved for $\dot{q}_{i4}$ and $\dot{q}_{i5}$ since, according to the above decomposition, its Jacobian has rank 2, provided that the Jacobian of the ith finger is of full rank. It results that $\dot{q}_{i4}$ and $\dot{q}_{i5}$ can be expressed as functions of $Y, \dot{Y}$

Let us now prove that the vectors of joint torques τ_i, $i = 1, 2, 3$ can be obtained as functions of $Y, \dot{Y}$ $\ddot{Y}$

By (2.48)-(2.49) and using $y_i = g_i(f_1, f_2, f_3)$, $i = 1, 2, 3$, the vector of contact forces f_1, f_2, f_3 can be computed as functions of $Y, \dot{Y}, \ddot{Y}$ Next, by (2.51) the same holds true for $\tau_{i,ext}$ since J_i and G_i don't depend on $\dot{q}_{i4}$ and $\dot{q}_{i5}$ by Condition 3. Finally, since q_{i4} and q_{i5} are cyclic coordinates (Condition 2), the dynamic equations of the fingers (2.50) allow to calculate τ_i, $i = 1, 2, 3$ as claimed.

We have shown that all the variables but q_{i4}, q_{i5} and $p_{C_i}^d$, ϕ_i^d, $i = 1, 2, 3$, are functions of Y and derivatives. It remains to show that if $\zeta = (q_{i4}, q_{i5})^T$ is chosen as the vector of integral variables, all the remaining system variables are functions of Y, its derivatives and ζ. This is obvious from the second equation of (2.93) and from (2.3) which achieves the proof. □

Remark 12. *It can be verified that the above proposition remains valid if the number of the joints is increased or decreased (the minimal number being three joints per finger) and if the number of fingers is increased. However, decreasing the number of joints will prevent from arbitrarily modifying simultaneously the position and orientation of the object and the position of the contact points on the object boundary.*

2.3 Motion planning

Recall, that for HOSs, the MPP is defined as a steering problem between an initial and a desired final configuration, denoted by q_I and q_F, respectively.

All solutions presented here are based on the fact that one can find a set of variables, denoted by Y and called the flat output (for the differentially flat case) or the partially flat output (for the Liouvillian case), allowing to obtain all or a subset of variables of the model as functions of $Y, \dot{Y}$ $Y^{(r)}$ with r finite integer. (See also Definitions 4 and 5.)

Using the flatness property, the MPP is equivalent to an interpolation problem for the variables Y since all variables of the HOS are functions of $Y, \dot{Y}$, $Y^{(r)}$. For the Liouvillian case, the integral variables cannot be simply (algebraic) functions of $Y, \dot{Y}$, but as integrals of such algebraic functions w.r.t. the time. In both cases, the motion planning algorithms can be divided into the following generic steps:

1. Calculate $Y_I, \dot{Y}_I$, $Y^{(r_I)}$ and $Y_F, \dot{Y}_F$, $Y^{(r_F)}$ using $q_I, \dot{q}_I$ $, q_I^{(r_I)}$ and $q_F, \dot{q}_F$ $, q_F^{(r_F)}$

2. Set the travelling duration T between the initial and final configurations.

3. Make an interpolation for each variable χ in Y such that

$$\chi(0) = \chi_I \qquad\qquad \chi(T) = \chi_F$$
$$\dot{\chi}(0) = \dot{\chi}_I \qquad\qquad \dot{\chi}(T) = \dot{\chi}_F$$

$$\chi^{(r_I)}(0) = \chi_I^{(r_I)} \qquad\qquad \chi^{(r_F)}(T) = \chi_F^{(r_F)}$$

4. Calculate the trajectory of the model variables as functions of Y and its derivatives. Two cases are to be distinguished:

   - flat case: all model variables can be obtained as (algebraic) functions of Y and its derivatives (see Equation (2.73) of Definition 4),
   - Liouvillian case: the trajectory of the integral variables have to be calculated by numerical integration w.r.t. the time of an (algebraic) expression involving Y and its derivatives (see Equation (2.74) of Definition 5).

Remark 13. *In the case of real-time applications, flatness is preferable to solve the MPP, since numerical integration is a heavy task in terms of processing time. This issue is also addressed in Section 3.3 dealing with motion planning in the case of crane control.*

Remark 14. *The integers r_I, r_F are determined by the following considerations:*

1. *By Definitions 4 and 5, the trajectory of Y must be sufficiently smooth in order to obtain continuous trajectories of x and u in Equations (2.73) and (2.75).*

2. *One imposes constraints on the derivatives of Y (e.g. starting and ending at rest points implies that higher order derivatives of Y vanish at $t = 0$ and $t = T$).*

To solve the interpolation problem in Step 3, one can choose a polynomial function for each variable χ in Y

$$\chi(t) = \sum_{j=0}^{\kappa} a_{\chi,j} t^j \qquad\qquad (2.101)$$

where $\kappa = r_I + r_F + 1$. Using polynomial functions, the vector of the coefficients $a_{\chi,j}$ can be obtained as a solution of a linear equation.

Assuming that the derivatives of Y vanish at the initial configuration, the number of coefficients in (2.101) can be decreased:

$$\chi(t) = \chi(0) + (\chi(T) - \chi(0)) \left(\frac{t}{T}\right)^{r_I+1} \sum_{j=0}^{r_F} a_{\chi,j} \left(\frac{t}{T}\right)^j \qquad\qquad (2.102)$$

The coefficients $a_{\chi,j}$ are obtained from the final configuration.

The remaining part of this section is divided into three parts following the classification made in Section 2.2, based on the holonomy, flatness and Liouvillian properties.

We treat first the MPP for planar structures (including Example 5), based on the flatness property of the model including the dynamics. Next, solutions for the MPP are given for the three-dimensional kinematic models obtained in Examples 1, 2, and 4. Finally, the case of three-dimensional hand structures with special morphology is studied (including Example 6) where the solution of the MPP is given again for the model including the dynamics.

2.3.1   Motion planning for planar structures

Proposition 4 asserts that the model of planar HOSs including the dynamics is differentially flat and the position and the orientation of the object are contained in the flat output Y provided that the hand has at least two fingers with at least two joints each. Hence, the polynomial interpolation method given by Equation (2.102) for the variables included in Y can be used. Let us give the solution of the MPP for the two-dimensional HOS presented in Example 5.

Example 7 (continuation of Example 5). First, we show that the kinematic constraints are indeed integrable by Proposition 3. Introduce the following polar coordinates for the contact points (see Figure 2.10):

$$x_{C_i}^d = r_i \cos \zeta_i \qquad x_{C_i}^o = R \cos \xi_i,$$
$$y_{C_i}^d = r_i \sin \zeta_i \qquad y_{C_i}^o = R \sin \xi_i.$$

Then Constraint (2.65) becomes

$$\begin{aligned} q_{i2} + r_i \cos \zeta_i &= x^o + R \cos(\xi_i + \phi^o) \\ q_{i1} + r_i \sin \zeta_i &= y^o + R \sin(\xi_i + \phi^o) \end{aligned} \qquad (2.103)$$

and developing Constraint (2.66) one obtains:

$$\sin(\xi_i + \phi^o - \zeta_i) = 0. \qquad (2.104)$$

Using (2.103)-(2.104) and eliminating ζ_i, $x^o = q_{i2}$, $\dot{x}^o = \dot{q}_{i2}$, $y^o = q_{i1}$, and $\dot{y}^o = \dot{q}_{i1}$ from (2.67) we get, after easy calculations which are omitted

$$\dot{\xi}_i + \frac{r_i}{r_i + R} \dot{\phi}^o = 0.$$

This can be integrated as

$$\xi_i = -\frac{r_i}{r_i + R} \phi^o + \xi_{i0} \quad i = 1, 2$$

where ξ_{i0} is the initial condition for ξ_i. Proposition 4 asserts that this HOS is flat with

$$Y = (x^o, y^o, \phi^o, y_1)$$

as a flat output, y_1 being defined as $y_1 = g_1(f_1, f_2)$ where g_1 is an arbitrary but fixed combination of the contact force components. Here, we choose y_1 as the sum of the squared norm of the net contact forces at the contact points: $y_1 = \|f_1\|^2 + \|f_2\|^2$

If we know the initial mechanical state of the KOS $(x^o(0),\ y^o(0),\ \phi^o(0),\ q_1(0),\ q_2(0))$ and we are given at time T a desired final configuration of the object $(x^o(T),\ y^o(T),\ \phi^o(T))$, since the flat output Y includes the position and the orientation of the object, it is enough to find smooth functions of time connecting $(x^o(0),\ y^o(0),\ \phi^o(0))$ to $(x^o(T),\ y^o(T),\ \phi^o(T))$, and to fix the trajectory of the remaining component of the flat output y_1 in order to deduce the corresponding inputs $\tau_{ij},\ (i, j = 1, 2)$ without integrating the system. We may also wish that the time derivatives of $x^o\ y^o$ and ϕ^o at $t = 0$ and $t = T$ vanish up to a finite order, to start and stop at rest points (i.e. with zero velocities and accelerations). Such functions for the trajectories of the orientation and position of the object can be chosen as polynomials given by Equation (2.102), with $\chi \in \{x^o, y^o, \phi^o\}$. A sample trajectory with zero velocities and accelerations at the initial and final configurations is given in Figure 2.13.
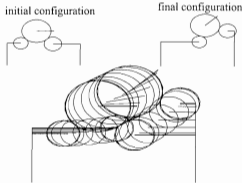

initial configuration   final configuration

Figure 2.13:   Trajectory of the object and the fingers.

Instead of defining an a priori trajectory of y_1 we may wish that the net contact force has minimal norm, to which case the trajectory of y_1 is deduced from the trajectory of the position and orientation of the object as follows: according to (2.60)-(2.61), the components of the contact forces satisfy

$$B \begin{bmatrix} f_1 \\ f_2 \end{bmatrix} \overset{\text{def}}{=} \begin{bmatrix} 1 & 0 & 1 & 0 \\ 0 & 1 & 0 & 1 \\ -y^o_{C_1} & x^o_{C_1} & -y^o_{C_2} & x^o_{C_2} \end{bmatrix} \begin{bmatrix} f_{11} \\ f_{12} \\ f_{21} \\ f_{22} \end{bmatrix} = \begin{bmatrix} m\dot{x}^o \\ m(\ddot{y}^o - g) \\ \Theta\ddot{\phi}^o \end{bmatrix}$$

and therefore the minimum norm of the net contact force is given by

$$y_1 = \left\| B^T (B B^T)^{-1} \begin{bmatrix} m\dot{x}^o \\ m(\ddot{y}^o - g) \\ \Theta\ddot{\phi}^o \end{bmatrix} \right\|.$$

The resulting configurations and net contact force for $\kappa = 4$ is shown in Figure 2.14.   ∎
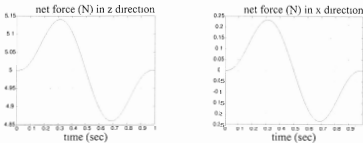
Figure 2.14: The net contact force (x and y components); $m = 0.5$kg

2.3.2   Motion planning for kinematic models (examples of Section 2.1.3)

Table 2.7 summarizes the results of Section 2.2 concerning Examples 1, 2, and 4.

Example	non-pivoting constraint	property	Proposition
1, 2	none	flat	5
1, 2	present	Liouvillian	7
4	none	Liouvillian	8

Table 2.7:   Properties of the examples of Section 2.1.3

The solution of the MPP for the flat case follows the same lines as the one presented in the previous subsection for flat planar structures. We address here the MPP for the Liouvillian cases. Let us consider Examples 1 and 2 first.

Motion planning for Examples 1 and 2 with spinning motions eliminated

Consider the driftless system obtained in Examples 1 and 2 eliminating the spinning motions (i.e. two inputs):

$$\dot{\varphi} = \frac{u_1}{R} \sin \varphi \tan \theta - \frac{u_2}{R} \cos \varphi \tan \theta$$

$$\dot{\theta} = \frac{u_1}{R} \cos \varphi + \frac{u_2}{R} \sin \varphi$$

$$\psi = \frac{u_1 \sin \varphi}{R \cos \theta} - \frac{u_2 \cos \varphi}{R \cos \theta}$$

$$\dot{x}_C^d = u_1$$

$$\dot{y}_C^d = u_2.$$

By Proposition 7, this driftless system is Liouvillian with $Y = \{\varphi, \theta\}$ as partially flat output. Observe that $Y = (\varphi, \theta)$ doesn't contain all orientation angles, hence one cannot determine

freely the trajectory of the orientation of the ball. Nevertheless, the following method may be used to overcome this difficulty.
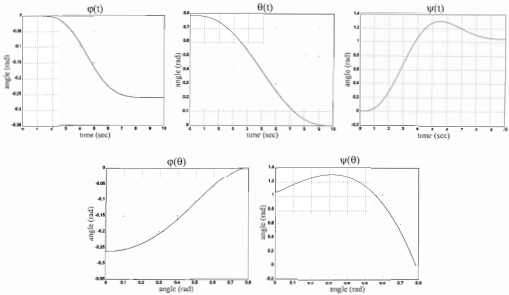

Figure 2.15: The solution of the MPP for the orientation angles.

Choose the trajectory of ψ as a polynomial function of θ:

$$\psi(\theta) = a_0 + a_1\theta + a_2\theta^2 + a_3\theta^3 \tag{2.105}$$

and we wish to obtain the trajectory of φ as a function of the angle θ. Noting that $\dot\varphi = \frac{d\varphi}{d\theta}\dot\theta$ and $\dot\psi = \frac{d\psi}{d\theta}\dot\theta$, the additional non-pivoting constraint (2.22) can be rewritten as

$$\frac{d\varphi}{d\theta} = \sin\theta \frac{d\psi}{d\theta}. \tag{2.106}$$

This expression can be integrated w.r.t. θ (such that $\varphi(\theta_I) = \varphi_I$) in order to obtain the function $\varphi(\theta)$. Reporting (2.105) in (2.106), the integration on the interval $[\theta_I, \theta]$ results

$$\varphi(\theta) = a_1(\cos\theta_I - \cos\theta) + 2a_2(\sin\theta - \sin\theta_I + \theta_I\cos\theta_I - \theta\cos\theta) \\ + 3a_3(\theta_I^2\cos\theta_I - 2\cos\theta_I - 2\theta_I\sin\theta_I - \theta^2\cos\theta + 2\cos\theta + 2\theta\sin\theta) + \varphi_I$$

which is linear w.r.t. the coefficients of the polynomial (2.105). Hence, these coefficients have to satisfy

$$\begin{aligned} \varphi_F &= \varphi(\theta_F) \\ \psi_I &= a_0 + a_1\theta_I + a_2\theta_I^2 + a_3\theta_I^3 \\ \psi_F &= a_0 + a_1\theta_F + a_2\theta_F^2 + a_3\theta_F^3 \end{aligned} \tag{2.107}$$

where φ_I, ψ_I, θ_I (resp. φ_F, ψ_F, θ_F) give the initial (resp. final) orientation of the ball. Since we have one more degree of freedom to chose a constraint, we wish that the second derivative of $\psi(\theta)$ vanish at the final point:

$$0 = a_2 + 3a_3\theta_F. \tag{2.108}$$

This system of equations given by (2.107)-(2.108) is linear in the coefficients of the polynomial (2.105). Once the trajectory of φ and ψ are given in function of θ, it remains to find a trajectory of θ w.r.t. the time, connecting θ_I to θ_F. Such a time function can be obtained using the expression (2.102). The input trajectories u_1 and u_2 are obtained using (2.92) in the proof of Proposition 7.

Remark 15. *The trajectory of the contact point on the plane is given by the integral variables x_C and y_C (see Proposition 7) and can be obtained by integrating the inputs in function of the time. This integration can be carried out numerically. Note also that no desired final position of the contact point is obtained for the motion planning, it is obtained as the result of the numerical integration. Recall that this contrasts significantly with the flat case. In fact, for those systems, the motion planning based of the flatness property allows to precise the desired final configuration for all variables. The proposed motion planning methods for Liouvillian system don't allow to give in advance the final values for some integral variables, they result from numerical integration.*

A sample trajectory is shown in Figure 2.15 connecting $\varphi_I = \frac{\pi}{3}$, $\theta_I = \frac{\pi}{4}$, $\psi_I = 0$ to $\varphi_F = \frac{\pi}{4}$, $\theta_F = 0$, $\psi_F = \frac{\pi}{3}$ in 10 seconds.

Next we present a motion planning algorithm for Example 4 which is proven to be Liouvillian by Proposition 8.

Motion planning for Example 4

Consider the driftless system

$$\dot{\varphi} = -\frac{u_1}{R} - \frac{u_2}{R}\sin\varphi\tan\theta + \frac{u_3}{R}\cos\varphi\tan\theta$$

$$\dot{\theta} = -\frac{u_2}{R}\cos\varphi - \frac{u_3}{R}\sin\varphi$$

$$\dot{w} = -\frac{u_2\sin\varphi}{R\cos\theta} + \frac{u_3\cos\varphi}{R\cos\theta}$$

$$\dot{x}^d_{C_1} = u_1$$

$$\dot{x}^d_{C_2} = u_2$$

$$\dot{x}^d_{C_1} = u_3$$

which is obtained in Example 4 and proven to be Liouvillian by Proposition 8, the partially flat output being $Y = \{\varphi, \theta, \psi\}$. Here all the orientation variables are included in Y. The motion planning is illustrated in the case of a sphere of radius $R = 1$cm.

The trajectory of the orientation of the sphere between its initial and desired final values is obtained using the polynomial interpolation proposed above (see Equation (2.102) and Figure 2.16). The trajectory of the contact points on the tangent planes are obtained by numerical integration and shown in Figure 2.17
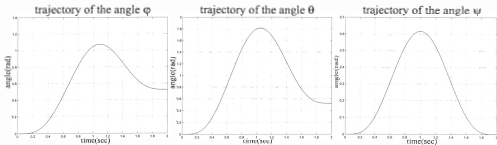
Figure 2.16: Trajectory of the orientation of the sphere (RPY angles: φ, θ, ψ)
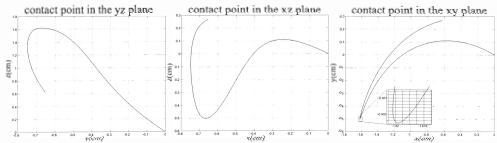
Figure 2.17: Trajectory of the contact points on the tangent planes

Remark 16. *Note that, due to integration, the final values of the $y_{C_1}^O$, $z_{C_1}^O$, $z_{C_2}^O$ cannot be chosen arbitrarily. Since in our case we are not particularly interested in the positions of the contact points in their respective planes this doesn't present a major restriction.*

2.3.3 Motion planning for hand-object structures with special morphology

Proposition 9 asserts that the *dynamic models of symmetric HOSs are Liouvillian*. Nevertheless, the inputs, i.e. the joint torques are functions of the partially flat output Y and their derivatives, hence no numerical integration is needed to obtain their trajectory from the trajectory of the variables in Y.

Example 8 (continuation of Example 6). Introduce the following polar coordinates for the contact points on the object surface:

$$x_{C_1}^O = R\cos\xi_{t,1}\cos\xi_{t,2}$$
$$y_{C_1}^O = R\cos\xi_{t,1}\sin\xi_{t,2} \tag{2.109}$$
$$z_{C_1}^O = R\sin\xi_{t,1}.$$

The dynamic equations of the object and the fingers are given by (2.48)-(2.49) and by (2.50).

This HOS is Liouvillian according to Proposition 9 and, using the polar coordinates of the contact points defined by (2.109), the partially flat output is given by

$$Y = (x^o, y^o, z^o, \varphi, \theta, \psi, y_i, \xi_{i,1}, \xi_{i,2})$$

with $i = 1, 2, 3$ and $y_i = g_i(f_1, f_2, f_3)$ where g_i are arbitrary but fixed combinations of the contact forces. Here, we choose $y_i = \|f_i\|^2$. The integral variables are q_{i4} and q_{i5}, $i = 1, 2, 3$.

Suppose, as in Example 7, that the initial mechanical state of the system is given at $t = 0$ by $(x^o(0), y^o(0), z^o(0), \varphi(0), \theta(0), \psi(0), \xi_{i,1}(0), \xi_{i,2}(0), q_i(0))$, $i = 1, 2, 3$, and that we are given at time $t = T$ a desired final position and orientation of the object $(x^o(T), y^o(T), z^o(T), \varphi(T), \theta(T), \psi(T))$ and final position of the contact points, $(\xi_{i,1}(T), \xi_{i,2}(T))$ on the object boundary.

Then, due to Proposition 9, the motion planning is reduced to an interpolation problem for the components of Y using polynomials given by (2.102) with the same number of initial and final conditions on each component of Y
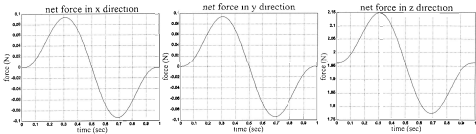
Figure 2.18: Components of the net force applied on the object by the fingers.

Once again, as in the Example 7, the trajectories of y_1, y_2, y_3 are not defined a priori, but determined such that the sum of the squared norms of the contact forces $\sum_{i=1}^{3} y_i$ be minimal: according to (2.48)-(2.49) the contact force components satisfy

$$B \begin{bmatrix} f_1 \\ f_2 \\ f_3 \end{bmatrix} \stackrel{\text{def}}{=} \begin{bmatrix} 1 & 0 & 0 & 1 & 0 & 0 & 1 & 0 & 0 \\ 0 & 1 & 0 & 0 & 1 & 0 & 0 & 1 & 0 \\ 0 & 0 & 1 & 0 & 0 & 1 & 0 & 0 & 1 \\ 0 & -z^o_{C_1} & y^o_{C_1} & 0 & -z^o_{C_2} & y^o_{C_2} & 0 & -z^o_{C_3} & y^o_{C_3} \\ z^o_{C_1} & 0 & -x^o_{C_1} & z^o_{C_2} & 0 & -x^o_{C_2} & z^o_{C_3} & 0 & -x^o_{C_3} \\ -y^o_{C_1} & x^o_{C_1} & 0 & -y^o_{C_2} & x^o_{C_2} & 0 & -y^o_{C_3} & x^o_{C_3} & 0 \end{bmatrix} \begin{bmatrix} f_1 \\ f_2 \\ f_3 \end{bmatrix} = \begin{bmatrix} m\ddot{x}^o \\ m\ddot{y}^o \\ m(\ddot{z}^o + g) \\ \Theta\dot{\omega}^o + [\omega^o \times]\Theta\omega^o \end{bmatrix}$$

thus $\sum_{i=1}^{3} y_i$ is minimal with the contact forces obtained by

$$
\begin{bmatrix} f_1 \\ f_2 \\ f_3 \end{bmatrix} = B^T (BB^T)^{-1} \begin{bmatrix} m\ddot{x}^o \\ m\ddot{y}^o \\ m(\ddot{z}^o + g) \\ \Theta\dot{\omega}^o + [\omega^o \times]\Theta\omega^o \end{bmatrix}
$$
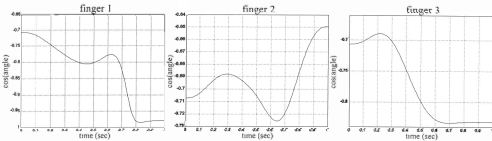
Figure 2.19: Cosine of angles between the contact forces and the surface normals.

An example trajectory is presented for the following numerical parameters: $m = 0.2$kg, $R = 0.1$m, $r = 0.02$m, $d_{x2} = 0.3$m. $d_{x3} = 0$m, $d_{y2} = 0$m, $d_{y3} = 0.3$m, $d_{z2} = 0$m, $d_{z3} = 0$m and $g = 9.81 \frac{m}{s^2}$. The trajectory connects the initial point $x^o(0) = 0.1$m. $y^o(0) = 0.1$m, $z^o(0) = 0.1$m, $\varphi(0) = 0$, $\theta(0) = 0$, $\psi(0) = 0$, $\xi_{11}(0) = \frac{7\pi}{6}$, $\xi_{12}(0) = -\frac{\pi}{4}$, $\xi_{21}(0) = \frac{11\pi}{6}$, $\xi_{22}(0) = -\frac{\pi}{4}$, $\xi_{31}(0) = \frac{\pi}{2}$, $\xi_{32}(0) = -\frac{\pi}{4}$ to a final point $x^o(T) = 0.15$m, $y^o(T) = 0.15$m, $z^o(T) = 0.2$m, $\varphi(T) = \frac{\pi}{8}$, $\theta(T) = \frac{\pi}{8}$, $\psi(T) = -\frac{\pi}{8}$, $\xi_{11}(T) = \frac{7\pi}{6}$, $\xi_{12}(T) = -\frac{\pi}{2}$, $\xi_{21}(T) = \frac{11\pi}{6}$, $\xi_{22}(T) = -\frac{\pi}{4}$, $\xi_{31}(T) = \frac{\pi}{2}$, $\xi_{32}(T) = -\frac{\pi}{4}$ such that $T = 1$s. The components of the net contact force are given in Figure 2.18.

The cosine of the angles between normal vectors to the object surface at the contact points and the contact forces applied by the fingers is given in Figure 2.19 showing that (2.52) is satisfied along the trajectory. Note that the minimality of $\sum_{i=1}^{3} y_i$ does not guarantee that the inequality constraints of Subsection 2.1.5 are satisfied. ∎

Chapter 3

Crane control

Many different types of weight handling equipment (WHE), and in particular cranes, are used in various industries including construction and naval transport [64]. From a mechanical point of view, cranes are typical examples of underactuated mechanical systems [15, 16, 51], since the number of actuators is less than the number configuration variables needed to describe the mechanical state of the system. For many WHEs, the payload is hoisted by a rope, hence an inherent pendulum-like oscillatory behaviour makes difficult the precise and fast positioning task. Such swinging motions, which are poorly damped in general, may be created by the crane operator himself when he moves the load or by external disturbances like winds and waves. Note that the time necessary to wait the end of oscillations of the load during weight handling operations using harbor cranes represents 30%-50% of the total time of operations depending on the experience of the crane operator and the weather conditions [57].

In all cases, the operator acts indirectly on the motion of the load and uses visual feedback in order to eliminate undesired oscillations. The difficulty of the operator's task is redoubled by the eventual presence of obstacles and personnel in the crane's workspace since the path of the load has to avoid them for obvious security reasons. Therefore, the aim of WHE control is to increase productivity and operational security by assisting the human crane operator.

Various techniques have been proposed to provide such assistance, the main objective being to attenuate undesired swinging of the load [23, 27, 50]. The industrial interest to this problem is attested by several patents (e.g. [57]). In papers [8, 26, 59, 66], linear methods are used including adaptive, robust or LQ techniques. Some authors use energetic methods based on the analogy with other mechanical systems. In particular, the model of an overhead (or gantry) crane is equivalent to that of a cart with a pendulum if one fixes the length of the rope attached to the load and considers it as a rod [14]. Another method starts from the analogy with the ball and beam example and uses passivity based techniques [66].

In this chapter we address the anti-sway problem as a special case of the general tracking problem. In fact, the elimination of swinging motions is equivalent to the stabilization of a special trajectory consisting of an equilibrium of the system. A more general problem would be the stabilization of any desired trajectory of the load connecting two different equilibria. This implies that a motion planning task has to be solved before addressing the closed loop tracking problem itself.

An additional objective of this chapter is to cover as many different WHEs as possible by

the analysis, allowing different geometries and including cantilever and overhead cranes besides the US Navy crane example. The small size model[1] of this last crane is at our disposal at the Centre Automatique et Systèmes (see Figure 3.1). The motivation of the generalization is that
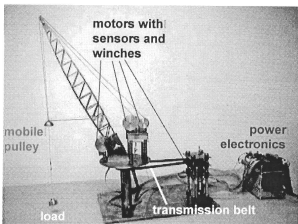

Figure 3.1. Reduced size model of the US Navy crane

a large class of WHEs have the same structural properties, namely, they can be decomposed into a fully actuated, articulated mechanical structure with in general one or two degrees of freedom (e.g. a crane with a rotate platform or a gantry crane with a moving bridge), and a hoisting system comprising ropes, winches, and pulleys.

Our goal is to give a systematic way to obtain dynamic models of a class of WHEs and to show how to find trajectories connecting two equilibria of the load exploiting the flatness property [19, 20, 22] of the dynamic model.

To this aim, the derived model of the class of WHEs involves Lagrange multipliers associated to geometric constraints on the generalized coordinates. This contrasts with choosing a minimal number of coordinates and eliminating the constraints.

The form of the deduced model shows that each member of the class is differentially flat and the coordinates of the load constitute all or part of the components of a flat output, depending on the number of motors. Thus the solution of the MPP becomes an interpolation problem using sufficiently smooth functions (e.g. polynomials).

The aim in closed loop is to stabilize asymptotically a desired equilibrium or a trajectory of the load using only partial information. This means that measurements on all configuration variables are not available. In particular, the load position and the angles between the ropes are not measured. We show that all equilibria of each WHE example presented in this chapter (3D cantilever, overhead, and US Navy cranes) can be globally stabilized using proportional-derivative type output feedback controllers. If, in the same proportional-derivative controller,

instead of the constant reference of the measured components of the end point, we use (time-varying) reference trajectories of the measured variables ending at an equilibrium, we prove the local stability of the system. In fact, simulations show that putting together motion planning and tracking results in more predictable transients (i.e. close to the desired reference trajectory) and in reduced oscillations at the final equilibrium.

The remaining part of the chapter starts with the study of the small size model of the US Navy crane (2D and 3D versions). Section 3.2 introduces a general method of WHE modelling which can be applied to a large class of systems. Three examples of this class are treated in details: the 3D cantilever, the 3D overhead, and the 3D US Navy cranes. It is also shown that all WHEs of the class are differentially flat.

Motion planning is addressed in Section 3.3 including the problem of obstacle avoidance and actuator dimensioning, the latter being an interesting application of motion planning aiming to find suitable actuators supporting fast displacements.

The last two sections of the chapter address the closed loop control of WHEs. The global stabilization of load equilibria is treated first for the different models of the US Navy crane and for the other examples (overhead and cantilever cranes). The last section studies the case where the PD controller uses time-varying feasible reference trajectories connecting load equilibria. These references are obtained using the motion planning method presented in Section 3.3.

Parts of this chapter have been published in [36, 38, 35].

3.1 Small size model of the US Navy crane

The model of the planar US Navy crane, described in [43, 42], is recalled first. This model is then extended to the case where the mass of the free (or mobile) pulley (see Figure 3.1) cannot be neglected w.r.t. the mass of the transported load. This is the case when the crane moves without load for example.

The three-dimensional model is presented next for the case with neglected and nonzero free pulley mass. The flatness property of each model is proven.

3.1.1 Crane in the plane

Let us start with the description of the crane in the plane, illustrated in Figure 3.2. The setup comprises:

- A boom making a fixed angle α w.r.t. the vertical, equipped with three winches: one located at the point P, a second one at the point A, at a fixed distance l from P and a third one at the point S, at fixed distance s from P

- A free pulley located at the point B.

- A vertical rope of variable length R, starting from P whose upper part makes an angle β with the boom, passing through the free pulley. The lower part of the rope connecting the points B and C makes an angle θ with the vertical. The length of the upper part
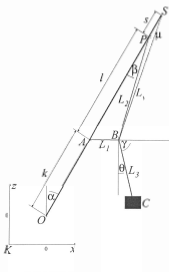
Figure 3.2: Planar version of the crane

connecting the points B and P is denoted by L_2 and the one of the lower part by L_3. Denoting the total length of the rope by R, we have $R = L_2 + L_3$.

- A horizontal rope of variable length L_4 relating the winch A to the pulley B.

- A suspension rope for the free pulley of variable length L_s, starting from S, ending at B.

- A load with mass m attached to the vertical rope at the point C, located at a distance L_3 from the free pulley B.

The winches at points P, A and S have radii ρ_1, ρ_2, and ρ_3, respectively, and they are torque controlled using electric motors with incremental encoders on their axes.

Note that for the real crane, the hoisting winches are not located at the points P, A and S. only pulleys are fixed to the boom at those points. However, since the rope lengths between these pulleys and the hoisting winches are constant, the pulleys at the points P A, and S can be considered directly as actuated winches winding up the corresponding ropes. When calculating the rotating inertia along a rope, the inertia of the winch is summed up with the inertia of the intermediate pulley(s).

All cables are supposed to be rigid (i.e. without elasticity). The plane of the boom and the ropes coincides with the xz-plane of the reference frame whose origin is at the point O (see Figure 3.2). The coordinates of the load at the point C are given by $(x, z)^T$ The coordinates of the free pulley at the point B are given by $(x_B, z_B)^T$

The inertial parameters are summarized in Table 3.1

notation	definition
m	mass of the load
m_0	mass of the free pulley
J_1	inertia of the winch at the point A
J_2	inertia of the winch at the point P
J_3	inertia of the winch at the point S

Table 3.1: Inertia parameters

The rope tensions are illustrated in Figure 3.3. The direction of the tension vectors t_1, t_2, t_3, t_s in the corresponding ropes are given by the geometry, thus the tensions in the ropes can be represented by the scalar variables T_1, T_2, T_3 and T_s. The sign conventions agree with that of Figure 3.3. Because of the neglected elasticity of the ropes we have

$$T_2 = T_3.$$

Two cases are distinguished: $m_0 = 0$ and $m_0 > 0$.

Neglected free pulley mass ($m_0 = 0$)

This case is also treated in [42, 43] and repeated here for completeness, since planar results and calculations are also used in order to prove the flatness of the three-dimensional models. The model is obtained by supposing $m_0 = 0$ (i.e. no dynamics associated to the free pulley) and suppressing the winch at the point S together with the corresponding rope and rope tension ($t_s = 0$).

The geometric relations read:

$$\begin{bmatrix} x_A \\ z_A \end{bmatrix} = \begin{bmatrix} k \sin \alpha \\ k \cos \alpha \end{bmatrix} \tag{3.1a}$$

$$\begin{bmatrix} x_P \\ z_P \end{bmatrix} = \begin{bmatrix} (k+l) \sin \alpha \\ (k+l) \cos \alpha \end{bmatrix} \tag{3.1b}$$

$$\begin{bmatrix} x_B \\ z_B \end{bmatrix} = \begin{bmatrix} (k+l) \sin \alpha - L_2 \sin(\alpha - \beta) \\ (k+l) \cos \alpha - L_2 \cos(\alpha - \beta) \end{bmatrix} \tag{3.1c}$$

$$\begin{bmatrix} x - x_B \\ z - z_B \end{bmatrix} = \begin{bmatrix} L_3 \sin \theta \\ -L_3 \cos \theta \end{bmatrix} \tag{3.1d}$$

$$\begin{bmatrix} x_B - k \sin \alpha \\ z_B - k \cos \alpha \end{bmatrix} = \begin{bmatrix} L_1 \sin(\theta + \gamma) \\ -L_1 \cos(\theta + \gamma) \end{bmatrix} \tag{3.1e}$$

The equilibrium of forces (tensions) at the free pulley (at the point B, see Figure 3.3) reads

$$t_1 + t_2 - t_3 = 0$$
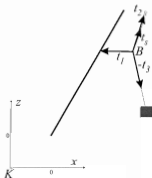
Figure 3.3: Rope tensions (at the free pulley)

or

$$0 = -T_1 \sin(\gamma + \theta) + T_3(\sin(\alpha - \beta) + \sin\theta)$$
$$0 = T_1 \cos(\gamma + \theta) + T_3(\cos(\alpha - \beta) - \cos\theta). \tag{3.2}$$

The dynamics of the load is given by

$$m \begin{bmatrix} \ddot{x} \\ \ddot{z} \end{bmatrix} = T_3 \begin{bmatrix} -\sin\theta \\ \cos\theta \end{bmatrix} - m \begin{bmatrix} 0 \\ g \end{bmatrix} \tag{3.3}$$

and those of the winches (see Figure 3.4) read

$$\frac{J_1}{\rho_1}\ddot{L}_1 = T_1\rho_1 + \eta_1(L_1, \dot{L}_1) - u_1 \tag{3.4}$$

$$\frac{J_2}{\rho_2}(\ddot{L}_2 + \ddot{L}_3) = T_3\rho_2 + \eta_2(L_2 + L_3, \dot{L}_2 + \dot{L}_3) - u_2 \tag{3.5}$$

where u_1 (resp. u_2) is the torque developed by the motor driving the winch at the point A (resp. P). The functions η_i give the friction torques. The proof of the flatness property relies on the following proposition.

Proposition 10. *The following properties hold true for the two-dimensional model of the crane:*

(ı) *The vectors $(x - x_B, z - z_B)^T$ and $(\ddot{x}, \ddot{z} + g)^T$ are parallel:*

$$\frac{x - x_B}{z - z_B} = \frac{\ddot{x}}{\ddot{z} + g}. \tag{3.6}$$

(ıı) *The section $\overline{AB}$ is the bisector of the angle $\widehat{CBP}$:*

$$\gamma = \frac{1}{2}(\pi + \beta - (\alpha + \theta)). \tag{3.7}$$
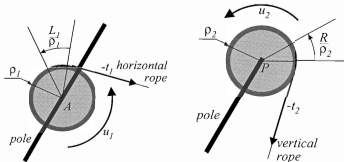
Figure 3.4: Torques at the winches

Proof. For part (i). Equation (3.3) gives

$$\frac{m}{T_3}\begin{bmatrix} \ddot{x} \\ \ddot{z}+g \end{bmatrix} = \begin{bmatrix} -\sin\theta \\ \cos\theta \end{bmatrix}$$

showing that the vector $(\ddot{x}, \ddot{z}+g)^T$ is parallel with the vector $(-\sin\theta, \cos\theta)^T$. On the other hand, from the geometry we have

$$-\frac{1}{L_3}\begin{bmatrix} x - x_B \\ z - z_B \end{bmatrix} = \begin{bmatrix} -\sin\theta \\ \cos\theta \end{bmatrix}$$

i.e. the vector $(x - x_B, z - z_B)^T$ is also parallel to $(-\sin\theta, \cos\theta)^T$. This proves (i).

To prove part (ii), consider Equation (3.2). Multiplying the first equation by $\cos(\gamma + \theta)$, the second one by $\sin(\gamma + \theta)$ and summing them up, one gets

$$\sin(\gamma + \theta + \alpha - \beta) = \sin(\pi - \gamma),$$

giving (3.7) by isolating γ. □

Proposition 11. *The planar crane model given by Equations (3.1)-(3.5) is differentially flat with (x, z) as a possible choice of the flat output.*

Proof. The proof consists of giving the calculations necessary to obtain the trajectory of all variables as functions of $x, \dot{x}, \ddot{x}, x^{(3)}, x^{(4)}$ and $z, \dot{z}, \ddot{z}, z^{(3)}, z^{(4)}$. First, we have from (3.3) that

$$\tan\theta = -\frac{\ddot{x}}{\ddot{z}+g}, \qquad T_3 = m((\ddot{z}+g)\cos\theta - \ddot{x}\sin\theta). \tag{3.8}$$

Let the point D be the intersection between the boom (section $\overline{OP}$) and the line connecting the points C and B (see Figure 3.5). We have

$$\frac{x + (d - k - l)\sin\alpha}{z + (d - k - l)\cos\alpha} = \frac{\dot{x}}{\ddot{z}+g}$$
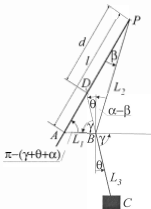
Figure 3.5: Geometry of the planar crane

which allows to express the distance d (see also Figure 3.5):

$$d = \frac{\ddot{x}(z - (k + l)\cos\alpha) - (\ddot{z} + g)(x - (k + l)\sin\alpha)}{(\ddot{z} + g)\sin\alpha - \ddot{x}\cos\alpha}. \tag{3.9}$$

Elementary geometric relations in the triangles PAB, PDB and DAB give

$$\frac{\sin\beta}{L_1} = \frac{\sin\gamma}{l} = \frac{\sin(\gamma - \beta)}{L_2} \tag{3.10a}$$

$$\frac{\sin\beta}{\parallel DB \parallel} = \frac{\sin 2\gamma}{d} = \frac{\sin(\alpha + \theta)}{L_2} \tag{3.10b}$$

$$\frac{\sin(\alpha + \theta)}{L_1} = \frac{\sin\gamma}{l - d} = \frac{\sin(\gamma - \beta)}{\parallel DB \parallel}. \tag{3.10c}$$

Isolating L_1 from the first and the last equations and equating the results we get

$$L_1 = l\frac{\sin\beta}{\sin\gamma} = (l + d)\frac{\sin(\alpha + \theta)}{\sin\gamma}$$

hence, provided that $\sin\gamma \neq 0$, we can express $\sin\beta$:

$$\sin\beta = \left(1 - \frac{d}{l}\right)\sin(\alpha + \theta)$$

allowing to calculate β in the interval $(0, \alpha)$ as function of θ and d which have been already expressed as functions of $x, \dot{x}, \ddot{x}, z, \dot{z}, \ddot{z}$. The angle γ is obtained from (3.7). Using Equation (3.10c) we get

$$\parallel DB \parallel = d\frac{\sin\beta}{\sin(\alpha + \theta - \beta)}$$

and the rope lengths L_1 and L_2 result from (3.10a), allowing to calculate the position (x_B, z_B) of the free pulley using (3.1c). The length L_3 is given by

$$L_3^2 = (x - x_B)^2 + (z - z_B)^2$$

and note that $L_3 > 0$. Then, from the equilibria of the rope tensions at the pulley (Equation (3.2)), the tension of the horizontal rope attached to the free pulley is

$$T_1 = 2T_3 \cos \gamma, \tag{3.11}$$

hence the motor torques u_1 and u_2 are obtained from the dynamics of the winches (Equations (3.4)-(3.5)). Since we have shown that all variables of the crane model are functions of x, z, and their successive time derivatives, the proposition follows. □

Remark 17 *Note that the geometric variables and the rope tensions are functions of x, z and derivatives up to the second order, and the expressions allowing to obtain the trajectory of the geometric variables don't depend on the inertial parameters (given in Table 3.1). However, one needs derivatives of x and z up to order four to obtain the motor torques u_1 and u_2.*

Nonzero free pulley's mass ($m_0 > 0$)

The free pulley mass is no more neglected and the winch at the point S is added to the model studied in the preceding paragraph. The additional geometric constraints read (see Figure 3.3):

$$\begin{bmatrix} x_S \\ z_S \end{bmatrix} = \begin{bmatrix} (k + l + s) \sin \alpha \\ (k + l + s) \cos \alpha \end{bmatrix} \tag{3.12a}$$

$$\begin{bmatrix} x_B \\ z_B \end{bmatrix} = \begin{bmatrix} (k + l + s) \sin \alpha - L_s \sin(\alpha - \mu) \\ (k + l + s) \cos \alpha - L_s \cos(\alpha - \mu) \end{bmatrix} \tag{3.12b}$$

where μ is the angle between the boom and the rope sustaining the free pulley at the point B. The dynamics of the free pulley is given by

$$m_0 \ddot{x}_B = -T_1 \sin(\gamma + \theta) + T_3 \sin(\alpha - \beta) + \sin \theta) + T_s \sin(\alpha - \mu)$$
$$m_0 (\ddot{z}_B + g) = T_1 \cos(\gamma + \theta) + T_3 (\cos(\alpha - \beta) - \cos \theta) + T_s \cos(\alpha - \mu) \tag{3.13}$$

where the relation $T_2 = T_3$ is already used. The dynamics of the additional winch at the point S reads

$$\frac{J_s}{\rho_3} \ddot{L}_s = T_s \rho_3 + \eta_3(\dot{L}_s) - u_3. \tag{3.14}$$

Note that the main difference w.r.t. *model of the* preceding paragraph is the loss of the bisector property of Proposition 10. Moreover, the number of inputs is increased by one, the new input u_3 being the torque of the motor hoising the suspension rope of the free pulley. Nevertheless, is it easy to prove that the flatness property is conserved.

Proposition 12. *The planar crane model given by Equations (3.1)-(3.5) and (3.12)-(3.14) is differentially flat with (x, z, L_3) as a choice of the flat output.*

Proof. We proceed as in the proof of Proposition 11. First, θ and T_3 are expressed by Equation (3.8). The coordinates of the pulley are calculated as

$$\begin{bmatrix} x_B \\ z_B \end{bmatrix} = \begin{bmatrix} x \\ z \end{bmatrix} + \frac{mL_3}{T_3} \begin{bmatrix} -\sin\theta \\ \cos\theta \end{bmatrix}$$

showing that x_B and z_B are functions of x, z, L_3, T_3, and θ, the last two variables being functions of x, z, $\ddot{x}$, and $\ddot{z}$. The rope lengths L_1, L_2, and L_s are obtained by expressing the distances between the free pulley and the corresponding winches. Knowing the side lengths of the triangles ABP and ABS, the corresponding angles γ, β and μ can be calculated.

Noting again that $T_2 = T_3$, the remaining rope tensions (T_1 and T_s) are expressed using (3.13):

$$\begin{bmatrix} T_s \\ T_1 \end{bmatrix} = \begin{bmatrix} \sin(\alpha - \mu) & -\sin(\gamma + \theta) \\ \cos(\alpha - \mu) & \cos(\gamma + \theta) \end{bmatrix}^{-1} \begin{bmatrix} m_0\ddot{x}_B - T_3\sin(\alpha - \beta) + \sin\theta \\ m_0(\ddot{z}_B + g) - T_3(\cos(\alpha - \beta) - \cos\theta) \end{bmatrix}$$

The motor torques are obtained, as before, using the dynamic equations (3.4)-(3.5) and (3.14) of the winches. □

Remark 18. *Note that for the model with nonzero free pulley mass, one needs derivatives up to the fourth order of the trajectory of the load to obtain the rope tensions. This contrasts to the case $m_0 = 0$ (see Remark 17) where the expression of the rope tensions involved only second order time derivatives of the flat output.*

Remark 19. *One may consider the bisector law as a "natural" way to give the trajectory of the free pulley during the motion. We can use the additional degree of freedom corresponding to the third component of the flat output to make the bisector property (3.7) respected. For, we choose*

$$y_3 = \pi + \beta - (\alpha + \theta) - 2\gamma$$

as the third flat output instead of L_3 and set it identically to zero.

Remark 20. *The state equations are not given explicitly, although they can be calculated by eliminating the geometric constraints. The state-space thus obtained is six-dimensional (three degrees of freedom) if the free pulley mass is neglected and eight-dimensional (four degrees of freedom) if $m_0 > 0$.*
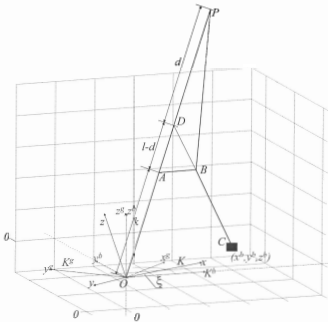
Figure 3.6: Crane in three dimensions

3.1.2 Crane in three dimensions

The 3D setup of the US Navy crane is depicted in Figure 3.6.

In three dimensions, additional variables are needed to describe the mechanical state of the crane. The origin of the inertial reference frame, denoted by K^b, is fixed again at O and its z-axis coincides with the vertical rotation axis of the crane. We introduce two additional frames, all having the origin at the point O:

1. The frame K is chosen such that the points P, A, and B determine its xz-plane. Note that the point C (i.e. the load) remains also in this plane if the free pulley (at the point B) has no mass.

2. The frame K^g is chosen such that the z_b-axis of the frame K^b and the point P determine its $x^g z^g$-plane.

The transformation between these frames (also illustrated in Figure 3.6) can be obtained by elementary rotations. We denote by ξ the rotation angle around the z^b axis of the frame K^b that transforms K^b to K^g. The rotation angle around the $\overline{OP}$ axis allowing to transform K^g to K is denoted by φ.

The corresponding transformation matrices read

$$\Omega_{K^b K^g}(\xi) = \begin{bmatrix} \cos\xi & -\sin\xi & 0 \\ \sin\xi & \cos\xi & 0 \\ 0 & 0 & 1 \end{bmatrix} \tag{3.15}$$

$$\Omega_{K^g K}(\varphi) = \begin{bmatrix} \sin^2\alpha(1-\cos\varphi)+\cos\varphi & -\cos\alpha\sin\varphi & \sin\alpha\cos\alpha(1-\cos\varphi) \\ \cos\alpha\sin\varphi & \cos\varphi & -\sin\alpha\sin\varphi \\ \sin\alpha\cos\alpha(1-\cos\varphi) & \sin\alpha\sin\varphi & \cos^2\alpha(1-\cos\varphi)+\cos\varphi \end{bmatrix} \tag{3.16}$$

such that the coordinate transformation between the frames K and K^b is given by

$$\Omega_{K^b K} = \Omega_{K^b K^g} \cdot \Omega_{K^g K}.$$

The additional inertial parameter is the rotational inertia of the platform which is denoted by M The cases with $m_0 = 0$ and $m_0 > 0$ are considered again separately.

Neglected free pulley mass ($m_0 = 0$)

Recall that the load remains in the plane determined by the points P A and B. The dynamics of the load are given by

$$m \begin{bmatrix} \ddot{x}^b \\ \ddot{y}^b \\ \ddot{z}^b + g \end{bmatrix} = \Omega_{K^b K^g} \cdot \Omega_{K^g K} \begin{bmatrix} -T_3\sin\theta \\ 0 \\ T_3\cos\theta \end{bmatrix} \tag{3.17}$$

such that θ gives the angle between the rope section $\overline{BC}$ and the z-axis of the frame K (this angle is also given in Figure 3.2. The force equilibrium at the free pulley reads

$$t_1 + t_2 - t_3 = 0 \tag{3.18}$$

and we have again $T_2 = T_3$. The dynamic equations of the winches at the points A and P are already given by Equations (3.4) and (3.5).

To obtain the dynamics of rotation of the platform, recall that the rope tensions generate torques rotating the platform. Hence the corresponding dynamic equation reads

$$J_{pf}\ddot{\xi} = proj_{z^b}\left(\overrightarrow{PO} \times (-t_2) + \overrightarrow{PA} \times (-t_1)\right) - \eta_4(\xi,\dot{\xi}) + u_4 \tag{3.19}$$

where $\times$ is the usual cross product in $\mathbb{R}^3$ and the operator $proj_{z^b}(.)$ gives the projection of a vector to the z^b axis of the frame K^b The function η_4 gives the friction torques.

The geometric constraints are expressed using the transformations (3.15)-(3.16):

$$\begin{bmatrix} x_B^b \\ y_B^b \\ z_B^b \end{bmatrix} = \Omega_{K^b K^g} \cdot \Omega_{K^g K} \begin{bmatrix} (k+l)\sin\alpha - L_2\sin(\alpha-\beta) \\ 0 \\ (k+l)\cos\alpha - L_2\cos(\alpha-\beta) \end{bmatrix} \tag{3.20a}$$

$$\begin{bmatrix} x^b - x_B^b \\ y^b - y_B^b \\ z^b - z_B^b \end{bmatrix} = \Omega_{K^b K^g} \cdot \Omega_{K^g K} \begin{bmatrix} L_3\sin\theta \\ 0 \\ -L_3\cos\theta \end{bmatrix} \tag{3.20b}$$

$$\begin{bmatrix} x_B^b - k\sin\alpha \\ y_B^b \\ z_B^b - k\cos\alpha \end{bmatrix} = \Omega_{K^b K^g} \cdot \Omega_{K^g K} \begin{bmatrix} L_1\sin(\theta+\gamma) \\ 0 \\ L_1\cos(\theta+\gamma) \end{bmatrix} \tag{3.20c}$$

Note that setting ξ and φ to zero we have $\Omega_{K^b K^g} \cdot \Omega_{K^g K} = I$ and one gets back the geometric constraints obtained for the planar case.

Proposition 13. *The following two properties are verified.*

(i) *The vectors* $(x^b - x_B^b, y^b - y_B^b, z^b - z_B^b)^T$ *and* $(\bar{x}^b, \bar{y}^b, \bar{z}^b + g)^T$ *are parallel, i.e.*

$$\frac{x^b - x_B^b}{z^b - z_B^b} = \frac{\bar{x}^b}{\bar{z}^b + g} \qquad \frac{y^b - y_B^b}{z^b - z_B^b} = \frac{\bar{y}^b}{\bar{z}^b + g}.$$

(ii) $\overline{AB}$ *bisects the angle* $\widehat{CBP}$:

$$\gamma = \frac{1}{2}\left(\pi + \beta - (\alpha+\theta)\right) \tag{3.21}$$

Proof. Rearranging (3.17) and (3.20b) one gets

$$\begin{bmatrix} \bar{x}^b \\ \bar{y}^b \\ \bar{z}^b + g \end{bmatrix} = \frac{T_3}{m} \Omega_{K^b K^g} \cdot \Omega_{K^g K} \begin{bmatrix} -\sin\theta \\ 0 \\ \cos\theta \end{bmatrix} = \frac{T_3}{m} \cdot v$$

$$\begin{bmatrix} x^b - x_B^b \\ y^b - y_B^b \\ z^b - z_B^b \end{bmatrix} = -L_3 \cdot \Omega_{K^b K^g} \cdot \Omega_{K^g K} \begin{bmatrix} -\sin\theta \\ 0 \\ \cos\theta \end{bmatrix} = -L_3 \cdot v.$$

These equations show that the vectors $(x^b - x_B^b, y^b - y_B^b, z^b - z_B^b)^T$ and $(\bar{x}^b, \bar{y}^b, \bar{z}^b + g)^T$ are both parallel to the vector v, hence (i) follows. To verify (ii), it is enough to note that transforming (3.18) in the frame K gives Equation (3.2), thus the property follows from the second part of Proposition 10. $\square$

Proposition 14. *The three-dimensional model of the crane given by the Equations (3.17), (3.18), (3.20), (3.4), (3.5), and (3.19) is differentially flat, a possible choice of the flat output is* (x^b, y^b, z^b)

Proof. In view of the proof of Proposition 11, it is enough to show that the angles ξ and φ are functions of (x^b, y^b, z^b) and their time derivatives. In fact, if the trajectories of ξ and φ are known, the transformations Ω_{K^bK} and $\Omega_{K^gK^b}$ are also known, thus the trajectory of the load in the xy-plane of the frame K can be calculated, hence the elements of the proof of Proposition 11 can be used.

Since the points A, B, P and C are in the same plane, there is an intersection between the lines determined by the sections $\overline{PA}$ and $\overline{CB}$. Let this intersection be denoted by D (see Figure 3.6).

The coordinates of the point D depend on the angle ξ and on the distance $h = k + l - d$:

$$\begin{bmatrix} x^b_D \\ y^b_D \\ z^b_D \end{bmatrix} = \begin{bmatrix} h\sin\alpha\cos\xi \\ h\sin\alpha\sin\xi \\ h\cos\alpha \end{bmatrix}$$

Since the point D is on the line determined by the section $\overline{CB}$, the vector $\overrightarrow{DB}$ is parallel with $(x^b, \dot{x}^b, \dot{z}^b + g)^T$. Hence, using Proposition 13, we get:

$$\frac{x^b - h\sin\alpha\cos\xi}{z^b - h\cos\alpha} = \frac{\dot{x}^b}{\ddot{z}^b + g} \qquad \frac{y^b - h\sin\alpha\sin\xi}{z^b - h\cos\alpha} = \frac{\dot{y}^b}{\ddot{z}^b + g} \qquad (3.22)$$

giving two equations to determine ξ and h as functions of $x^b, \dot{x}^b, \ddot{x}^b, y^b, \dot{y}^b, \ddot{y}^b, z^b, \ddot{z}^b$. Eliminating h we get an equation of type

$$A\sin\xi + B\cos\xi = D \qquad (3.23)$$

where

$$A = \sin\alpha(\ddot{z}^b + g)(\ddot{x}^b z^b - x^b(\ddot{z}^b + g))$$
$$B = -\sin\alpha(\ddot{z}^b + g)(\ddot{y}^b z^b - y^b(\ddot{z}^b + g))$$
$$D = \ddot{y}^b\cos\alpha(\ddot{x}^b z^b - x^b(\ddot{z}^b + g)) - \ddot{x}^b\cos\alpha(\ddot{y}^b z^b - y^b(\ddot{z}^b + g)).$$

Equation (3.23) gives two solutions for ξ in the interval $[-\pi, +\pi)$. Then h can be calculated from one of the following relations

$$h(\ddot{x}^b\cos\alpha - \sin\alpha\cos\xi(\ddot{z}^b + g)) = \ddot{x}^b z^b - x^b(\ddot{z}^b + g)$$
$$h(\ddot{y}^b\cos\alpha - \sin\alpha\sin\xi(\ddot{z}^b + g)) = \ddot{y}^b z^b - y^b(\ddot{z}^b + g)$$

where one may chose the numerically more precise expression (i.e. the more stable division).

It remains to find the trajectory of the variable φ as function of x^b, y^b, z^b and derivatives. Since ξ is expressed as function of the flat output and derivatives, the same is true for the transformation $\Omega_{K^bK^g}$ and thus for the coordinates of the vector $\overrightarrow{DC}$ in the frame K^g.

By the definition of the frame K^g, the y-coordinate of the vector $\overrightarrow{DC}$ vanish. Hence

$$proj_y\left(\Omega^T_{K^gK}\begin{bmatrix} x^g - h\sin\alpha \\ y^g \\ z^g - h\cos\alpha \end{bmatrix}\right) = 0.$$

Using the expression (3.16) of the transformation $\Omega_{K^g K}$ this gives

$$\sin\varphi(z^g \sin\alpha - x^g \cos\alpha) + y^g \cos\varphi = 0$$

allowing to calculate φ in the interval $(-\frac{1}{2}\pi; \frac{1}{2}\pi)$.

Now, it is possible to calculate the trajectory of the load in the xz-plane of the frame K and to reuse the elements of the proof of Proposition 11. Finally, the trajectory of the input u_3 is obtained using Equation (3.19). □

Remark 21. *Equation (3.22) gives the intersection of a line, determined by the acceleration of the load, and a cone, given by the possible positions of the boom. This geometric problem has two complex or two real solutions. Complex solutions mean that the required acceleration cannot be realized by the crane at all (no intersection point D). Even for real solutions, not all values of h are physically realizable. For, note that if h is out of the range $(k, k+l)$, at least one rope tension becomes negative which is not excluded from the model, but cannot be physically realized.*

Nonzero free pulley mass ($m_0 > 0$)

The main consequence of a nonzero free pulley mass is that the load at the point C is no longer constrained to evolve in the plane determined by the boom and the free pulley at the point B (see Figure 3.7). Recall that the coordinates of the free pulley in the frame K^b are denoted by $(x_B^b, y_B^b, z_B^b)^T$. The dynamics of the load read

$$m \begin{bmatrix} \ddot{x}^b \\ \ddot{y}^b \\ \ddot{z}^b + g \end{bmatrix} = \frac{T_3}{L_3} \begin{bmatrix} x_B^b - x^b \\ y_B^b - y^b \\ z_B^b - z^b \end{bmatrix} \tag{3.24}$$

The geometric constraints for the rope sections $\overline{PB}$, $\overline{AB}$ are already given by Equation (3.20). The geometric constraint for the rope section $\overline{SB}$ reads (see also Figure 3.6)

$$\begin{bmatrix} x_B^b \\ y_B^b \\ z_B^b \end{bmatrix} = \Omega_{K^b K^g} \cdot \Omega_{K^g K} \begin{bmatrix} (k+l+s)\sin\alpha - L_s\sin(\alpha - \beta) \\ 0 \\ (k+l+s)\cos\alpha - L_s\cos(\alpha - \beta). \end{bmatrix} \tag{3.25}$$

Instead of introducing two angles in order to give the orientation of the rope section $\overline{BC}$, we simple add a new quadratic expression to the constraints:

$$L_3^2 = (x_B^b - x^b)^2 + (y_B^b - y^b)^2 + (z_B^b - z^b)^2 \tag{3.26}$$

Remark 22. *One may replace all geometric constraints introduced so far by quadratic ones similar to Equation (3.26). The advantage of this kind of constraints is that they eliminate the use of angles between the rope sections as variables. The general and systematic modelling procedure presented in Section 3.2 uses quadratic constraints like (3.26).*
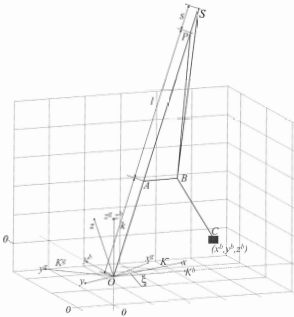
Figure 3.7: Crane in three dimensions

The force equilibrium at the free pulley is expressed by

$$m_B \begin{bmatrix} \ddot{x}_B^b \\ \ddot{y}_B^b \\ \ddot{z}_B^b + g \end{bmatrix} = t_1 + t_2 - t_3 + t_s. \tag{3.27}$$

The dynamics of the three winches (located at the points A, P and S) are already given by Equations (3.4)-(3.5) and (3.14). The dynamics associated to the rotation of the platforms are easily obtained from (3.19) by adding the torque generated by t_s:

$$J_{pf}\ddot{\xi} = proj_{z^b}\left(\overrightarrow{OP} \times (-t_2) + \overrightarrow{OA} \times (-t_1) + \overrightarrow{OS} \times (-t_s)\right) - \eta_4(\xi, \dot{\xi}) + u_4. \tag{3.28}$$

Proposition 15. *The 3D model of the crane such that $m_0 > 0$, given by Equations (3.24), (3.20a), (3.20c). (3.25)-(3.27), (3.4)-(3.5), (3.14), (3.28) is differentially flat. A possible choice of the flat output is given by x^b y^b z^b and L_3.*

Proof. Taking the norm of both sides of (3.24) and using the geometric constraint (3.26), the rope tensions in the main rope attached to the load can be obtained as

$$m \parallel \left(\ddot{x}^b, \ddot{y}^b, \ddot{z}^b + g\right)^T \parallel = T_3. \tag{3.29}$$
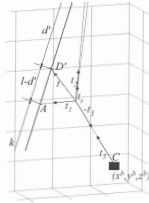
Figure 3.8: Rope tensions

This allows to express the coordinates of the free pulley as function of $x^b, \ddot{x}^b$ $y^b, \ddot{y}^b, z^b, \ddot{z}^b$ L_3:

$$\begin{bmatrix} x_B^b \\ y_B^b \\ z_B^b \end{bmatrix} = \begin{bmatrix} x^b \\ y^b \\ z^b \end{bmatrix} + \frac{mL_3}{T_3} \begin{bmatrix} \ddot{x}^b \\ \ddot{y}^b \\ \ddot{z}^b + g \end{bmatrix}$$

Introduce the tension t as

$$t = \begin{bmatrix} t_x \\ t_y \\ t_z \end{bmatrix} = l_3 + m_B \begin{bmatrix} \ddot{x}_B^b \\ \ddot{y}_B^b \\ \ddot{z}_B^b + g \end{bmatrix}$$

From Equation (3.27), we have

$$t = t_1 + t_2 + t_s.$$

Since t_1, t_2 and t_s are in the plane determined by the points P, A and B, t must also be in the same plane. Hence, the line determined by the vector t intersects the boom at a point denoted by D' which is at a distance d' from P (see Figure 3.8).

To calculate the position of the intersection point D' on the boom, one obtains similar equations to (3.22) with unknowns ξ and $h' = k + l - d'$:

$$\frac{x_B^b - h' \sin \alpha \cos \xi}{z_B^b - h' \cos \alpha} = \frac{t_x}{t_z} \qquad \frac{y_B^b - h' \sin \alpha \sin \xi}{z_B^b - h' \cos \alpha} = \frac{t_y}{t_z}. \qquad (3.30)$$

Eliminating h', one gets again an equation of type $A' \sin \xi + B' \cos \xi = D'$ with

$$A' = t_z(t_z z_B^b - x_B^b t_z) \sin \alpha$$
$$B' = -t_z(t_y z_B^b - y_B^b t_z) \sin \alpha$$
$$D' = t_y \cos \alpha (t_z z_B^b - x_B^b t_z) - t_x \cos \alpha (t_y z_B^b - y_B^b t_z).$$

giving two solutions for ξ in the interval $[-\pi, +\pi)$. The variable h' can be obtained from any of the following relations:

$$h'(t_x \cos \alpha - \sin \alpha \cos \xi t_z) = t_z z_B^b - x_B^b t_z,$$
$$h'(t_y \cos \alpha \sin \alpha \sin \xi t_z) = t_y z_B^b - y_B^b t_z,$$

choosing the numerically more stable division.

To find the trajectory of the variable φ as function of x^b, y^b, z^b, L_3, and derivatives, observe that by the definition of the frame K^9, the y coordinate of the vector $\overrightarrow{D'B}$ vanish. Hence

$$proj_y \left(\Omega_{K^9K}^T \begin{bmatrix} x_B^9 - h' \sin \alpha \\ y_B^9 \\ z_B^9 - h' \cos \alpha \end{bmatrix} \right) = 0.$$

Using the expression (3.16) of the transformation Ω_{K^9K} this gives

$$\sin \varphi (z_B^9 \sin \alpha - x_B^9 \cos \alpha) + y_B^9 \cos \varphi = 0,$$

allowing to calculate φ in the interval $(-\frac{1}{2}\pi; \frac{1}{2}\pi)$. This makes possible to calculate the angles β, γ, and μ in the PAB-plane together with the rope lengths L_1, L_2, and L_4, using the geometric constraints (3.20a), (3.20c) and (3.25).

Finally, the dynamics of the winches (3.4)-(3.5), (3.14) and the dynamics of the rotation (3.28) give the motor torques u_1, u_2, u_3, and u_4, respectively. $\square$

Remark 23. *A different choice of the fourth flat output (L_3) can be also envisaged. For instance, the height of the free pulley z_B^b (or any of its coordinates) is also a possible choice.*

Remark 24. *Note that the bisector property has no meaning in this framework since the points P, A, B, and C are no longer in the same plane.*

However, one may wish to find a trajectory that respects this property as closely as possible in an intuitive way. Given a trajectory of the load, this is carried out by choosing the trajectory of the fourth variable of the flat output (e.g. L_3 or z_B^b) by calculating it from the trajectory of the load as if the free pulley's mass were neglected (i.e. using the calculations described in the proof of Proposition 14). Then, the trajectory thus obtained gives the trajectory of the fourth variable in the flat output, and it can be used for further calculations.

Remark 25. *It is no longer true that the trajectories of the geometric variables (i.e. angles, rope lengths) are independent of the mass of the load.*

3.2   A general modelling method for a class of weight handling equipments

Notice that most WHEs (see [64]) use ropes and winches to displace the load. This hoising system is mounted on a mechanical structure with one or two articulations (e.g. rotate platform or moving bridge). These common characteristics, which will be defined more precisely later in this section, lead to a general modelling process. The interest of this generalization is that properties, in particular flatness, can be verified for a larger class of similar equipments.

To motivate further the interest of the generalization, consider the examples depicted in Figures 3.9, 3.10, 3.11, and 3.12, representing a 2D overhead, a 3D cantilever, a 3D overhead, and a 3D US Navy crane, respectively. Let us enumerate their common characteristics and introduce some notations:

- The load moves in a working space of either dimension $p = 2$ such as the overhead crane of Figure 3.9, or $p = 3$ as portrayed in Figures 3.10, 3.11, and 3.12.
- All considered WHEs comprise the following elements:
  - A working load of mass m whose coordinates are x_i, $i = 1, \ldots, p$.
  - A hoisting system composed of ropes, pulleys, and winches. The motors actuating the winches are supposed to be torque controlled and each one delivers a force noted by T_j where j numbers the winch. The different rope lengths are denoted by L_j.
  - A fully articulated mechanical structure on which are attached the winches winding the ropes. For the overhead crane depicted in Figure 3.9 it is a rail structure without articulation and for the 3D cranes of Figures 3.10 and 3.12 it corresponds to a boom that can rotate under motor actuation (the mechanical structure has one articulation with one actuator).
  - A free or main pulley which guides the rope attached to the load. Its coordinates are denoted by x_{0i}, $i = 1, \ldots, p$.
  - A rail constraining the movement of the free pulley might (see the 2D and 3D overhead crane and the cantilever crane in Figures 3.9, 3.11, and 3.10, respectively) or might not (see the 3D US Navy crane in Figure 3.12) be present.
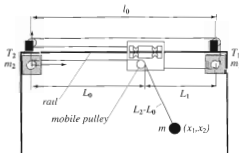

Figure 3.9: 2D overhead crane

3.2.1   Weight handling equipment definition and modelling

Let p be the dimension of the working space with $p \in \{2,3\}$. The definition of a WHE is as follows.

Definition 6 (WHE). *A WHE is constituted by the following elements:*

   i. a rigid articulated actuated mechanical structure with $d \in \{0,1\}$ degrees of freedom.

   ii. motors (winches).

   iii. ropes.

   iv. pulleys.

   v. a load.

and enjoys the following topographic properties:

   1. There is at least one motor fixed on the articulated structure. Let $s+1$ be the number of such motors, $s \geq 0$.

   2. There are as many ropes as motors fixed on the articulated mechanical structure.

   3. Each motor is linked to a pulley or to the load with a rope.

   4. s ropes end on a unique pulley, called the free pulley. If $s=0$ there is no free pulley. All pulleys but the free pulley are fixed to the structure.

   5. There is a unique rope going through the free pulley and ending on the load.

   6. Between the load and the free pulley there is no other pulley.

Moreover, the following physical property is assumed. The free pulley moves in a manifold of dimension $n \in (p-1, p)$. This manifold is determined thanks to the constraints imposed by the ropes and by possibly restricting the free pulley to move along a rail. If $n = p - 1$ the manifold is transversal to the gravitational field.

Let us enumerate and order the fixed pulleys on the structure along each rope starting from the motor winding the rope (i.e. from the winch) to the free pulley or to the load. This is possible due to the previous definition. Denote by r_i the number of fixed pulleys along the ith rope ($i = 1, \ldots, s + 1$).

We present here a Lagrangian approach to the WHE modelling. Hence, we start with the choice of generalized coordinates, then express the Lagrangian and the geometric constraints. The model is given in Theorem 2 below.

Consider an inertial base frame such that its pth axis is pointed in the direction opposite to g, the gravity acceleration. We introduce the following coordinates:

   1. position of the working load: $(x_1, \ldots, x_p)$,

2. position of the free pulley (if it exists): $(x_{01}, \quad , x_{0p})$,

3. positions of the motors winding ropes: $(x_{i1}, \quad , x_{ip})$ for $i = 1, \quad , s + 1$,

4. positions of the fixed pulleys: $(w_{ij1}, \quad , w_{ijp})$ for $i = 1, \quad , s + 1$ and $j = 1, \quad , r_i$,

5. rope lengths: L_i for $i = 1, \quad , s + 1$,

6. rope length L_0 between the free pulley (if it exists) and the motor hoisting the load.

The following inertia parameters are introduced. Let m denote the load mass and m_0 the free pulley mass. Denote by J_i, $i = 1, \quad , s + 1$, the inertia of the winches hoisting the ropes (including the inertia of the motors) and let J_{ij}, $i = 1, \quad , s + 1$, $j = 1, \quad , r_i$, denote the inertia of the fixed pulleys along the ropes. Moreover, denote by ρ_i and by ρ_{ij}, $i = 1, \quad , s + 1$, $j = 1, \quad , r_i$, the radii of the winches and the fixed pulleys, respectively.

Since all winches and fixed pulleys are located on the moving part of the mechanical structure the rope distances between them are constant. This implies that all rope distances can be virtually eliminated from the model by placing the winches at positions of the last fixed pulleys (the r_ith one) along the ropes. Each rope length is then reduced by the sum of the *constant* rope distances between the pulleys wound along that rope. For notational convenience we keep the notation L_i for the new rope lengths. The rotating inertia are then summed up along each rope to obtain

$$ m_i = \frac{J_i}{\rho_i} + \sum_{j=1}^{r_i} \frac{J_{ij}}{\rho_{ij}} \qquad i = 1, \quad , s + 1 $$

associated to the rope length L_i, $i = 1, \quad , s + 1$. Note that no inertia parameter is associated to the rope length L_0 since the corresponding rope section is part of the rope attached to the load with total length L_{s+1}.

Let m_{stc} be the mass of the moving part of the mechanical structure comprising the mass of all winches and fixed pulleys. Denote by J_{stc} the corresponding rotating inertia w.r.t. the joint axis in the case of a rotational joint. Define M as

$$ M = \begin{cases} m_{stc} & \text{for translational articulation} \\ \dfrac{J_{stc}}{r} & \text{for rotational articulation} \end{cases} $$

where r is the distance between the joint axis and the winch of the rope of length L_{s+1}. The inertia parameter M is not defined if the mechanical structure has no articulation, i.e. if $d = 0$.

Let us make the following assumptions which are satisfied by most of the WHEs used in practice. These assumptions also allow further notational simplification which do not impart on generality.

A1. The free pulley is present. Consequently, $s \geq 1$

A2. The crane has no redundant actuator or motor: $s - p - d - c$.

A3. If $d = 1$, the origin of the base frame is on the joint axis of the articulated mechanical structure. The articulated mechanical structure consists of either a rotational joint, to

which case the joint axis is colinear with g, or a translational joint, to which case the joint axis is orthogonal to g. This assumption eliminates the variable $x_{(s+1)p}$. (The vertical position of the motor winching the load remains constant.)

A4. The angular velocities of the fixed pulleys are small enough to neglect their quadratic effects (if any) w.r.t. the motions of the mechanical structure. Note that no such quadratic effect appears in our examples.

A5. If the free pulley moves along a rail, the rail is then fixed to the moving part of the structure. We suppose that the line determining the direction of the rail passes through the winch hoisting the load (with coordinates $(x_{(s+1)1}, \quad , x_{(s+1)p})$) and a point given by the vector v_{rail}:

$$v_{rail} = P_{rail} \cdot (x_{(s+1)1}, \quad , x_{(s+1)p})^T + p_{rail} \neq (x_{(s+1)1}, \quad , x_{(s+1)p})^T \tag{3.31}$$

where P_{rail} is a constant parameter matrix and p_{rail} a constant parameter vector. The vector $(x_{(s+1)1}, \quad , x_{(s+1)p})^T - v_{rail} \neq 0$ gives the direction of the rail. Moreover, introduce a parameter c such that $c = 1$ if the rail is present and $c = 0$ otherwise.

A6. We suppose that all the winches hoisting ropes are located on the moving part of the structure along a line such that

$$(x_{j1}, \quad , x_{jp})^T = \begin{cases} \alpha_j (x_{(s+1)1}, \quad , x_{(s+1)p})^T & \text{if } c = 0 \\ v_{rail} + \alpha_j \left((x_{(s+1)1}, \quad , x_{(s+1)p})^T - v_{rail} \right) & \text{if } c = 1 \end{cases} \quad j = 1, \quad , s,$$

i.e. the winches are situated along the rail if it is present.

p	d	c	s	d+s+1
2	0	0	2	3
2	0	1	1	2
3	1	0	2	4
3	1	1	1	3

Table 3.2: Parameter values compatible with the assumptions

The number of actuators (i.e. the actuator of the articulated structure and the motors winding ropes taken together) equals to $d + s + 1$. Table 3.2 gives the possible values of the parameters: p (dimension of the working space), d (number of articulations of the mechanical structure), c (presence of a rail system), and s (number of ropes attached to the free pulley) compatible with the assumptions.

The elimination of the fixed pulleys from the model and the above assumptions reduced the number of variables, thus the vector of the generalized coordinates reads

$$q = (x_1, \quad , x_p, x_{01}, \quad , x_{0p}, x_{(s+1)1}, \quad , x_{(s+1)(p-1)}, L_0, L_1, \quad , L_{s+1})^T \tag{3.32}$$

Using these generalized coordinates, the Lagrangian of a WHE in the sense of Definition 6 which is subject to the above assumptions reads:

$$\mathcal{L} = \frac{1}{2}\left(m \sum_{i=1}^{p} \dot{x}_i^2 + m_0 \sum_{i=1}^{p} \dot{x}_{0i}^2 + M \sum_{i=1}^{p-1} \dot{x}_{(s+1)i}^2 + \sum_{i=1}^{s+1} m_i \dot{L}_i^2 \right) - g(m x_p + m_0 x_{0p}). \quad (3.33)$$

Let us study next the constraints on the variables in q. Constraints on the rope lengths are present either due to ropes terminating at the free pulley:

$$C_j(x_{01}, \quad , x_{0p}, x_{(s+1)1}, \quad , x_{(s+1)p-1}, L_j) = 0 \qquad j = 1, \quad , s. \quad (3.34)$$

or due to the rope terminating at the working load. Two constraints are obtained for the latter rope, one for the length between the free pulley and the corresponding winch fixed to the structure (denoted by L_0) and one for the length between the load and the free pulley:

$$C_{s+1}(x_{01}, \quad , x_{0p}, x_{(s+1)1}, \quad , x_{(s+1)p-1}, L_0) = 0 \quad (3.35)$$

$$C_{s+2}(x_{01}, \quad , x_{0p}, x_1, \quad , x_p, L_0, L_{s+1}) = 0. \quad (3.36)$$

An additional constraint is imposed by the motion compatible with the degree of freedom of the structure if $d = 1$. In view of the above assumptions, this constraint exists only if $p = 3$ (see Table 3.2):

$$C_{s+3}(x_{(s+1)1}, \quad , x_{(s+1)p-1}) = 0 \quad (3.37)$$

The motion constraint of the free pulley along the rail (if it is present) is of the form:

$$C_{s+p-k}(x_{01}, \quad , x_{0p}, x_{(s+1)1}, \quad , x_{(s+1)p-1}) = 0 \qquad k = 1, \quad , p - 1 \quad (3.38)$$

Denote by l the total number of constraints. If the rail (i.e. Constraint (3.38)) is present, $l = s + 2p - 1$ and $l = s + p$ otherwise.

Here, $C_1, \quad , C_l$ are at most quadratic functions of all their arguments (note that this also allows linear terms). Moreover, $C_1, \quad C_{s+2}$ contain no nested product involving L_j and x_{ij}. The exact form of the constraints is not needed in the sequel (nevertheless they are explicitly given in Remark 27 below).

In place of obtaining an explicit differential model, we prefer an implicit formulation with additional variables, known as *Lagrange multipliers*.

Theorem 2. *Assume that the constraints are independent in an open subset of the generalized coordinate space. The dynamical model associated to a WHE corresponding to Definition 6*

reads:

$$m\ddot{x}_i = \lambda_{s+2}\frac{\partial C_{s+2}}{\partial x_i} - \delta_{ip}mg \qquad i = 1, \quad ,p \tag{3.39a}$$

$$m_0\ddot{x}_{0i} = \sum_{j=1}^{l}\lambda_j\frac{\partial C_j}{\partial x_{0i}} - \delta_{ip}m_0g \qquad i = 1, \quad ,p \tag{3.39b}$$

$$0 = \sum_{j=1}^{l}\lambda_j\frac{\partial C_j}{\partial L_0} \tag{3.39c}$$

$$m_s\ddot{L}_s = \sum_{j=1}^{l}\lambda_j\frac{\partial C_j}{\partial L_s} + T_s \qquad s = 1, \quad ,s+1 \tag{3.39d}$$

$$M\ddot{x}_{(s+1)i} = \sum_{j=1}^{l}\lambda_j\frac{\partial C_j}{\partial x_{(s+1)i}} + F_i(T_{s+2}) \qquad i = 1, \quad ,p-1 \tag{3.39e}$$

subject to Constraints (3.34)-(3.38), where $\delta_{ip} = 1$ if $i = p$ and $\delta_{ip} = 0$ otherwise. T_1, , T_{s+1} are the torques produced by the motors on the structure and T_{s+2} the one produced by the structure actuator. F_1, , F_{p-1} are the generalized external forces depending on the torque delivered by the structure actuator and the λ_i denote the Lagrange multipliers.

Proof. We compute

$$\frac{d}{dt}\frac{\partial \mathcal{L}}{\partial \dot{q}} - \frac{\partial \mathcal{L}}{\partial q} = F_q + \tau_q$$

where τ_q are the constraint forces and

$$F_q = (\underbrace{0, \quad ,0}_{2p+1}, T_1, \quad ,T_{s+1}, F_1(T_{s+2}), \quad ,F_{(p-1)}(T_{s+2}))^T$$

gives the external forces.

Taking total differential of the constraints leads to

$$\sum_{j=1}^{\dim q}\frac{\partial C_i}{\partial q_j}dq_j = 0, \qquad i = 1, \quad ,l,$$

expressing that virtual displacements are in ker $DC(q)$ where $DC(q)$ is the matrix whose entries are $\frac{\partial C_i}{\partial q_j}$. Since the constraint forces compatible with the virtual displacements are workless, we have $\sum_{i=1}^{\dim q}\tau_i dq_i = 0$. Therefore, $\tau = (\tau_1, \quad \tau_{\dim q})$ is a linear combination of the lines of $DC(q)$:

$$\tau_i = \sum_{j=1}^{l}\lambda_j\frac{\partial C_j}{\partial q_i} \qquad i = 1, \quad ,\dim q \tag{3.40}$$

and the theorem is proved.   □

Remark 26. *Note that the LHS^2 $\frac{d}{dt}\frac{\partial \mathcal{L}}{\partial \dot{q}}$ of the model (3.39) is independent of the specific topography of the WHE, whereas the RHS consists of the exterior forces F_q plus gravity terms $\frac{\partial \mathcal{L}}{\partial q}$ and the terms given by (3.40) which sum up the topographic specificity.*

Remark 27 *The exact form of the constraints C_j, $j = 1, \ldots, l$ are:*

$$C_j = \frac{1}{2}\sum_{i=1}^{p}(x_{0_i} - x_{j_i})^2 - \frac{L_j^2}{2} = 0 \qquad j = 1, \ldots, s. \tag{3.41a}$$

$$C_{s+1} = \frac{1}{2}\sum_{i=1}^{p-1}(x_{0_i} - x_{(s+1)_i})^2 - \frac{L_0^2}{2} = 0. \tag{3.41b}$$

$$C_{s+2} = \frac{1}{2}\sum_{i=1}^{p}(x_{0_i} - x_{1_i})^2 - \frac{(L_{s+1} - L_0)^2}{2} - 0. \tag{3.41c}$$

$$C_{s-3} = \begin{cases} \frac{1}{2}\sum_{i=1}^{p-1}x_{(s+1)_i}^2 - r^2 = 0 & \text{for rotational joint} \\ t_{a1}x_{(s+1)2} - x_{(s+1)1}t_{a2} = 0 & \text{for prismatic joint.} \end{cases} \tag{3.41d}$$

$$C_{s-p-k} = \sum_{i=1}^{p}(x_{0_i} - x_{(s+1)_i})\varrho_{k_i} = 0 \qquad k = 1, \ldots, p-1 \tag{3.41e}$$

where $t_a = (t_{a1}, \ldots, t_{ap})^T$ is the vector of the joint axis of the articulated structure and $\varrho_k = (\varrho_{k1}, \ldots, \varrho_{kp})^T \neq 0$, $k = 1, \ldots, p-1$ are orthogonal vectors to $(x_{(s+1)_1}, \ldots, x_{(s+1)_p})^T - v_{rail}$ which gives the direction of the rail as defined in **A5**. *Note that these formulae are not needed to state and prove our main results.*

3.2.2 Flatness

Assume that we exclude free fall trajectories of the load, namely such that $\ddot{x}_p = \ldots g$ (here g stands for the norm of the gravity acceleration) and such that $\frac{\partial C_{s+2}}{\partial x_p} = 0$.

Theorem 3. *WHEs defined by Definition 6 and satisfying* **A1**–**A5** *of Section 3.2.1 are differentially flat. The flat output, denoted by Y in the sequel, can be chosen as $(x_1, \ldots, x_p)$, the coordinates of the load, and $s + 1 + d - p$ coordinates of the free pulley.*

Proof. In view of the assumptions we need to distinguish the four cases of Table 3.2. We provide the proof for $p = 3$, the simplest cases with $p = 2$ can be dealt in a similar way. (Recall that $p = 2$ implies that $d = 0$.)

Assume first that $s = 2 = p - 1$ and consider $Y = (x_1, \ldots x_p, x_{0p})$ as a candidate flat output. Combining the pth equation of (3.39a) and (3.36) and the fact that the C_i's contain no cross-terms involving L_0, L_{s+2} by assumption, one obtains λ_{s+2} as a function of x_p, $\ddot{x}_p$ and x_{0p} since $\lambda_{s+2} \neq 0$ which is guaranteed by the assumption that $\ddot{x}_p \neq -g$, the $p-1$ first equations of (3.39a) express the remaining coordinates $x_{01}, \ldots, x_{0(p-1)}$ as functions of x_j, $\ddot{x}_j$, $j = 1, \ldots, p$, and x_{0p}. Next, we use the $2p + 1$ equations (3.35)-(3.37)

---

^{2}Left Hand Side

and (3.39b)-(3.39c) to express the $2p + 1$ variables $L_0, L_{s+1}, x_{(s+1)1}, \ldots, x_{(s+1)p-1}, \lambda_1, \ldots, \lambda_p$ as functions of $x_{01}, \ldots, x_{0p}, x_1, \ldots, x_p, \dot{x}_{s+2}$ and derivatives up to order 2 which in turn can be expressed as functions of Y and derivatives up to order 4. Now, by (3.34), one can express $L_1, \ldots, L_s$ as functions of variables which are already expressed as functions of the flat output and its derivatives. By (3.39d), $T_1, \ldots, T_p$ are also obtained as functions of the previous ones and derivatives of Y up to order 6, and finally, T_{s+2} and λ_{s+3} are obtained in a similar way by (3.39e) which proves that $Y = (x_1, \ldots, x_p, x_{0p})$ is a flat output.

Consider now the case with $s = c = 1$ (i.e. the rail constraints (3.38) are present) and let $Y = (x_1, \ldots, x_p)$ be the candidate flat output. First, we use the $2p$ equations (3.37)-(3.38) and (3.39a) to express $2p$ variables $x_{01}, \ldots, x_{0p}, x_{s+2}, x_{(s+1)1}, \ldots, x_{(s+1)p-1}$ as functions of x_j, $\ddot{x}_j$, $j = 1, \ldots, p$. We proceed using equations (3.34)-(3.36) and (3.39c) to express the rope lengths L_0, L_1, L_2 and λ_{s+1} as functions of Y $\dot{Y}$ Next, we use Equation (3.39b) to obtain $\lambda_s, \lambda_{s+p+1}, \lambda_{s+p+2}$ as functions of $Y = (x_1, \ldots, x_p)$ and its derivatives up to order 4. Finally, we use equations (3.39d) and (3.39e) to express $T_1, \ldots, T_{s+2}$ and λ_{s+3} as functions of Y and their derivatives up to order 6 which proves that $Y = (x_1, \ldots, x_p)$ is indeed a flat output. $\square$

3.2.3   Numerical simulation of the dynamics

The simulation of a dynamical system consists of numerically integrating its state equations. For the cranes we advocate to integrate the equations of the implicit model without reducing these equations by choosing a particular set of independent coordinates and eliminating the rest. The system to be integrated (3.39) being affine w.r.t. $\Lambda = (\lambda_1, \ldots \lambda_l)^T$ the vector of Lagrange multipliers, is of the form

$$\ddot{q} = F(q, \dot{q})\Lambda + F_0(q, \dot{q}) \tag{3.42}$$

where q stands for the vector of generalized coordinates given by (3.32). For this system to be well determined, expressions of λ_i be the functions of q and $\dot{q}$ need to be obtained. To do so, we differentiate twice the constraints $C_j(q)$, $j = 1, \ldots l$ which gives, in matrix form

$$A(q, \dot{q}) + \frac{\partial C}{\partial q}\ddot{q} = 0,$$

with

$$A(q, \dot{q}) = \left(\dot{q}^T \left(\frac{\partial^2 C_1}{\partial q^2} \right) \dot{q}, \ldots, \dot{q}^T \left(\frac{\partial^2 C_l}{\partial q^2} \right) \dot{q} \right)^T$$

We then replace $\ddot{q}$ by its expression given by (3.42) to yield

$$\frac{\partial C}{\partial q} F(q, \dot{q})\Lambda = -A(q, \dot{q}) - \frac{\partial C}{\partial q} F_0(q, \dot{q}).$$

It can be shown that $\frac{\partial C}{\partial q} F(q, \dot{q})$ is always an invertible matrix and thus

$$\Lambda = - \left(\frac{\partial C}{\partial q} F(q, \dot{q}) \right)^{-1} \left(A(q, \dot{q}) + \frac{\partial C}{\partial q} F_0(q, \dot{q}) \right) \tag{3.43}$$

Equation (3.42) with Λ replaced by (3.43) is then integrated using a standard algorithm. Numerical simulations show that the constraints are satisfied throughout the integration process once the initial condition satisfy them.

3.2.4 Examples of weight handling equipment modelling

Let us illustrate the general modelling approach by giving the resulting equations for the 3D cantilever, 3D overhead, and 3D US Navy cranes (the latter being the subject of Section 3.1.2).

Example 9. *3D Cantilever Crane.* The crane depicted in Figure 3.10 comprises a trolley restricted to move along a rail. The trolley is considered as a free pulley. The rail rotates around a vertical axis together with the winches no.1 and no.2 whose coordinates are $(x_{11}, x_{12}, x_{13})^T$ and $(x_{21}, x_{22}, x_{23})^T$ respectively. Winch no.2 hoists the load and winch no.1 moves the trolley. The winches are located on a line passing through the origin of the base frame, thus $x_{1j} = \alpha_1 x_{2j}$, $j = 1$, , 3. Since the rail passes through the origin of the base frame, one can choose $v_{rail} = 0$ (i.e. the $P_{rail} = 0$ and $p_{rail} = 0$ in Equation (3.31)), hence the direction of the rail is simply given by the vector $(x_{21}, x_{22}, x_{23})^T$ All assumptions are satisfied, thus the crane fits the general modelling setup with the following parameters: $n = 2$, $p = 3$, $d = s = c = 1$

Let the vectors ϱ_1 and ϱ_2, both orthogonal to the direction of the rail, be chosen as $\varrho_1 = (0, 0, 1)^T$ and $\varrho_2 = (-x_{22}, x_{21}, 0)^T$ The generalized coordinates are

$$q = (x_1, x_2, x_3, x_{21}, x_{01}, x_{02}, L_0, L_1, L_2)^T$$

where x_{03} is omitted since it equals to zero. Note that this also makes trivial the constraint corresponding to ϱ_1 in Equation (3.41e). The constraints, obtained using (3.41), read
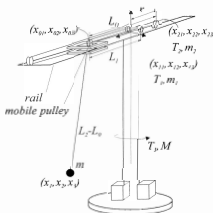

Figure 3.10: 3D Cantilever crane

$$C_1(q) = \frac{1}{2}\left((x_{01} - \alpha_1 x_{21})^2 + (x_{02} - \alpha_1 x_{22})^2 - L_1^2\right) = 0 \tag{3.44a}$$

$$C_2(q) = \frac{1}{2}\left((x_{01} - x_{21})^2 + (x_{02} - x_{22})^2 - L_0^2\right) = 0 \tag{3.44b}$$

$$C_3(q) = \frac{1}{2}\left((x_{01} - x_1)^2 + (x_{02} - x_2)^2 + x_3^2 - (L_2 - L_0)^2\right) = 0 \tag{3.44c}$$

$$C_4(q) = \frac{1}{2}\left(x_{21}^2 + x_{22}^2 - r^2\right) = 0 \tag{3.44d}$$

$$C_5(q) = -x_{01} x_{22} + x_{02} x_{21} = 0. \tag{3.44e}$$

Define the set

$$\mathcal{S} = \left\{(q, \dot{q}) \in \mathbb{R}^{20} \mid C_i(q) = 0, i = 1, \ldots, 5\right\} \tag{3.45}$$

The dynamics of the cantilever crane evolve on $\mathcal{S}$ by construction. The model is obtained using Theorem 2. The kinetic and potential energies are defined by

$$W_k = \frac{1}{2}\sum_{i=1}^{3} m\dot{x}_i^2 + \frac{1}{2}\sum_{i=1}^{2}\left(m_0\dot{x}_{0i}^2 + M\dot{x}_{2i}^2\right) + \frac{1}{2}\sum_{i=1}^{2} m_i\dot{L}_i^2 \qquad W_p = mgx_3 \tag{3.46}$$

and the Lagrangian reads $\mathcal{L} = W_k - W_p$. Thus the dynamics are given by

$$m\ddot{x}_1 = -\lambda_3(x_{01} - x_1) \tag{3.47a}$$

$$m\ddot{x}_2 = -\lambda_3(x_{02} - x_2) \tag{3.47b}$$

$$m\ddot{x}_3 = \lambda_3 x_3 - mg \tag{3.47c}$$

$$m_0\ddot{x}_{01} = \lambda_3(x_{01} - x_1) + \lambda_1(x_{01} - \alpha_1 x_{21}) + \lambda_2(x_{01} - x_{21}) - \lambda_5 x_{22} \tag{3.47d}$$

$$m_0\ddot{x}_{02} = \lambda_3(x_{02} - x_2) + \lambda_1(x_{02} - \alpha_1 x_{22}) + \lambda_2(x_{02} - x_{22}) + \lambda_5 x_{21} \tag{3.47e}$$

$$0 = \lambda_3(L_2 - L_0) - \lambda_2 L_0 \tag{3.47f}$$

$$m_1\ddot{L}_1 = -\lambda_1 L_1 + T_1 \tag{3.47g}$$

$$m_2\ddot{L}_2 = -\lambda_3(L_2 - L_0) + T_2 \tag{3.47h}$$

$$M\ddot{x}_{21} = -\lambda_1\alpha_1(x_{01} - \alpha_1 x_{21}) - \lambda_2(x_{01} - x_{21}) + \lambda_4 x_{21} + \lambda_5 x_{02} - T_3 x_{22} \tag{3.47i}$$

$$M\ddot{x}_{22} = -\lambda_1\alpha_1(x_{02} - \alpha_1 x_{22}) - \lambda_2(x_{02} - x_{22}) + \lambda_4 x_{22} - \lambda_5 x_{01} + T_3 x_{21}. \tag{3.47j}$$

Using Theorem 3, a possible flat output is given by $Y = (x_1, x_2, x_3)^T$ the position of the load.

The dynamics and the constraints have the same expressions if we rotate the base frame by any fixed angle around its vertical axis which coincides with the rotation axis of the crane. This invariance property will be used in Section 3.4.3 to show our stability results in closed loop.   ∎

Example 10. *3D Overhead Crane.* The crane is depicted in Figure 3.11. In contrast to the cantilever crane of Example 9, the rail with the trolley (free pulley) cannot be rotated but translated. The axis of the corresponding joint of the mechanical structure is given by the vector $\mathbf{t}_a = (0, 1, 0)^T$. Winch no.1, whose coordinates are $(x_{11}, x_{12}, x_{13})^T$ moves the trolley along the rail and winch no.2, whose coordinates are $(x_{21}, x_{22}, x_{23})^T$ hoists the load. The

choice of the origin of the base frame is such that $x_{03} = x_{13} = x_{23} = 0$. The rail passes through the winch no.2 and the point of coordinates $v_{rail} = (x_{21}-1, x_{22}, 0)^T$ (i.e. $P_{rail} = l$ and $p_{rail} = (-1, 0, 0)^T$ in Equation (3.31)). Let us choose $\varrho_1 = (0, 0, 1)^T$ and $\varrho_2 = (0, 1, 0)^T = t_4$. The constraint along ϱ_1 is again trivial since $x_{03} = 0$ by the choice of the base frame). The parameters are $n = 2$, $p = 3$, $d = 1$, $c = 1$, and $s = 1$. The generalized coordinates read
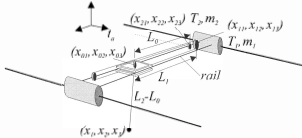
Figure 3.11:   3D Overhead crane

$$q = (x_1, x_2, x_3, x_{21}, x_{22}, x_{01}, L_0, L_1, L_2)^T$$

and the constraints are given by

$$C_1(q) = \frac{1}{2}\left((x_{01} - x_{21} + 1 - \alpha_1)^2 + (x_{02} - x_{22})^2 - L_1^2\right) = 0$$

$$C_2(q) = \frac{1}{2}\left((x_{01} - x_{21})^2 + (x_{02} - x_{22})^2 - L_0^2\right) = 0$$

$$C_3(q) = \frac{1}{2}\left((x_{01} - x_1)^2 + (x_{02} - x_2)^2 + x_3^2 - (L_2 - L_0)^2\right) = 0$$

$$C_4(q) = x_{21} = 0$$

$$C_5(q) = x_{02} - x_{22} = 0.$$

The last two constraints are linear, hence they can be used to eliminate the coordinates x_{21} and x_{22} in a straightforward way. The remaining generalized coordinates read

$$q = (x_1, x_2, x_3, x_{01}, x_{02}, L_0, L_1, L_2)^T$$

and the remaining constraints are

$$C_1(q) = \frac{1}{2}\left((x_{01} + 1 - \alpha_1)^2 - L_1^2\right) = 0 \tag{3.48a}$$

$$C_2(q) = \frac{1}{2}\left(x_{01}^2 - L_0^2\right) = 0 \tag{3.48b}$$

$$C_3(q) = \frac{1}{2}\left((x_{01} - x_1)^2 + (x_{02} - x_2)^2 + x_3^2 - (L_2 - L_0)^2\right) = 0. \tag{3.48c}$$

Due to these constraints, the dynamics of the 3D overhead crane evolve on the set

$$\mathcal{S} = \left\{(q, \dot{q}) \in \mathbb{R}^{16} \mid C_i(q) = 0, \imath = 1, \quad .3\right\} \tag{3.49}$$

The kinetic and potential energies are given by

$$W_k = \frac{1}{2} \sum_{i-1}^{3} m \dot{x}_i^2 + \frac{1}{2} \sum_{i=1}^{2} m_0 \dot{x}_{0_i}^2 + \frac{1}{2} M \dot{x}_{02}^2 + \frac{1}{2} \sum_{i=1}^{2} m_i \dot{L}_i^2 \qquad W_p = mgx_3. \qquad (3.50)$$

Then we use Theorem 2 to obtain the dynamics:

$$m \ddot{x}_1 = -\lambda_3 (x_{01} - x_1) \qquad (3.51a)$$

$$m \ddot{x}_2 = -\lambda_3 (x_{02} - x_2) \qquad (3.51b)$$

$$m \ddot{x}_3 = \lambda_3 x_3 - mg \qquad (3.51c)$$

$$m_0 \ddot{x}_{01} = \lambda_1 (x_{01} + 1 - \alpha_1) + \lambda_2 x_{01} \qquad (3.51d)$$

$$(m_0 + M) \ddot{x}_{02} = \lambda_3 (x_{02} - x_2) + T_3 \qquad (3.51e)$$

$$0 = -\lambda_2 L_0 + \lambda_3 (L_2 - L_0) \qquad (3.51f)$$

$$m_1 \ddot{L}_1 = -\lambda_1 L_1 + T_1 \qquad (3.51g)$$

$$m_2 \ddot{L}_2 = -\lambda_3 (L_2 - L_0) + T_2. \qquad (3.51h)$$

A possible flat output is given by the position of the load: $Y = (x_1, x_2, x_3)^T$ ∎

Example 11. *3D US Navy Crane.* This is the only crane among the examples without a rail system. Instead, the number of winches is increased since two ropes terminate on the free pulley. The detailed description of this type of crane, depicted in Figure 3.12 with the notations used here, has been already given in Section 3.1. The parameters are: $p = n = 3$, $d = 1$, $c = 0$ (there is no rail system), and $s = 2$. The vector of generalized coordinates is

$$q = (x_1, x_2, x_3, x_{31}, x_{32}, x_{01}, x_{02}, x_{03}, L_0, L_1, L_2, L_3)^T \qquad (3.52)$$

The constraints read:

$$C_1(q) = \frac{1}{2} \left((x_{01} - \alpha_1 x_{31})^2 + (x_{02} - \alpha_1 x_{32})^2 + (x_{03} - \alpha_1 x_{33})^2 - L_1^2 \right) = 0 \qquad (3.53a)$$

$$C_2(q) = \frac{1}{2} \left((x_{01} - \alpha_2 x_{31})^2 + (x_{02} - \alpha_2 x_{32})^2 + (x_{03} - \alpha_2 x_{33})^2 - L_2^2 \right) = 0 \qquad (3.53b)$$

$$C_3(q) = \frac{1}{2} \left((x_{01} - x_{31})^2 + (x_{02} - x_{32})^2 + (x_{03} - x_{33})^2 - L_0^2 \right) = 0 \qquad (3.53c)$$

$$C_4(q) = \frac{1}{2} \left((x_{01} - x_1)^2 + (x_{02} - x_2)^2 + (x_{03} - x_3)^2 - (L_3 - L_0)^2 \right) = 0 \qquad (3.53d)$$

$$C_5(q) = \frac{1}{2} \left(x_{31}^2 + x_{32}^2 - r^2 \right) = 0. \qquad (3.53e)$$

The 3D US Navy crane may evolve on the set

$$\mathcal{S} = \left\{ (q, \dot{q}) \in \mathbb{R}^{24} \mid C_i(q) = 0, i = 1, \quad , 5 \right\} \qquad (3.54)$$

The kinetic and potential energies are defined by

$$W_k = \frac{1}{2} \sum_{i=1}^{3} \left(m \dot{x}_i^2 + m_0 \dot{x}_{0i}^2 \right) + \frac{1}{2} M \dot{x}_{3i}^2 + \frac{1}{2} \sum_{i=1}^{3} m_i \dot{L}_i^2 \qquad W_p = mgx_3 + m_0 g x_{03}. \qquad (3.55)$$

The Lagrangian reads $\mathcal{L} = W_k - W_p$. The dynamics are given by Theorem 2:

$$m\ddot{x}_1 = -\lambda_4(x_{01} - x_1) \tag{3.56a}$$

$$m\ddot{x}_2 = -\lambda_4(x_{02} - x_2) \tag{3.56b}$$

$$m\ddot{x}_3 = -\lambda_4(x_{03} - x_3) - mg \tag{3.56c}$$

$$m_0\ddot{x}_{02} = \lambda_4(x_{01} - x_1) + \lambda_1(x_{01} - \alpha_1 x_{31}) + \lambda_2(x_{01} - \alpha_2 x_{31}) + \lambda_3(x_{01} - x_{31}) \tag{3.56d}$$

$$m_0\ddot{x}_{02} = \lambda_4(x_{02} - x_2) + \lambda_1(x_{02} - \alpha_1 x_{32}) + \lambda_2(x_{02} - \alpha_2 x_{32}) + \lambda_3(x_{02} - x_{32}) \tag{3.56e}$$

$$m_0\ddot{x}_{03} = \lambda_4(x_{03} - x_3) + \lambda_1(x_{03} - \alpha_1 x_{33}) + \lambda_2(x_{03} - \alpha_2 x_{33}) + \lambda_3(x_{03} - x_{33}) - m_0 g \tag{3.56f}$$

$$0 = \lambda_4(L_3 - L_0) - \lambda_3 L_0 \tag{3.56g}$$

$$m_1\ddot{L}_1 = -\lambda_1 L_1 + T_1 \tag{3.56h}$$

$$m_2\ddot{L}_2 = -\lambda_2 L_2 + T_2 \tag{3.56i}$$

$$m_3\ddot{L}_3 = -\lambda_4(L_3 - L_0) + T_3 \tag{3.56j}$$

$$M\ddot{x}_{31} = -\lambda_1\alpha_1(x_{01} - \alpha_1 x_{31}) - \lambda_2\alpha_2(x_{01} - \alpha_2 x_{31}) - \lambda_3(x_{01} - x_{31}) + \lambda_5 x_{31} - T_4 x_{32} \tag{3.56k}$$

$$M\ddot{x}_{32} = -\lambda_1\alpha_1(x_{02} - \alpha_1 x_{32}) - \lambda_2\alpha_2(x_{02} - \alpha_2 x_{32}) - \lambda_3(x_{02} - x_{32}) + \lambda_5 x_{32} + T_4 x_{31}. \tag{3.56l}$$

One can prove using Theorem 3 that the coordinates of the load and the height of the free pulley form a flat output: $Y = (x_1, x_2, x_3, x_{03})^T$
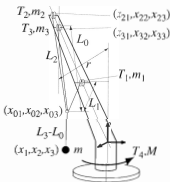
Figure 3.12:   3D US Navy crane

The model of this crane (i.e. the dynamic equations (3.56) and the constraints (3.53)) is invariant w.r.t. the rotation of the base frame around its vertical axis by any fixed angle. This will be used in Section 3.4.   ∎

3.3   Motion planning

To motivate the necessity of the motion planning, recall first that undesired oscillations of the load are created in part by the crane operator himself. In fact, when the operator wishes to displace the load to a desired equilibrium position along a trajectory avoiding obstacles in the

crane's workspace, he manipulates the load indirectly by acting on motors rotating winches. Hence the operator tries to find the trajectory of the motor forces corresponding to the desired trajectory of the load. This is considered to be a difficult task even for experienced crane operators since it requires simultaneous actions on several actuators (e.g. four winches for the 3D US Navy crane).

We propose to assist the crane operator by solving the MPP corresponding to his desired displacement. More precisely, the human operator gives the desired equilibrium position of the load and the motion planning algorithm calculates the corresponding trajectory of the motor forces. This requires the knowledge of the parameters of the model.

The motion planning algorithm is based on the flatness property of the WHEs (see Theorem 3). Assume that the position, velocity, acceleration, jerk, and all derivatives up to the $6th$ order of the flat output (including the position of the load) are given at the starting time t_I by $\left(Y_I, \dot{Y}_I, \ddot{Y}_I, \quad Y_I^{(5)} \; Y_I^{(6)}\right)$ and the desired final configuration of the flat output and its successive time derivatives are $\left(Y_F, \dot{Y}_F, \ddot{Y}_F, \quad Y_F^{(5)} \; Y_F^{(6)}\right)$ at time t_F.

The flatness property implies that for any trajectory connecting the initial and final points, the motor torques can be calculated without integration of the model equations. It is enough to follow the steps of the proof of Theorem 3. The trajectory can be obtained using polynomial interpolation as it has been already proposed in Chapter 2.

To see this, suppose that the initial and final conditions correspond to two different equilibria of the load: $Y_I = \bar{Y}_I$, $\dot{Y}_I = \ddot{Y}_I = \quad = Y_I^{(5)} = Y_I^{(6)} = 0$ and $Y_F = \bar{Y}_F$, $\dot{Y}_F = \ddot{Y}_F = \quad = Y_F^{(5)} = Y_F^{(6)} = 0$. Note that derivatives up to the 6th order are needed to calculate the reference inputs (i.e. motor forces). To satisfy these constraints with the trajectory of the flat output, we can construct a $13th$ degree polynomial

$$\chi_c(t) = \bar{\chi}_I + (\bar{\chi}_F - \bar{\chi}_I) \left(\frac{t - t_I}{t_F - t_I}\right)^7 \sum_{j=7}^{13} a_j \left(\frac{t - t_I}{t_F - t_I}\right)^{(j-7)} \tag{3.57}$$

where $\chi_c(t)$ is the reference trajectory of a variable of the flat output Y (using similar notation as in Section 2.3). This polynomial satisfies all initial conditions and the coefficients a_j are computed by solving a linear equation, independent of Y_I, Y_F, t_I and t_F. In fact, the numerical values of these coefficients are

$$a_{13} = 924 \qquad a_{12} = -6006$$
$$a_{11} = 16380 \qquad a_{10} = -24024$$
$$a_9 = 20020 \qquad a_8 = -9009$$
$$a_7 = 1716.$$

Using such polynomials for each variable of the flat output Y we get a straight line trajectory of the load in the workspace of the crane connecting the two equilibria

Remark 28. *The off-line calculations of the coefficients are of interest in the case of real-time applications where the desired end-point of the trajectory is modified continually by the human operator*

Let us illustrate the solution[3] of the MPP for the 3D US Navy crane modelled in Example 11 The parameters used are that of a reduced size model (1:80) realized in the Centre Automatique et Systèmes of the École Nationale Supérieure des Mines de Paris, depicted in Figure 3.1. The mass of the load is 250[g]. Recall that, by Proposition 14 (or by Theorem 3), the flat output includes the coordinates of the load, i.e. $\{x_1, x_2, x_3\} \subset Y$ and that we wish to find an idle to idle trajectory for the load implying that the reference trajectory will have no sway at the final equilibrium.
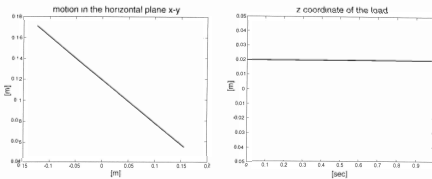

Figure 3.13: Horizontal displacement of the load

The trajectory depicted in Figure 3.13 is a horizontal idle to idle displacement of the load obtained using polynomial interpolation as in Equation (3.57). Some of the corresponding motor torques are given in Figure 3.14.

Obstacle avoidance

The flatness property furnishes an easy way to find trajectories avoiding obstacles present in the crane's workspace. Suppose that the positions of the obstacles are known in the base frame. The geometry of a trajectory avoiding the obstacle can be given by the functions

$$x_2 = x_2(x_1) \qquad x_3 = x_3(x_1)$$

where the variables x_2 and x_3 depend on the values of x_1. The geometry of the trajectory can be also specified by

$$x_1 = x_1(\lambda) \qquad x_2 = x_2(\lambda) \qquad x_3 = x_3(\lambda)$$

with $\lambda(0) = 0$. Here $\lambda(T)$ is the length of the trajectory between the initial and final equilibria and T is the travelling duration. Thus, given the time function $x_1(t)$ or $\lambda(t)$ (for the latter, $\dot{\lambda}$ gives the velocity along the trajectory), the other variables are given as their functions. For the variables x_1 or λ, the polynomial interpolation of Equation (3.57) can be used.

For cranes, parabolic trajectories are natural to avoid obstacles. Such a trajectory, connecting the same two equilibria of the load as the straight line trajectory depicted in Figure 3.13 is presented in Figure 3.15. The corresponding motor torques are given in Figure 3.16.

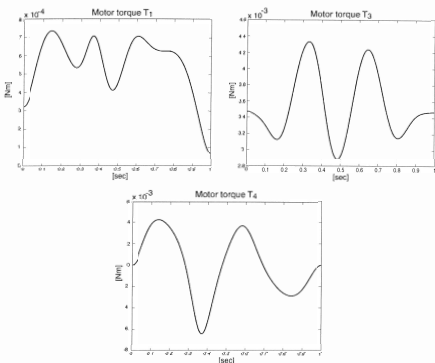[3]All calculations are made using Matlab

Figure 3.14: Motor torques generating the horizontal displacement; see Figure 3.12 for the notations T_1, T_3 and T_4

Actuator dimensioning

Flatness based motion planning was used for dimensioning the actuators (i.e. DC motors) of the small size model of the 3D US Navy crane. The problem of actuator dimensioning in our case consisted of finding the characteristics of the DC motors winding the ropes and rotating the platform with the boom such that sufficiently high masses (say up to one kilogram) can be displaced at a sufficiently high velocity.

A possible solution consists of calculating the static tensions corresponding to some equilibrium of the load with the maximal mass, multiplying the obtained values by a number estimating the necessary overload during dynamic displacements, and finally choosing the motor-gearbox pair with the suitable power. The crucial point of this method is the estimation of the forces which are necessary to overcome the dynamic effects along the trajectory. It turns out that one has a certain tendency to underestimate these dynamic effects, in particular for the motor winding the horizontal rope attached to the free pulley and for the motor rotating the platform, since these motors deliver low (or zero) torques if the load is in equilibrium.

Based on the flatness property and the above presented motion planning algorithm, one can calculate the necessary motor torques for any load trajectory together with the corresponding
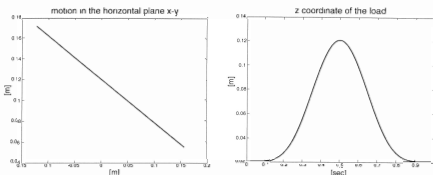
Figure 3.15: Parabolic displacement of the load

velocities of the motor axes. This allows to consider the maximum values along any kind of trajectory and to find the satisfactory motor-gearbox combinations without underestimating the dynamic effects. For displacements considered to be best, simulations show that the dynamic effects overcome largely the static effects as shown in Figures 3.14, 3.18, and 3.16. This holds true both for the presented straight line and parabolic displacements.

3.4 Global measurement feedback stabilization

The aim of the closed loop control is to stabilize an equilibrium or a reference trajectory of the load. This section deals with the stabilization of an equilibrium, the closed loop tracking problem is studied in the next section.

For real cranes, measurements of all configuration variables are not available. In particular, there is no direct information about the position of the load and the angles between the rope sections because of the lack of sufficiently robust sensors resisting to shocks, dust, oil, and abrupt changes of the environment (e.g. an artificial vision system providing information about the position of the load, or more precisely about the position of the hook, should deliver exact measurements in all weather and lightening conditions). The uncompleteness of the measurement information obstructs the use of state feedback techniques.

Nevertheless, robust sensors are mounted on the axes of the motors actuating the moving part of the mechanical structure and the winches. These sensors measure the angular positions of the motor axes and/or their velocities. In the sequel we suppose that the angular positions and velocities of all motors are measured.

One of the "simplest" regulators which can be constructed from these measurements is a linear proportional-derivative type controller on the rope lengths and the position of the moving part of the mechanical structure. We show that this regulator is able to globally stabilize any desired equilibrium of the load. Our notion of global stability assures the convergence to the desired equilibrium in closed loop from most initial configurations in the crane's workspace with pulling tension in the ropes.
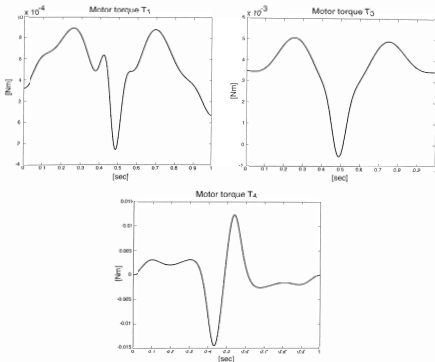
Figure 3.16:   Motor torques generating the parabolic trajectory; see Figure 3.12 for the notations T_1, T_3 and T_4

Some stability definitions and theorems are recalled first. Next, we show that any equilibrium in the workspace of the 2D model of the US Navy crane (studied in Section 3.1.1) can be globally stabilized using PD controllers. Finally, global stability in closed loop is also shown for all 3D examples of Section 3.2.4, including the 3D US Navy crane.

3.4.1   Stability definitions and theorems

This material is standard and repeated here for completeness. More details can be found in [29]. Consider the system

$$\dot{x} = f(x), \qquad x \in \mathbb{R}^n \qquad (3.58)$$
$$f(0) = 0$$

where $f(x)$ is Lipschitz continuous and let $x(t, x_0)$ denote the unique solution of the above system with initial condition $x(0) = x_0$.

Definition 7 (stability). The equilibrium $x = 0$ of (3.58) is stable if for all $\epsilon > 0$, there exists a $\delta > 0$, such that $\| x_0 \| < \delta \Rightarrow \| x(t, x_0) \| < \epsilon$, for all $t \geq 0$.
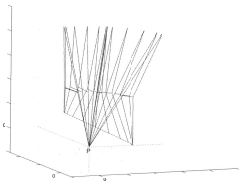
Figure 3.17: Straight line displacement in three dimensions

Definition 8 (asymptotic stability). *The equilibrium $x = 0$ of (3.58) is asymptotically stable if it is stable and*

$$\lim_{t \to \infty} x(t, x_0) = 0.$$

A sufficient stability condition is given by the following theorem.

Theorem 4 (Lyapunov's second method). *If there is a function $V(x)$ such that*

1. $V(x) > 0, \ \forall x \in \mathcal{U} \subset \mathbb{R}^n, x \neq 0$

2. $L_f V(x) < 0, \ \forall x \in \mathcal{U} \subset \mathbb{R}^n, x \neq 0$ *and* $L_f V(0) = 0$

where $\mathcal{U}$ is a neighborhood of 0, then 0 is locally asymptotically stable. Moreover, if $\mathcal{U} = \mathbb{R}^n$ and $V(x)$ is radially unbounded, i.e. $V(x) \to \infty$ as $\| x \| \to \infty$, then 0 is globally stable.

If $L_f V(x)$ vanishes for a set of points including the origin then the stability of the origin is not guaranteed. In order to deal with this case one needs some additional definitions.

Definition 9 (invariant set). *A set $\mathcal{I}$ is said to be invariant with respect to (3.58) if,*

$$\forall x_0 \in \mathcal{I} \qquad x(t, x_0) \in \mathcal{I}, \quad \forall t \in \mathbb{R}.$$

Definition 10 (positively invariant set). *A set $\mathcal{I}$ is said to be positively invariant with respect to (3.58) if,*

$$\forall x_0 \in \mathcal{I} \qquad x(t, x_0) \in \mathcal{I}, \quad \forall t \geq 0.$$

Definition 11 (approaching a set). *We say that a solution $x(t)$ of (3.58) approaches a set $\mathcal{M}$ as $t \to \infty$, if for each $\epsilon > 0$, there is a $T > 0$ such that*

$$\inf_{\bar{x} \in \mathcal{M}} \| x(t) - \bar{x} \| < \epsilon, \quad \forall t > T$$

velocity of the fourth motor axis

torque delivered by motor 4

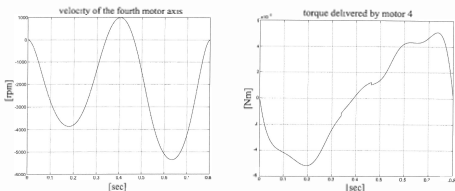Figure 3.18: The rpm (revolutions per minute) and the torque delivered by the fourth motor (rotating the platform with the boom), corresponding to the trajectory illustrated in Figure 3.17 (travelling duration equals to 0.8 sec)

Theorem 5 (LaSalle's Invariance Theorem). *Let $\mathcal{C} \subset \mathcal{U} \subset \mathbb{R}^n$ be a compact set that is positively invariant w.r.t. (3.58). Let V $\mathcal{U} \to \mathbb{R}$ be a continuously differentiable function such that $L_f V(x) \leq 0$ for all $x \in \mathcal{U}$. Let $\mathcal{N}$ be the set of all points in $\mathcal{C}$ where $L_f V(x) = 0$. Let $\mathcal{M}$ be the largest invariant set in $\mathcal{N}$ Then, every solution starting in $\mathcal{C}$ approaches $\mathcal{M}$ as $t \to \infty$.*

3.4.2 PD controller for the 2D US Navy crane

The modelling of the 2D US Navy crane has been undertaken in Section 3.1.1 and an implicit model given by Equations (3.1)-(3.5) has been obtained. Recall that (x, z) are the coordinates of the load at the point C. The masses of the load and the ropes are assumed unstretchable, hence $T_2 = T_3$.

The information provided by the sensors allow to calculate (after a suitable initialization process) the rope lengths L_1 and R. We consider also the velocity of these variables as measured.

Note that Equations (3.1c)-(3.1e) can be rewritten as

$$(x_B - (k+l)\sin\alpha)^2 + (z_B - (k+l)\cos\alpha)^2 - L_2^2 = 0 \qquad (3.59a)$$
$$(x_B - x)^2 + (z_B - z)^2 - L_3^2 = 0 \qquad (3.59b)$$
$$(x_B - k\sin\alpha)^2 + (z_B - k\cos\alpha)^2 - L_1^2 = 0. \qquad (3.59c)$$

These equations have the same form as the geometric constraints in Section 3.2 and will be used in the stability analysis.

The planar US Navy crane has three degrees of freedom, hence the minimal number of generalized coordinates is three. A possible choice is $q = (\gamma, L_1, R)^T$ including the measured variables L_1 and R. All remaining variables can be expressed as functions of q using the geometry of the crane given by (3.1). The only external *efforts are* the torques u_1 and u_2 delivered by the DC motors hoisting the ropes.

Let $(\bar{x}, \bar{z})$ denote an open-loop equilibrium position of the load. Then, one may calculate the equilibrium of the remaining variables using the following relations:

$$
\begin{aligned}
\bar{\theta} &= 0 & \sin \bar{\beta} &= \frac{\bar{x} - k \sin \alpha}{l} & \bar{\gamma} &= \frac{1}{2}\left(\pi + \beta - \alpha\right) \\
\bar{R} &= l\left(1 - \cos(\alpha - \bar{\beta})\right)\frac{\sin(\bar{\gamma} - \bar{\beta})}{\sin \bar{\gamma}} + (k + l)\cos \alpha - \bar{z} \\
\bar{L}_1 &= l\frac{\sin \bar{\beta}}{\sin \bar{\gamma}} & \bar{T}_2 &= T_3 = mg & \bar{T}_1 &= 2mg \cos \bar{\gamma}.
\end{aligned}
\tag{3.60}
$$

Notice that due to the geometry of the crane, $\gamma \in (\frac{\pi - \alpha}{2}, \frac{\pi}{2})$, hence $\sin \bar{\gamma} > 0$.

Remark 29. *The open-loop equilibria given by (3.60) are not isolated points in the configuration space of the model, they form a two-dimensional manifold.*

The aim of the closed loop control is to stabilize the load at a given equilibrium $(\bar{x}, \bar{z})$ such that $(\bar{x}, \bar{z})$ is a point under the boom. We claim that this can be achieved using (linear) PD controllers, provided that the friction terms η_1 and η_2, which are assumed to depend only on the measured variables $L_1, \dot{L}_1, R, \dot{R}$, are exactly compensated, namely

$$
\tilde{u}_1 = u_1 - \eta_1(L_1, \dot{L}_1) \qquad \tilde{u}_2 = u_2 - \eta_2(R, \dot{R}).
\tag{3.61}
$$

(See Remarks 31 and 32 concerning the methods used to compensate friction effects for experiments on the small size model). The PD controllers read

$$
\tilde{u}_1 = \rho_1\left(\bar{T}_1 + k_{dL_1}\dot{L}_1 + k_{pL_1}(L_1 - \bar{L}_1)\right)
\tag{3.62}
$$

$$
\tilde{u}_2 = \rho_2\left(\bar{T}_2 + k_{dR}\dot{R} + k_{pR}(R - \bar{R})\right)
\tag{3.63}
$$

where the *a priori* rope tensions $\bar{T}_1$ and $\bar{T}_2$ are determined using Equation (3.60) and k_{pL_1}, k_{pR}, k_{dL_1}, and k_{dR} are constant gains to be determined to achieve satisfactory performance.

The crane has, in the absence of the controllers, kinetic and potential energy due to the load with mass m and kinetic energy due to the inertia J_1 and J_2 of the winches. Let W_k denote the total kinetic energy and W_p the potential gravitational energy. Extra energy can be stored in the controller in closed loop, due to the constant a priori and proportional terms. This energy will be denoted by W_{ctrl}.

Thus, the energy function W consists of three terms:

$$
W = W_k + W_p + W_{ctrl},
\tag{3.64}
$$

with

$$
\begin{aligned}
W_k &= \frac{1}{2}\left(m(\dot{x}^2 + \dot{z}^2) + \frac{J_1}{\rho_1^2}\dot{L}_1^2 + \frac{J_2}{\rho_2^2}\dot{R}^2\right) \\
W_p &= mgz \\
W_{ctrl} &= \frac{1}{2}k_{pL_1}(L_1 - \bar{L}_1)^2 + T_1 L_1 + \frac{1}{2}k_{pR}(R - \bar{R})^2 + \bar{T}_2 R.
\end{aligned}
$$

Since x and z can be expressed as functions of the generalized coordinates as

$$x = (k+l)\sin\alpha - l\frac{\sin\left(\gamma - \arcsin\left(\frac{L_1\sin\gamma}{l}\right)\right)}{\sin\gamma}\sin\left(\alpha - \arcsin\left(\frac{L_1\sin\gamma}{l}\right)\right) +$$
$$\left(R - l\frac{\sin\left(\gamma - \arcsin\left(\frac{L_1\sin\gamma}{l}\right)\right)}{\sin\gamma}\right)\sin\left(\pi - 2\gamma - \alpha + \arcsin\left(\frac{L_1\sin\gamma}{l}\right)\right)$$

$$z = (k+l)\cos\alpha - l\frac{\sin\left(\gamma - \arcsin\left(\frac{L_1\sin\gamma}{l}\right)\right)}{\sin\gamma}\cos\left(\alpha - \arcsin\left(\frac{L_1\sin\gamma}{l}\right)\right) -$$
$$\left(R - l\frac{\sin\left(\gamma - \arcsin\left(\frac{L_1\sin\gamma}{l}\right)\right)}{\sin\gamma}\right)\cos\left(\pi - 2\gamma - \alpha + \arcsin\left(\frac{L_1\sin\gamma}{l}\right)\right)$$

the crane dynamics in *closed loop* can be obtained by applying

$$\frac{d}{dt}\frac{\partial\mathcal{L}}{\partial\dot{q}_i} - \frac{\partial\mathcal{L}}{\partial q_i} = F_{q_i} \qquad i=1, \quad .3$$

where $\mathcal{L} = W$ $q_1 = \gamma$, $q_2 = L_1$, $q_3 = R$, and F_{q_i} is the associated generalized force, i.e. $F_\gamma = 1$, $F_R = k_{dR}\dot{R}$, and $F_{L_1} = k_{dL_1}\dot{L}_1$ due to the derivative terms in the controllers. Notice that the proportional terms and the constant a priori forces are already in the function W due to the term W_{ctrl}, and thus absent in the F_{q_i}. Notice also that the actual choice of the generalized coordinates does not lead to the most compact formulation of the dynamics, but will make the derivation of the necessary lemmas easy.

The proof of the global stability of the equilibrium $(\bar{x}, \bar{z})$ in closed loop uses LaSalle's Invariance Theorem. Its application needs some preparatory lemmas.

Lemma 3. *The time derivative of the energy function is*

$$\frac{dW}{dt} = -k_{dL_1}\dot{L}_1^2 - k_{dR}\dot{R}^2$$

Proof. The proof is an easy adaptation of derivations appearing in most textbooks on classical mechanics that prove energy conservation in purely Lagrangian systems (without dissipation) [25, 65]. Here extra terms are present due to the derivative components in the controller.   □

Let us now characterize the trajectories of the closed loop system such that $\dot{R} = 0$ and $\dot{L}_1 = 0$, (i.e. $\frac{d}{dt}W = 0$). Note that the use of $x(t) \equiv \bar{x}$ means that the variable x stays for all times at the value $\bar{x}$ and that barred variables refer to the desired equilibrium to be stabilized, determined from $(x,\bar{z})$ using Equation (3.60).

Lemma 4. *The unique invariant trajectory in closed loop along which $\frac{dW}{dt} = 0$, namely $\dot{R} = 0$ and $\dot{L}_1 = 0$, is the desired equilibrium, i.e. $x(t) \equiv \bar{x}$, $z(t) \equiv \bar{z}$.*

Proof. First, let us show that $\dot{R} = \dot{L}_1 = 0$ implies that the closed loop system is at its equilibrium. The input torques u_1 and u_2 drive directly the dynamics of the winches winding ropes of lengths L_1 and R and generate the rope tensions. From Equations (3.4)-(3.5) we have

$$\tilde{u}_1 = T_1\rho_1 - \frac{J_1}{\rho_1}\ddot{L}_1$$

$$\tilde{u}_2 = T_2\rho_2 - \frac{J_2}{\rho_2}\ddot{R}$$

(recall that the friction terms η_1 and η_2 are compensated). Applying the PD feedback law, given by Equation (3.62) and (3.63) where $\bar{T}_1$ and $\bar{T}_2$ are the forces corresponding to the equilibrium position $(\bar{x}, \bar{z})$, determined by Equation (3.60), we get

$$\rho_1 \left(\bar{T}_1 + k_{dL_1} \dot{L}_1 + k_{pL_1}(L_1 - \bar{L}_1) \right) = T_1 \rho_1 - \frac{J_1}{\rho_1} \ddot{L}_1$$

$$\rho_2 \left(\bar{T}_2 + k_{dR} \dot{R} + k_{pR}(R - \bar{R}) \right) = T_2 \rho_2 - \frac{J_2}{\rho_2} \ddot{R}.$$

Since $\dot{R} = \dot{L}_1 = 0$ by assumption, denote the constant values of L_1 and R by $\hat{L}_1$, $\hat{R}$. ($\bar{R}$ is the desired equilibrium and $\hat{R}$ is the real equilibrium. We wish to show precisely that these equilibria coincide.) This yields,

$$T_1 = T_1 + k_{pL_1}(\hat{L}_1 - L_1) = \hat{T}_1 \tag{3.65}$$

$$T_2 = T_2 + k_{pR}(\hat{R} - \bar{R}) = \hat{T}_2, \tag{3.66}$$

showing that the motors deliver constant torques. Notice that by Equation (3.11) we have that

$$2\cos\gamma(t) = \frac{T_1(t)}{T_2(t)}.$$

Since $T_1(t) \equiv \hat{T}_1$ and $T_2(t) \equiv \hat{T}_2$ are constant, so must be $\gamma(t) \equiv \hat{\gamma}$ thus γ is also constant. But this shows that all configuration variables are constant if $\dot{L}_1 = 0$ and $\dot{R} = 0$. It follows that all variables of the system are constant, hence the only trajectory compatible with $\frac{dW}{dt} = 0$ is an equilibrium of the system.

It remains to show that the equilibrium characterized by the hatted variables coincides with the desired equilibrium given by the barred variables. First, observe that for every equilibrium position of the load $\bar{T}_2 = \hat{T}_2 = mg$ (see Equation (3.60)). Reporting this in (3.66) we get

$$0 = \hat{R} - \bar{R}$$

and we conclude that $\hat{R} = \bar{R}$. The equalities $\bar{L}_1 = \hat{L}_1$ and $\gamma = \hat{\gamma}$ will be proved by contradiction (see Figure 3.19). For, suppose that $\bar{\gamma} > \hat{\gamma}$. Recall that $\ddot{\theta} = \ddot{\theta} = 0$, thus (3.7) implies $\bar{\beta} > \hat{\beta}$. Since $\hat{\gamma}, \bar{\gamma} \in (\frac{\pi - \alpha}{2}, \frac{\pi}{2}]$ it is easily verified that

$$\bar{L}_1 = l\frac{\sin\beta}{\sin\gamma} = l\frac{\sin(2\bar{\gamma} - \pi + \alpha)}{\sin\bar{\gamma}}$$

is a strictly increasing function of its argument, thus we conclude that $L_1 > \hat{L}_1$. Noticing that $k_{pL_1} > 0$ and using (3.65) we have that $\hat{T}_1 > \bar{T}_1$. But then the relations $\bar{T}_1 = 2mg\cos\bar{\gamma}$ and $\hat{T}_1 = 2mg\cos\hat{\gamma}$ imply that $\bar{\gamma} < \hat{\gamma}$, a contradiction. One arrives to a similar contradiction supposing that $\gamma < \hat{\gamma}$ thus we conclude that $\bar{\gamma} = \hat{\gamma}$ and $L_1 = \hat{L}_1$. Since the equilibria of the configuration variables coincide, the same holds true for all variables of the system, and in particular for the position of the load as claimed. $\square$

Lemma 5. *The function W defined by (3.64) is bounded from below, i.e. there exists a real number c such that $W > c$.*
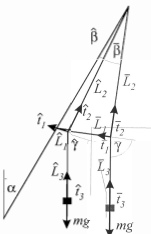
Figure 3.19:   The two equilibria coincide: reasoning by contradiction

Proof. All quadratic terms in W are bounded from below. The terms $\bar{T}_1 L_1$ and $\bar{T}_2 R$ are also bounded from below since both L_1, R, and $\bar{T}_i$, $i = 1, 2$, are positive. It remains to show that the term mgz is dominated if $z \to -\infty$. For, observe that Equations (3.59a) and (3.59b) implies that L_2 or L_3 tends to $+\infty$ if $z \to -\infty$. Since $R = L_2 + L_3$, all rope length being positive, this implies that R goes to $+\infty$ if z goes to $-\infty$. But then the quadratic term $\frac{1}{2} k_{pR}(R - \bar{R})^2$ dominates the term mgz and thus W is bounded from below. $\square$

Lemma 6. *Consider the set U in the configuration space defined by $W \leq C$ with $C \in \mathbb{R}$ such that $C > c$, c being the lower bound of W. All state variables are bounded on U.*

Proof. From the definition of W and since W is bounded from below by Lemma 5, it is clear that $\dot{x}$, $\dot{z}$, L_1, R, and $\bar{R}$ are bounded on U. But, using the quadratic relation given by Equation (3.59c), x_B and x_B are also bounded, and using (3.59b), the same holds true for x and z. Thus, by the geometric constraints, γ and $\dot{\gamma}$ are also bounded. $\square$

The main stability theorem for the planar model of the US Navy crane together with the PD controllers given by Equations (3.62)-(3.63) is as follows.

Theorem 6. *The equilibrium $(x, \bar{z})$ of the two-dimensional US Navy crane is globally asymptotically stabilized in closed loop using the PD controllers (3.62)-(3.63) with positive but otherwise arbitrary gains k_{pL_1}, k_{dL_1}, k_{pR}, k_{dR} and with friction compensation (3.61).*

Proof. Choose a sufficiently large C such that, for both the initial condition (in the crane's workspace with pulling rope tensions) and the equilibrium, $W < C$ with W being the function defined in (3.64). Define the set $\mathcal{C} = \{(q, \dot{q}) \mid W(q, \dot{q}) \leq C\}$. Using Lemma 3, we get $\frac{dW}{dt} = -k_{dR}\dot{R}^2 - k_{dL_1}\dot{L}_1^2$. Since $\frac{dW}{dt} \leq 0$, the system's trajectories stay in $\mathcal{C}$, hence $\mathcal{C}$ is positively invariant. By Lemma 6, the set $\mathcal{C}$ is compact. Lemma 4 characterizes the set $\mathcal{M} = \{(q, \dot{q})$

$\frac{dW}{dt} = 0\}$ as being the equilibrium point $(\bar{x}, \bar{z})$ to be stabilized. The claim follows by applying Theorem 5 with the previously defined sets $\mathcal{C}$ and $\mathcal{M}$, and $V = W$ □

Remark 30. *Notice that the model was obtained under the hypothesis that the cables were rigid and thus could transmit positive and negative forces to the winches which is not the case for real cranes. As long as $0 < \gamma < \frac{\pi}{2}$, T_1 is guaranteed to be positive and the force can be transmitted.*

Simulation study

Note that, though the PD controller presented in the previous section (and its 3D version, studied in the next one) has been successfully experimented on the reduced size model of the US Navy crane, we can only present simulation results[4] since we do not have sensors to measure the position of the load or the angles of the ropes nor to record them. Such measurements should be made possible in the future by processing the images of a camera.

The crane model is simulated using the following parameters: $m_1 = 0.2$ [kg], $J_1 = J_2 = 6.25 \cdot 10^{-3}$ [kg/m²], $l = 0.35$ [m], $\alpha = 0.445$ [rad]. These parameters correspond to the 1:80 small scale model of a real US Navy crane at disposal at the Centre Automatique et Systèmes.

The equilibrium position is set to $\bar{x} = -0.1$ [m] and $z = -0.5[m]$. The simulation results are given in Figure 3.20. The tuning of the gains has been done in simulation and the gains have been set to $k_{pR} = 20$, $k_{pL_1} = 10$, $k_{dR} = 10$ and $k_{dL_1} = 20$. Note that the global stability of the regulator is not sensitive to the values of the design parameters as shown by Theorem 6.

Friction compensation for real experiments

The following two remarks are in order about the methods and results concerning friction compensation on the motor axes.

Remark 31. *For the real closed loop experiments on the small size model of the US Navy crane, the compensation of friction relies on a simple friction model including kinetic, negative viscous (Stribeck Effect). and viscous frictions (see [4]). The corresponding coefficients are identified experimentally. Moreover, small amplitude sinusoidal excitations (in tensions) are applied permanently on the motors in order to avoid as much as possible the region of small velocities.*

Remark 32. *It has been observed during the experiments on the small size model of the US Navy crane that a residual, poorly damped oscillation, which remains inside a vertical cone, is present due to the uncompensated (or under-compensated) friction effects. In fact, the residual frictions make unobservable these oscillations since they "dissipate" completely the corresponding tension variations in the ropes. Moreover, the amplitude of the residual oscillation depends on the mass of the load since oscillations with higher amplitudes of a load with less mass result identic variations of the tensions in the ropes as lower amplitude oscillations with higher mass. Nevertheless, during the experiments, the residual oscillations remained always small w.r.t. the oscillations generated by external disturbances.*

---

[4]Some camera recorded experiences can be downloaded at the site of the Centre Automatique et Systèmes (http://cas.ensmp.fr).
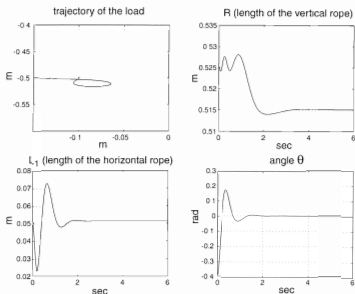
Figure 3.20: Closed-loop behaviour under PD control

3.4.3 PD controller for the 3D examples of Section 3.2.4

We show in this section that for all cranes, studied in Section 3.2.4, any equilibrium of the load can be globally stabilized using PD controllers.

Recall that global stability means convergence to the desired equilibrium in closed loop from almost all initial configurations in the crane's workspace (this is precisely defined in the theorem on closed loop stability). Recall that pushing tensions in the ropes have no physical meaning for real cranes.

All proofs use LaSalle's Invariance Theorem, given in Section 3.4.1. For each example we start with the formulae giving the equilibrium values of all variables corresponding to the desired equilibrium of the load and give the expression of the PD controller. Then we construct and energy function W to be used in the stability proof. In all cases, the proof of the main global stability theorem relies on a series of lemmas as in the previous subsection. The first lemma shows that the time derivative of W along the integral curves in closed loop is negative or zero. Next we show that the equilibrium to be stabilized is one of the finite isolated equilibria in closed loop. This is followed by the characterization of the trajectories along which the time derivative of W vanish. Finally, the boundedness of the level sets of W is shown on $\mathcal{S}$, the set on which the considered crane may evolve.

The proofs of similar lemmas may be identical or may differ only in some details of calculations. In those cases the proof is presented for only one of the three studied cranes.

3D cantilever crane

The model of this crane is given in Example 9. We wish to stabilize the load equilibrium $(\bar{x}_1, \bar{x}_2, \bar{x}_3)^T$ such that $\bar{x}_1^2 + \bar{x}_2^2 \neq 0$ and $\bar{x}_3 < 0$ (i.e. the load is under the rotating rail at a nonzero distance from the rotation axis). Setting to zero the LHS of the dynamics given by Equation (3.47) and using the constraints (3.44), one can calculate the equilibria of all configuration variables, all Lagrange multipliers, and all input forces, denoted by $\bar{q}$, $\bar{\lambda}_i$, $i = 1, \ldots, 5$, and $\bar{T}_i$, $i = 1, \ldots, 3$, respectively:

$$
\begin{aligned}
&\bar{x}_{01} = \bar{x}_1 && \bar{x}_{02} = \bar{x}_2 && \bar{x}_{21} = \frac{r\bar{x}_1}{\sqrt{\bar{x}_1^2 + \bar{x}_2^2}} \\
&\bar{x}_{22} = \frac{r\bar{x}_2}{\sqrt{\bar{x}_1^2 + \bar{x}_2^2}} && \bar{L}_0 = r + \sqrt{\bar{x}_1^2 + \bar{x}_2^2} && \bar{L}_1 = \alpha_1 r + \sqrt{\bar{x}_1^2 + \bar{x}_2^2} \\
&\bar{L}_2 = r + \sqrt{\bar{x}_1^2 + \bar{x}_2^2} - \bar{x}_3 && \bar{\lambda}_1 = \frac{mg}{\alpha_1 r - \sqrt{\bar{x}_1^2 + \bar{x}_2^2}} && \bar{\lambda}_2 = -\frac{mg}{r + \sqrt{\bar{x}_1^2 + \bar{x}_2^2}} \\
&\bar{\lambda}_3 = \frac{mg}{\bar{x}_3} && \bar{\lambda}_4 = \frac{(1-\alpha_1)mg}{r} && \bar{\lambda}_5 = 0 \\
&\bar{T}_1 = mg && \bar{T}_2 = -mg && \bar{T}_3 = 0.
\end{aligned}
\tag{3.67}
$$

The sensors are mounted on the motor axes and measure the angular positions and velocities, hence the rope lengths L_1, L_2, and the rotation angle of the rail, defined as

$$
\xi = \begin{cases}
\arctan\left(\frac{x_{22}}{x_{21}}\right) & \text{if } x_{21} \geq 0 \\
-\pi + \arctan\left(\frac{x_{22}}{x_{21}}\right) & \text{if } x_{21} < 0 \text{ and } x_{22} < 0 \\
\pi + \arctan\left(\frac{x_{22}}{x_{21}}\right) & \text{if } x_{21} < 0 \text{ and } x_{22} \geq 0.
\end{cases}
\tag{3.68}
$$

such that $\xi \in (-\pi, +\pi]$, can be calculated together with the corresponding velocities $\dot{L}_1$, $\dot{L}_2$, and $\dot{\xi}$. Define the error variables as $e_{q_i} = \bar{q}_i - q_i$ where q_i stands for the ith component of q and q_i for its equilibrium value. Moreover, define similarly $e_\xi = \bar{\xi} - \xi$. Consider the following PD controller:

$$
\begin{aligned}
T_1 &= \bar{T}_1 + k_{d1}\dot{e}_{L_1} + k_{p1}e_{L_1} \\
T_2 &= \bar{T}_2 + k_{d2}\dot{e}_{L_2} + k_{p2}e_{L_2} \\
T_3 &= k_{d3}\dot{e}_\xi + k_{p3}e_\xi
\end{aligned}
\tag{3.69}
$$

where k_{pi} and k_{di}, $i = 1, \ldots, 3$ are positive numbers and according to the fact that $\bar{T}_3 = 0$. Let

$$
W_{ctrl} = \frac{1}{2}\left(\sum_{i=1}^{2} k_{pi}e_{L_i}^2 + k_{p3}r^2 e_\xi^2\right) + \sum_{i=1}^{2} \bar{T}_i e_{L_i}
\tag{3.70}
$$

denote the "potential" energy stored in the controller and define the following energy-like function:

$$
W = W_k + W_p + W_{ctrl}
\tag{3.71}
$$

where W_k and W_p are defined by (3.46) and W_{ctrl} by (3.70).

Lemma 7 *The derivative of W along the closed loop trajectories of the system is given by*

$$
\frac{dW}{dt} = -k_{d1}\dot{e}_{L_1}^2 - k_{d2}\dot{e}_{L_2}^2 - k_{d3}r^2\dot{e}_\xi^2.
$$

Proof. Differentiating W and replacing the closed loop accelerations obtained from Equation (3.47) using (3.69) of the PD controller, we get

$$\frac{dW}{dt} = \sum_{i=1}^{5} \lambda_i \frac{d}{dt} C_i(q) - \sum_{i=1}^{2} k_{di} \dot{L}_i^2 + k_{d3} \dot{\xi}(\dot{x}_{21} x_{22} - \dot{x}_{22} x_{21}) + k_{p3} e_{\xi}(\dot{x}_{22} x_{22} - \dot{x}_{21} x_{21} - r^2 \dot{\xi}).$$

(3.72)

Differentiating Equation (3.68) and using Constraint (3.44c) we have

$$r^2 \dot{\xi} = (\dot{x}_{22} x_{21} - \dot{x}_{21} x_{22})$$

Reporting this expression in (3.72) and noting that $\frac{d}{dt} C_i(q) = 0$, $i = 1, \ldots, 5$, the lemma follows.   □

Lemma 8. *Consider the closed loop system obtained from the dynamics (3.47) with the PD controller (3.69). It has two isolated equilibria, one of which being given by* $(\bar{x}_1, \bar{x}_2, \bar{x}_3)$.

Proof. Let a closed loop equilibrium of the system be denoted by $\hat{q}$ and assume that $\hat{x}_3 < 0$. The vector $\hat{q}$ satisfies the following set of equations:

$$0 = -\hat{\lambda}_3(\hat{x}_{01} - \hat{x}_1) \tag{3.73a}$$

$$0 = -\hat{\lambda}_3(\hat{x}_{02} - \hat{x}_2) \tag{3.73b}$$

$$0 = -\hat{\lambda}_3 \hat{x}_3 - mg \tag{3.73c}$$

$$0 = -\hat{\lambda}_3(\hat{x}_{01} - \hat{x}_1) + \hat{\lambda}_1(\hat{x}_{01} - \alpha_1 \hat{x}_{21}) + \hat{\lambda}_2(\hat{x}_{01} - \hat{x}_{21}) - \hat{\lambda}_5 \hat{x}_{22} \tag{3.73d}$$

$$0 = -\hat{\lambda}_3(\hat{x}_{02} - \hat{x}_2) + \hat{\lambda}_1(\hat{x}_{02} - \alpha_1 \hat{x}_{22}) + \hat{\lambda}_2(\hat{x}_{02} - \hat{x}_{22}) + \hat{\lambda}_5 \hat{x}_{21} \tag{3.73e}$$

$$0 = -\hat{\lambda}_3(\hat{L}_2 - \hat{L}_0) - \hat{\lambda}_2 \hat{L}_0 \tag{3.73f}$$

$$0 = -\hat{\lambda}_1 \hat{L}_1 + mg + k_{p1}(\bar{L}_1 - \hat{L}_1) \tag{3.73g}$$

$$0 = -\hat{\lambda}_3(\hat{L}_2 - \hat{L}_0) - mg + k_{p2}(\bar{L}_2 - \hat{L}_2) \tag{3.73h}$$

$$0 = -\hat{\lambda}_1 \alpha_1(\hat{x}_{01} - \alpha_1 \hat{x}_{21}) - \hat{\lambda}_2(\hat{x}_{01} - \hat{x}_{21}) + \hat{\lambda}_4 \hat{x}_{21} + \hat{\lambda}_5 \hat{x}_{02} - k_{p3}(\bar{\xi} - \hat{\xi}) \hat{x}_{22} \tag{3.73i}$$

$$0 = -\hat{\lambda}_1 \alpha_1(\hat{x}_{02} - \alpha_1 \hat{x}_{22}) - \hat{\lambda}_2(\hat{x}_{02} - \hat{x}_{22}) + \hat{\lambda}_4 \hat{x}_{22} - \hat{\lambda}_5 \hat{x}_{01} + k_{p3}(\bar{\xi} - \hat{\xi}) \hat{x}_{21} \tag{3.73j}$$

together with Constraints (3.44).

We proceed as in (3.67). Considering (3.73a), (3.73b), (3.73c) with $\hat{x}_3 < 0$, and (3.44d), (3.44e), we have $\hat{x}_i = \bar{x}_{0i}$, $i = 1, 2$, $\hat{\lambda}_3 = \frac{mg}{\hat{x}_3}$, $\hat{x}_{21} = -\frac{r \bar{x}_1}{\sqrt{\hat{x}_1^2 + \hat{x}_2^2}}$, $\hat{x}_{22} = -\frac{r \bar{x}_2}{\sqrt{\hat{x}_1^2 + \hat{x}_2^2}}$ and, according to (3.44a)–(3.44c), $\hat{L}_0 = r + \sqrt{\hat{x}_1^2 + \hat{x}_2^2}$, $\hat{L}_1 = \alpha_1 r + \sqrt{\hat{x}_1^2 + \hat{x}_2^2}$ and $\hat{L}_2 = r + \sqrt{\hat{x}_1^2 + \hat{x}_2^2} - \hat{x}_3$. Then, using (3.73d)–(3.73f), we get $\hat{\lambda}_5 = 0$ and $\hat{\lambda}_1 = \frac{mg}{\alpha_1 r + \sqrt{\hat{x}_1^2 + \hat{x}_2^2}}$, $\hat{\lambda}_2 = -\frac{mg}{r + \sqrt{\hat{x}_1^2 + \hat{x}_2^2}}$. Again, according to (3.73i), (3.73j), we obtain $\bar{\xi} - \hat{\xi} = 0$ and $\hat{\lambda}_4 = \frac{(1 - \alpha_1) mg}{r}$. Thus, comparing the latter expression of $\hat{L}_1$ with (3.73g), we conclude that $\hat{L}_1 = \bar{L}_1$. Again, comparing the expression of $\hat{L}_2$ with (3.73h), we conclude that $\hat{L}_2 = \bar{L}_2$. It results that $\hat{x}_i = \bar{x}_i$, $i = 1, 2$, $\hat{x}_{2i} = \bar{x}_{2i}$, $i = 1, 2$, $\hat{\lambda}_i = \bar{\lambda}_i$, $i = 1, \ldots, 5$ and $\hat{x}_3 = \bar{x}_3$ which achieves to prove that $\hat{q} = \bar{q}$ if $\hat{x}_3 < 0$.

Consider now the opposite case $\hat{x}_3 > 0$. Since $\hat{L}_2 - \hat{L}_0$ must be positive and according to Constraint 3.44c, $\hat{x}_3 = \hat{L}_2 - \hat{L}_0$. Reporting this relation and the results of the previous discussion in (3.73), the remaining nontrivial equations are

$$
\begin{aligned}
0 &= 2mg + k_{p1}(\bar{L}_1 - \hat{L}_1) \\
0 &= -2mg + k_{p2}(\hat{L}_2 - \hat{L}_2) \\
0 &= (\alpha_1 - 1)mg + \hat{\lambda}_4 r
\end{aligned}
\tag{3.74}
$$

which allows to calculate the equilibrium values $\hat{L}_1$, $\hat{L}_2$ and $\hat{\lambda}_4$, different from the desired equilibrium and the lemma follows. □

Remark 33. *Notice that, in the case $\hat{x}_3 > 0$, the load stands above the trolley and the resulting tension of the rope attached to the load is $\bar{T}_1 + k_{p1}(\bar{L}_1 - \hat{L}_1) = mg - 2mg = -mg < 0$ which means that the rope is pushed, a highly unrealistic situation in practice.*

Lemma 9. *$\frac{dW}{dt} = 0$ implies that the system in closed loop is in equilibrium.*

Proof. We need to show that all variables are constant if $\frac{dW}{dt} = 0$. According to Lemma 7 $\frac{dW}{dt} = 0$ implies that all measured variables are in equilibrium i.e. $\dot{L}_1 = 0$, $\dot{L}_2 = 0$ and $\dot{\xi} = 0$. Denote the equilibrium values of these variables by a hat, i.e. $L_1 = \hat{L}_1$, $L_2 = \hat{L}_2$, and $\xi = \hat{\xi}$. Since the RHS of Equation (3.69) is constant, the same holds true for the motor forces. Let us denote their constant values by $\bar{T}_1$, $\bar{T}_2$, and $\bar{T}_3$, respectively.

Observe that $\dot{\xi} = 0$ implies that $\dot{x}_{21} = \dot{x}_{22} = 0$. Constraint (3.44d) implies that $\dot{x}_{21}x_{21} + \dot{x}_{22}x_{22} = 0$ and, together with $r^2\dot{\xi} = \dot{x}_{22}x_{21} - \dot{x}_{21}x_{22} = 0$, which proves that $\dot{x}_{21} = \dot{x}_{22} = 0$, or $x_{21} = \hat{x}_{21}$ and $x_{22} = \hat{x}_{22}$. Further, using Constraints (3.44a) and (3.44e), we get that x_{01} and x_{02} are constant, namely $x_{01} = \hat{x}_{01}$ and $x_{02} = \hat{x}_{02}$ and, by (3.44b), we immediately deduce that L_0 is constant, i.e. $L_0 = \hat{L}_0$.

We next prove that λ_1 is constant by remarking that (3.47g) reads $0 = -\lambda_1\hat{L}_1 + \bar{T}_1 + k_{p1}(\bar{L}_1 - \hat{L}_1)$, thus $\lambda_1 = \hat{\lambda}_1$. Accordingly, since (3.47h) reads $0 = -\lambda_3(\hat{L}_2 - \hat{L}_0) + \bar{T}_2 + k_{p2}(\bar{L}_2 - \hat{L}_2)$, we have $\lambda_3 = \hat{\lambda}_3$ and, by (3.47f), $\lambda_2 = \hat{\lambda}_2$. Now, (3.47i) and (3.47j) read

$$
\begin{aligned}
0 &= -\hat{\lambda}_1\alpha_1(\hat{x}_{01} - \alpha_1\hat{x}_{21}) - \hat{\lambda}_2(\hat{x}_{01} - \hat{x}_{21}) + \lambda_4\hat{x}_{21} + \lambda_5\hat{x}_{02} - k_{p3}(\hat{\xi} - \hat{\xi})\hat{x}_{22} \\
0 &= -\hat{\lambda}_1\alpha_1(\hat{x}_{02} - \alpha_1\hat{x}_{22}) - \hat{\lambda}_2(\hat{x}_{02} - \hat{x}_{22}) + \lambda_4\hat{x}_{22} - \lambda_5\hat{x}_{01} + k_{p3}(\hat{\xi} - \hat{\xi})\hat{x}_{21}
\end{aligned}
$$

which proves, by remarking that $\det\begin{pmatrix} \hat{x}_{21} & \hat{x}_{02} \\ \hat{x}_{22} & \hat{x}_{01} \end{pmatrix} = -\hat{x}_{21}\hat{x}_{01}(1 + \tan^2\hat{\xi}) \neq 0$, that $\lambda_4 = \hat{\lambda}_4$ and $\lambda_5 = \hat{\lambda}_5$. Finally, using (3.47d) and (3.47e), the same argument yields $x_1 = \hat{x}_1$ and $x_2 = \hat{x}_2$ and, combined with (3.44c), $x_3 = \hat{x}_3$ which achieves to prove the Lemma. □

Lemma 10. *The function W defined by (3.71) is bounded from below on S (defined by (3.45)), i.e. there exists a finite real number c such that $c \leq W(q, \dot{q})$ for all $(q, \dot{q}) \in S$.*

Proof. Since $W = W_k + (\frac{1}{2}k_{p1}e_{L_1}^2 + \bar{T}_1 e_{L_1}) + (\frac{1}{2}k_{p2}e_{L_2}^2 + \bar{T}_2 e_{L_2} + mgx_3)$ and since $W_k \geq 0$ and $\frac{1}{2}k_{p1}e_{L_1}^2 + \bar{T}_1 e_{L_1} = \frac{1}{2}k_{p1}\left(e_{L_1} + \frac{\bar{T}_1}{k_{p1}}\right)^2 - \frac{\bar{T}_1^2}{2k_{p1}}$, we have $W \geq -\frac{\bar{T}_1^2}{2k_{p1}} + (\frac{1}{2}k_{p2}e_{L_2}^2 + \bar{T}_2 e_{L_2} + mgx_3)$ But, taking into account (3.44c), we have $x_3^2 = (L_2 - L_0)^2 - (x_{01} - x_1)^2 - (x_{02} - x_3)^2 \leq (L_2 - L_0)^2 \leq L_2^2$ and since $x_3 \leq 0$, we get $x_3 \geq -L_2$. Thus $mgx_3 \geq -mgL_2 = mge_{L_2} - mg\bar{L}_2$ and $\frac{1}{2}k_{p2}e_{L_2}^2 + \bar{T}_2 e_{L_2} + mgx_3 \geq \frac{1}{2}k_{p2}e_{L_2}^2 + (\bar{T}_2 + mg)e_{L_2} - mg\bar{L}_2 = \frac{1}{2}k_{p2}\left(e_{L_2} + \frac{\bar{T}_2 + mg}{k_{p2}}\right)^2 - \frac{(\bar{T}_2 + mg)^2}{2k_{p2}} - mg\bar{L}_2$. Using the fact that $\bar{T}_2 = -mg$, we have proved that $W \geq -\frac{\bar{T}_1^2}{2k_{p1}} - mg\bar{L}_2 = c$ and the lemma follows. $\square$

Lemma 11. *Every level set $W(q, \dot{q}) = C$ on S, with $C > c$, c being the lower bound of W on S, is bounded.*

Proof. Assume that $W = C$. Following the same lines as in the previous lemma, we get:

$$C' = C + \frac{\bar{T}_1^2}{2k_{p1}} + mg\bar{L}_2 \geq W_k + \frac{1}{2}k_{p1}\left(e_{L_1} + \frac{\bar{T}_1}{k_{p1}}\right)^2 + \frac{1}{2}k_{p2}e_{L_2}^2 + \frac{r^2}{2}k_{p3}e_\xi^2 \tag{3.75}$$

with

$$W_k = \frac{1}{2}\left[\sum_{i=1}^{3} m_i \dot{x}_i^2 + \sum_{i=1}^{2}(m_0 \dot{x}_{0_i}^2 + M\dot{x}_{2_i}^2) + \sum_{i} m_i \dot{L}_i^2\right]$$

From the inequality (3.75), we immediately deduce that

$$\dot{x}_i^2 \leq C_{1,i} \quad \dot{x}_{0_i}^2 \leq C_{1,0_i} \quad \dot{x}_{2_i}^2 \leq C_{1,2_i} \quad \dot{L}_i^2 \leq C_{1,L_i} \quad i = 1, 2 \quad \dot{x}_3^2 \leq C_{1,3}$$

and

$$\left(e_{L_1} + \frac{\bar{T}_1}{k_{p1}}\right)^2 \leq C_1 \quad e_{L_2}^2 \leq C_2 \quad e_\xi^2 \leq C_\xi$$

where $C_{1,i}$, $C_{1,0_i}$, $C_{1,2_i}$, C_{1,L_i}, C_1, C_2, C_ξ are suitable positive constants and since $\bar{L}_1$, $\bar{L}_2$, $\bar{\xi}$ are bounded L_1, L_2 and ζ are also bounded. Now, Constraint (3.44d) yields $x_{21}^2 \leq r^2$ and $x_{22}^2 \leq r^2$. Next, using Constraint (3.44a), we obtain $x_{01}^2 \leq C_{01}$ and $x_{02}^2 \leq C_{02}$ for suitable constants C_{01}, C_{02}. It follows, using Constraint (3.44b), that $L_0^2 \leq C_{L0}$ and, again, since $(L_2 - L_0)^2 \leq C_{L20}$, by (3.44c), we get $x_1^2 \leq C_1'$, $x_3^2 \leq C_2'$. Finally, we have already proved that $0 \geq x_3 \geq -L_2$ which achieves to prove that q and $\dot{q}$ are bounded. $\square$

Theorem 7 *Denote by $\tilde{q}$ the equilibrium different from $\bar{q}$, the desired equilibrium given by the position of the load $(\bar{x}_1, \bar{x}_2, \bar{x}_3)^T$. There exists a positive number $\tilde{C}$ such that for all initial conditions $(q_I, \dot{q}_I) \in S$ with $W(q_I, \dot{q}_I) < \tilde{C}$, the trajectory of the closed loop system converges to $\bar{q}$.*

Proof. Recall first that $W(\bar{q}, 0) = mg\bar{x}_3 < 0$ by construction. Let $\tilde{C} = W(\tilde{q}, 0)$. Using the definition of W (Equation (3.71)) we have

$$\tilde{C} = \frac{1}{2}\sum_{i=1}^{2}k_{pi}(L_i - \tilde{L}_i)^2 + \sum_{i=1}^{2}\bar{T}_i(\bar{L}_i - \tilde{L}_i) + mg\tilde{x}_3. \tag{3.76}$$

Observe that $\bar{T}_1 = mg$ and $\bar{T}_2 = -mg$ by Equation (3.67), and further, by Equation (3.74), we have $\hat{L}_1 - \bar{L}_1 = -\frac{2mg}{k_{p1}}$ and $\hat{L}_2 - \bar{L}_2 = \frac{2mg}{k_{p2}}$. By the proof of Lemma 8, the equilibrium $\hat{q}$ is such that $\hat{x}_3 > 0$. Replacing in (3.76) we get $\hat{C} = mg\hat{x}_3$, hence $W(\bar{q}, 0) < \hat{C}$

Define the set $\mathcal{S}_{\hat{C}} = \left\{ (q, \dot{q}) \in \mathcal{S} \quad W(q, \dot{q}) < \hat{C} \right\}$ By the preceding discussion, the set $\mathcal{S}_{\hat{C}}$ contains the equilibrium $\bar{q}$. Moreover, $\mathcal{S}_{\hat{C}}$ is bounded by Lemma 11 and positively invariant by Lemma 7. Applying LaSalle's Invariance Theorem, all trajectories starting in $\mathcal{S}_{\hat{C}}$ approach $\bar{q}$ as $t \to \infty$. □

Remark 34. *The set $\mathcal{S}_{\hat{C}}$ cannot be easily described by a set of inequalities on the components of q and $\dot{q}$. However, it can be seen that it contains all feasible configurations where the load is under the crane at the condition that the initial velocity is small enough if the initial distance to the equilibrium point is large.*

3D overhead crane

The model of this crane is obtained in Example 10. The control objective is the same as for the cantilever crane of the preceding subsection: the stabilization of a load equilibrium given by $(\bar{x}_1, \bar{x}_2, \bar{x}_3)^T$ such that $\bar{x}_3 < 0$. From the dynamics (3.51), the equilibrium values of the remaining variables can be obtained as

$$
\begin{array}{llll}
\bar{x}_{02} = \bar{x}_2 & \bar{x}_{01} = \bar{x}_1 & \bar{L}_0 = \bar{x}_1 \\
\bar{L}_1 = \bar{x}_1 + 1 - \alpha_1 & \bar{L}_2 = -\bar{x}_3 + \bar{x}_1 & \bar{\lambda}_1 = \frac{mg}{\bar{x}_1 + 1 - \alpha_1} \\
\bar{\lambda}_2 = -\frac{mg}{\bar{x}_1} & \bar{\lambda}_3 = \frac{mg}{\bar{x}_3} & \bar{T}_1 = mg \\
\bar{T}_2 = -mg & \bar{T}_3 = 0.
\end{array}
\tag{3.77}
$$

The measured variables are L_1, L_2, and x_{02}, the position of the moving part of the structure (i.e. the bridge with the rail). Defining the error variables as in the preceding subsection, the PD controller reads

$$
\begin{aligned}
T_1 &= \bar{T}_1 + k_{d1}\dot{e}_{L_1} + k_{p1}e_{L_1} \\
T_2 &= \bar{T}_2 + k_{d2}\dot{e}_{L_2} + k_{p2}e_{L_2} \\
T_3 &= k_{d3}\dot{e}_{x_{02}} + k_{p3}e_{x_{02}},
\end{aligned}
\tag{3.78}
$$

with k_{di} and k_{pi}, $i = 1, \quad , 3$, real positive numbers and using that $\bar{T}_3 = 0$ by (3.77). Let the potential energy stored in the above PD controller be defined as

$$
W_{ctrl} = \frac{1}{2}\left(\sum_{i=1}^{2} k_{pi}e_{L_i}^2 + k_{p3}e_{x_{02}}^2 \right) + \sum_{i=1}^{2}\bar{T}_i e_{L_i},
$$

and introduce

$$
W = W_k + W_p + W_{ctrl}
\tag{3.79}
$$

where W_k and W_p are defined by Equation (3.50). We can now state similar lemmas as for the 3D cantilever crane in the preceding paragraph with similar proofs which are omitted.

Lemma 12. *The derivative of W along the closed loop trajectories of the system is given by*

$$\frac{dW}{dt} = -k_{d1}\dot{e}_{L_1}^2 - k_{d2}\dot{e}_{L_2}^2 - k_{d3}\dot{e}_{x_{02}}^2.$$

Lemma 13. *Consider the closed loop system obtained from the dynamics (3.51) with the PD controller (3.78). It has two isolated equilibria, one of which is given by $(\bar{x}_1, \bar{x}_2, \bar{x}_3)^T$.*

Lemma 14. $\frac{dW}{dt} = 0$ *implies that the system in closed loop is in equilibrium.*

Lemma 15. *The function W defined by (3.79) is bounded from below on S (the set S is defined by (3.49)), i.e. there exists a finite real number c such that $c \leq W(q, \dot{q})$ for all $(q, \dot{q}) \in S$.*

Lemma 16. *Consider a level set of $W(q, \dot{q})$ on S, such that $W = C$, where $C > c$, c being the lower bound of W on S. This level set is bounded.*

Theorem 8. *Denote by $\tilde{q}$ the equilibrium different from $\bar{q}$. For all initial conditions $(q_I, \dot{q}_I) \in S$ such that $W(q_I, \dot{q}_I) < W(\tilde{q}, 0) = \tilde{C}$, the closed loop trajectories approach the desired equilibrium $\bar{q}$, given by the position of the load $(\bar{x}_1, \bar{x}_2, \bar{x}_3)^T$.*

Note that Remark 34 also applies here.

3D US Navy crane

The model of the 3D US Navy crane is presented in Example 11. We wish to stabilize the equilibrium $(\bar{x}_1, \bar{x}_2, \bar{x}_3, \bar{x}_{03})^T$ such that $\alpha_1 r < \sqrt{\bar{x}_1^2 + \bar{x}_2^2} < r$ and $\bar{x}_3 < \bar{x}_{03} < \frac{\sqrt{\bar{x}_1^2 + \bar{x}_2^2}}{r}x_{33}$ (i.e. both the free pulley and the load are under the boom). The equilibria of the configuration variables, Lagrange multipliers, and input forces are:

$$
\begin{aligned}
&\bar{x}_{01} = \bar{x}_1 && \bar{x}_{02} = \bar{x}_2 && \bar{x}_{31} = \frac{r\bar{x}_1}{\sqrt{\bar{x}_1^2 + \bar{x}_2^2}} \\
&\bar{x}_{32} = \frac{r\bar{x}_2}{\sqrt{\bar{x}_1^2 + \bar{x}_2^2}} && \bar{L}_0 = \sqrt{(x_{33} - \bar{x}_{03})^2 + (r - \sqrt{\bar{x}_1^2 + \bar{x}_2^2})^2} && \bar{\lambda}_4 = -\frac{mg}{\bar{x}_{03} - \bar{x}_3} \\
&\bar{L}_1 = \sqrt{(\alpha_1 x_{33} - \bar{x}_{03})^2 + (\alpha_1 r - \sqrt{\bar{x}_1^2 + \bar{x}_2^2})^2} && \bar{T}_3 = -mg \\
&\bar{L}_2 = \sqrt{(\alpha_2 x_{33} - \bar{x}_{03})^2 + (\alpha_2 r - \sqrt{\bar{x}_1^2 + \bar{x}_2^2})^2} && \bar{\lambda}_3 = -\frac{mg}{\bar{L}_0} \\
&L_3 = \bar{x}_{03} - \bar{x}_3 + \sqrt{(x_{33} - \bar{x}_{03})^2 + (\alpha_2 r - \sqrt{\bar{x}_1^2 + \bar{x}_2^2})^2} && \bar{T}_4 = 0.
\end{aligned}
\tag{3.80}
$$

(Recall that x_{33} is a geometric parameter and not a configuration variable, hence it has no equilibrium value.) The equilibrium values $\bar{\lambda}_1$, $\bar{\lambda}_2$, $\bar{\lambda}_5$, $\bar{T}_1$, and $\bar{T}_2$ can be obtained by solving the (linear) Equations (3.56h), (3.56i), (3.56f), (3.56d), and (3.56k) (resp. Equations (3.56h), (3.56i), (3.56f), (3.56e), and (3.56l)) if $\dot{x}_1 \neq 0$ (resp. $\dot{x}_1 = 0$) with vanishing LHS.

Moreover, define the rotation angle of the platform as

$$\xi = \begin{cases} \arctan(\frac{x_{32}}{x_{31}}) & \text{if } x_{31} \geq 0 \\ -\pi + \arctan(\frac{x_{32}}{x_{31}}) & \text{if } x_{31} < 0 \text{ and } x_{32} < 0 \\ \pi + \arctan(\frac{x_{32}}{x_{31}}) & \text{if } x_{31} < 0 \text{ and } x_{32} \geq 0 \end{cases} \quad (3.81)$$

which is similar to (3.68). Let the error variables be calculated the same way as for the cantilever crane (including e_ξ). The PD controller reads

$$\begin{aligned} T_1 &= \bar{T}_1 + k_{d1}\dot{e}_{L_1} + k_{p1}e_{L_1} \\ T_2 &= \bar{T}_2 + k_{d2}\dot{e}_{L_2} + k_{p2}e_{L_2} \\ T_3 &= \bar{T}_3 + k_{d3}\dot{e}_{L_3} + k_{p3}e_{L_3} \\ T_4 &= \bar{T}_4 + k_{d4}\dot{e}_\xi + k_{p4}e_\xi \end{aligned} \quad (3.82)$$

and the potential energy stored in the controller is given by

$$W_{ctrl} = \frac{1}{2} \left(\sum_{i=1}^{3} k_{pi}e_{L_i}^2 + r^2 k_{p4}e_\xi^2 \right) + \sum_{i=1}^{3} \bar{T}_i e_{L_i}. \quad (3.83)$$

Introduce the function

$$W = W_k + W_p + W_{ctrl} \quad (3.84)$$

where W_k and W_p are defined by (3.55) and W_{ctrl} by (3.83).

Lemma 17 *The derivative of W along the closed loop trajectories of the system is given by*

$$\frac{dW}{dt} = -k_{d1}\dot{e}_{L_1}^2 - k_{d2}\dot{e}_{L_2}^2 - k_{d3}\dot{e}_{L_3}^2 - k_{d4}r^2\dot{e}_\xi^2.$$

Proof. Simple adaptation of the proof of Lemma 7 $\qquad\square$

Lemma 18. *Consider the closed loop system obtained from the dynamics (3.56) with the PD controller (3.82). It has a finite number of isolated equilibria, one of which is given by $(\bar{x}_1, \bar{x}_2, \bar{x}_3)^T$ and $\bar{x}_{03}$.*

Proof. Recall that all rope lengths L_1, L_2, L_3, and $L_3 - L_0$ are assumed to be positive. Denote by $\hat{q}$ an equilibrium of the closed loop system and by $\hat{\lambda}_i$, $i = 1, \ldots, 5$, the equilibria of the

corresponding Lagrange multipliers. Then $\hat{q}$ and $\hat{\lambda}_i$ satisfy

$$0 = -\hat{\lambda}_4(\hat{x}_{01} - \hat{x}_1) \tag{3.85a}$$

$$0 = -\hat{\lambda}_4(\hat{x}_{02} - \hat{x}_2) \tag{3.85b}$$

$$0 = -\hat{\lambda}_4(\hat{x}_{03} - \hat{x}_3) - mg \tag{3.85c}$$

$$0 = \hat{\lambda}_4(\hat{x}_{01} - \hat{x}_1) + \hat{\lambda}_1(\hat{x}_{01} - \alpha_1\hat{x}_{31}) + \hat{\lambda}_2(\hat{x}_{02} - \alpha_2\hat{x}_{31}) + \hat{\lambda}_3(\hat{x}_{01} - \hat{x}_{31}) \tag{3.85d}$$

$$0 = \hat{\lambda}_4(\hat{x}_{02} - \hat{x}_2) + \hat{\lambda}_1(\hat{x}_{02} - \alpha_1\hat{x}_{32}) + \hat{\lambda}_2(\hat{x}_{02} - \alpha_2\hat{x}_{32}) + \hat{\lambda}_3(\hat{x}_{02} - \hat{x}_{32}) \tag{3.85e}$$

$$0 = \hat{\lambda}_4(\hat{x}_{03} - \hat{x}_3) + \hat{\lambda}_1(\hat{x}_{03} - \alpha_1 x_{33}) + \hat{\lambda}_2(\hat{x}_{03} - \alpha_2 x_{33}) + \hat{\lambda}_3(\hat{x}_{03} - x_{33}) - m_0g \tag{3.85f}$$

$$0 = \hat{\lambda}_4(\hat{L}_3 - \hat{L}_0) - \hat{\lambda}_3\hat{L}_0 \tag{3.85g}$$

$$0 = -\hat{\lambda}_1\hat{L}_1 + \hat{T}_1 + k_{p1}(\bar{L}_1 - \hat{L}_1) \tag{3.85h}$$

$$0 = -\hat{\lambda}_2\hat{L}_2 + \hat{T}_2 + k_{p2}(\bar{L}_2 - \hat{L}_2) \tag{3.85i}$$

$$0 = -\hat{\lambda}_4(\hat{L}_3 - \hat{L}_0) + \hat{T}_3 + k_{p3}(\bar{L}_3 - \hat{L}_3) \tag{3.85j}$$

$$0 = -\hat{\lambda}_1\alpha_1(\hat{x}_{01} - \alpha_1\hat{x}_{31}) - \hat{\lambda}_2\alpha_2(\hat{x}_{01} - \alpha_2\hat{x}_{31}) - \hat{\lambda}_3(\hat{x}_{01} - \hat{x}_{31}) + \hat{\lambda}_5\hat{x}_{31} - k_{p4}(\bar{\xi} - \hat{\xi})\hat{x}_{32} \tag{3.85k}$$

$$0 = -\hat{\lambda}_1\alpha_1(\hat{x}_{02} - \alpha_1\hat{x}_{32}) - \hat{\lambda}_2\alpha_2(\hat{x}_{02} - \alpha_2\hat{x}_{32}) - \hat{\lambda}_3(\hat{x}_{02} - \hat{x}_{32}) + \hat{\lambda}_5\hat{x}_{32} + k_{p4}(\bar{\xi} - \hat{\xi})\hat{x}_{31}. \tag{3.85l}$$

A similar proof to the ones of the previous examples, roughly speaking using elimination arguments, can be done here. However, to break the monotony, we now propose a different proof based on more physical and geometric ideas.

From Equation (3.85c) we have that $\hat{\lambda}_4 \neq 0$ and $\hat{x}_3 - \hat{x}_{03} \neq 0$, hence it follows from Equations (3.85a)-(3.85b) that $\hat{x}_1 = \hat{x}_{01}$ and $\hat{x}_2 = \hat{x}_{02}$, i.e. the rope section between the free pulley and the load is vertical. The equilibrium implies that the net force at the free pulley is zero, hence the resultant force transmitted by the ropes of lengths L_1 and L_2, and by the rope section of length L_0 must be also vertical. Since these rope sections are coplanar, their common plane is again vertical. Hence both the free pulley and the load are in the same vertical plane which is determined by the boom.

Without loss of generality, we may assume that the choice of the base frame is such that $\hat{x}_{02} = \hat{x}_2 = \hat{x}_{32} = 0$. Reporting this in Equation (3.85l), we have that

$$0 = k_{p4}(\bar{\xi} - \hat{\xi})\hat{x}_{31}$$

hence $\bar{\xi} = \hat{\xi}$ (since $k_{p4} > 0$ and $\hat{x}_{31} \neq 0$). Using Constraint (3.53e) and the definition of the rotation angle ξ (Equation (3.81)), we have that $\hat{x}_{31} = \bar{x}_{31}$, and by the choice of the base frame $\bar{x}_{32} = \hat{x}_{02} - \hat{c}_2 = 0$. Thus we conclude again (as for the 3D cantilever crane) that for all equilibria in closed loop, the orientation of the boom with the winches coincide with its desired position.

For the equilibria positions of the free pulley and the load in the vertical plane determined by the boom, one can distinguish four cases to obtain four different equilibria:

1. $\hat{x}_3 < \hat{x}_{03} < \frac{\hat{x}_{01}}{\hat{x}_{31}} x_{33}$: the equilibrium $\hat{q}$ coincides with $\bar{q}$

2. $\hat{x}_3 > \hat{x}_{03}$ and $\hat{x}_{03} < \frac{\hat{x}_{01}}{\hat{x}_{31}} x_{33}$ (the load is higher than the free pulley): $\hat{q}$ differs from $\bar{q}$

3. $\hat{x}_3 < \hat{x}_{03}$ and $\hat{x}_{03} > \frac{\hat{x}_{01}}{\hat{x}_{31}} x_{33}$ (the free pulley is over the boom): $\hat{q}$ differs from q

4. $\hat{x}_3 > \hat{x}_{03}$ and $\hat{x}_{03} > \frac{\hat{s}_{21}}{\hat{s}_{31}}\hat{x}_{33}$ (the free pulley is over the boom and the load is higher than the free pulley). $\hat{q}$ differs from $\bar{q}$.

The last three equilibria exist mathematically but have no physical meaning for real cranes because they imply pushing forces along one or more rope sections.   □

Lemma 19. $\frac{dW}{dt} = 0$ implies that the system in closed loop is in equilibrium.

Proof. $\frac{dW}{dt} = 0$ implies that $\dot{L}_1 = \dot{L}_2 = \dot{L}_3 = \dot{\xi} = 0$ using Lemma 17, hence the rope lengths L_i, $i = 1, \ldots, 3$, are constant. Denote the constant values by a hat so that $L_i(t) \equiv \hat{L}_i$ and $\xi(t) \equiv \hat{\xi}$. The constant rope lengths $\hat{L}_i$ also imply that L_0 is constant since the rope sections of length L_1, L_2, and L_0 terminate all on the free pulley, thus $L_0(t) \equiv \hat{L}_0$. From the expression of the PD controller (3.82), we have that $T_i(t) \equiv \hat{T}_i$, $i = 1, \ldots, 4$.

The constant rope lengths imply that the LHS of equations (3.56h)-(3.56j) vanish and the Lagrange multipliers λ_1, λ_2, and λ_4 are constant, their constant values being $\hat{\lambda}_1 = \frac{\hat{T}_1}{\hat{L}_1}$, $\hat{\lambda}_2 = \frac{\hat{T}_2}{\hat{L}_2}$, and $\hat{\lambda}_4 = \frac{\hat{T}_3}{\hat{L}_3 - \hat{L}_0}$. Then Equation (3.56g) gives $\hat{\lambda}_3 = \hat{\lambda}_4 \frac{\hat{L}_3 - \hat{L}_0}{\hat{L}_0}$.

Now, let us use the fact that ξ is also constant which implies, using its definition (3.81) and Constraint (3.53e), that x_{31} and x_{32} are constant. Denote their constant values by $\hat{x}_{31}$ and $\hat{x}_{32}$. Without loss of generality, we may chose the orientation of the base frame such that $\hat{x}_{32} = 0$. Then Equation (3.56l) can be rewritten as

$$0 = -x_{02}(\hat{\lambda}_1\alpha_1 + \hat{\lambda}_2\alpha_2 + \hat{\lambda}_3) + \hat{T}_4\hat{x}_{31},$$

hence $x_{02}(t) \equiv \hat{x}_{02}$. With a different choice of the orientation of the base frame, such that $\hat{x}_{31} = 0$, we have similar result for x_{01}, thus $x_{01}(t) \equiv \hat{x}_{01}$. (The constant values of these variables are different for different orientations of the base frame. However, to prove the lemma, it is unnecessary to give the equilibria values, it is enough to show that these variables remain constant). Next, replacing in Equation (3.56k) or in Equation (3.56l), all variables are constant except λ_5 which implies $\lambda_5(t) \equiv \hat{\lambda}_5$.

Replacing in Constraint (3.53a):

$$\frac{1}{2}\left((\hat{x}_{01} - \hat{x}_{31})^2 + (\hat{x}_{02} - \hat{x}_{32})^2 + (x_{03} - x_{33})^2 - \hat{L}_0^2\right) = 0,$$

it follows that $x_{03}(t) \equiv \hat{x}_{03}$ since all variables are shown to be constant except x_{03}. Then the LHS of equations (3.56d)-(3.56f) vanish and the only variables which are not proven to be constant on the RHS of these equations are x_1, x_2, and x_3. Hence $x_i(t) \equiv \hat{x}_i$, $i = 1, \ldots, 3$ and the Lemma follows.   □

Lemma 20. The function W defined by (3.84) is bounded from below on $\mathcal{S}$ (the set $\mathcal{S}$ is defined by (3.54)), i.e. there exists a finite real number c such that $c \leq W(q, \dot{q})$ for all $(q, \dot{q}) \in \mathcal{S}$.

Proof. $W_k \geq 0$ by construction. Before studying the terms $W_{ctrl} + W_p$, observe that Constraint (3.53a) implies $(x_{03} - \alpha_1 x_{33})^2 = L_1^2 - (x_{01} - \alpha_1 x_{31})^2 - (x_{02} - \alpha_1 x_{31})^2 \leq L_1^2$, hence, x_{33} being constant, $\alpha_1 x_{33} - L_1 \leq x_{03}$. Similarly, using Constraint (3.53c) we obtain that

$x_{33} - L_0 \leq x_{03} \leq x_{33} + L_0$. Further, using this inequality together with Constraint (3.53d), we get $x_3 - L_3 \leq x_3 \leq x_3 + L_3$. (This inequality is also clear geometrically, since the load cannot be lowered, from the winch of its rope, more than the corresponding rope length.) Let us use now these inequalities to find the lower bound of $W_{ctrl} + W_p$:

$$
\begin{aligned}
W_{ctrl} + W_p &= \sum_{i=1}^{3} \left(\frac{1}{2} k_{pi} e_{L_i}^2 + \bar{T}_i e_{L_i} \right) + r^2 \frac{1}{2} k_{p4} e_\xi^2 + m g x_{03} + m g x_3 \\
&\geq \frac{1}{2} k_{p1} e_{L_1}^2 + \bar{T}_1 e_{L_1} + m g \alpha_1 x_{33} - m g L_1 + m g L_1 - m g \bar{L}_1 + \\
&\quad \frac{1}{2} k_{p2} e_{L_2}^2 + T_2 e_{L_2} + \frac{1}{2} k_{p3} e_{L_3}^2 + \bar{T}_3 e_{L_3} + m g x_{33} - m g L_3 + m g L_3 - m g \bar{L}_3 \\
&= \frac{1}{2} k_{p1} \left(e_{L_1} + \frac{\bar{T}_1 + m g}{k_{p1}} \right)^2 - \frac{(\bar{T}_1 + m g)^2}{2 k_{p1}} + m g (\alpha_1 x_{33} - \bar{L}_1) + \\
&\quad \frac{1}{2} k_{p2} \left(e_{L_2} + \frac{\bar{T}_2}{k_{p2}} \right)^2 - \frac{\bar{T}_2^2}{2 k_{p2}} + \\
&\quad \frac{1}{2} k_{p3} \left(e_{L_3} + \frac{\bar{T}_3 + m g}{k_{p3}} \right)^2 - \frac{(T_3 + m g)^2}{2 k_{p3}} + m g (x_{33} - \bar{L}_3) \\
&\geq - \frac{(\bar{T}_1 + m g)^2}{2 k_{p1}} + m g (\alpha_1 x_{33} - \bar{L}_1) - \frac{\bar{T}_2^2}{2 k_{p2}} - \frac{(\bar{T}_3 + m g)^2}{2 k_{p3}} + m g (x_{33} - \bar{L}_3),
\end{aligned}
$$
(3.86)

hence W is bounded from bellow. $\qquad \square$

Lemma 21. *Consider a level set of $W(q, \dot{q})$ on S, such that $W = C$, where $C > c$, c being the lower bound of W on S. This level set is bounded.*

Proof. Let $W = C$. Using the proof of the previous lemma (see (3.86)) we have that

$$
\begin{aligned}
C' &= C + \frac{(\bar{T}_1 + m g)^2}{2 k_{p1}} - m g (\alpha_1 x_{33} - \bar{L}_1) + \frac{\bar{T}_2^2}{2 k_{p2}} + \frac{(\bar{T}_3 + m g)^2}{2 k_{p3}} - m g (x_{33} - \bar{L}_3) \\
&\geq W_k + \frac{1}{2} k_{p1} \left(e_{L_1} + \frac{\bar{T}_1 + m g}{k_{p1}} \right)^2 + \frac{1}{2} k_{p2} \left(e_{L_2} + \frac{\bar{T}_2}{k_{p2}} \right)^2 + \\
&\quad \frac{1}{2} k_{p3} \left(e_{L_3} + \frac{\bar{T}_3 + m g}{k_{p3}} \right)^2 + r^2 \frac{1}{2} k_{p4} e_\xi^2
\end{aligned}
$$
(3.87)

where W_k is defined by (3.55). It follows that

$$
\dot{x}_i^2 \leq C_{1,i}, \quad \dot{x}_{0i}^2 \leq C_{1,0i}, \quad \dot{L}_i^2 \leq C_{1,Li}, \quad i = 1, \quad, 3 \quad \dot{x}_{3i}^2 \leq C_{1,3i} \quad i = 1, 2
$$

$$
\frac{1}{2} k_{p1} \left(e_{L_1} + \frac{\bar{T}_1 + m g}{k_{p1}} \right)^2 \leq C_{L1} \quad \left(e_{L_2} + \frac{\bar{T}_2}{k_{p2}} \right)^2 \leq C_{L2} \quad \left(e_{L_3} + \frac{\bar{T}_3 + m g}{k_{p3}} \right)^2 \leq C_{L3} \quad e_\xi^2 \leq C_\xi
$$

where $C_{1,i}$, $C_{1,0i}$, $C_{1,Li}$, $i = 1, \quad, 3$, $C_{1,3i}$, $i = 1, 2$, C_{L1}, C_{L2}, C_{L3}, and C_ξ are suitable positive constants. Since $\bar{L}_i$, $i = 1, \quad, 3$, and $\bar{\xi}$ are constant, the variables L_i, $i = 1, \quad, 3$, and ξ are bounded. By Constraint (3.53e), we have that $x_{3i}^2 \leq r$ for $i = 1, 2$.

We use Constraints (3.53) to show that the remaining variables are bounded. For observe that by Constraint (3.53a) there exist positive constants C_{01}, C_{02}, and C_{03} such that $x_{01}^2 \leq C_{01}$, $x_{02}^2 \leq C_{02}$, and $x_{03}^2 \leq C_{03}$. Hence L_0 is also bounded by (3.53c): $L_0^2 \leq C_{L0}$. The variables x_1, x_2, and x_3 are then bounded by (3.53d). The boundedness of $\dot{L}_0$ follows by differentiating (3.53c). □

Theorem 9. *There exists a positive number $\tilde{C}$ such that for all initial conditions $(q_I, \dot{q}_I) \in \mathcal{S}$ with $W(q_I, \dot{q}_I) < \tilde{C}$ the closed loop trajectories approach the desired equilibrium $\bar{q}$, given by the position of the load $(\bar{x}_1, \bar{x}_2, \bar{x}_3)^T$ and by the height of the free pulley $\bar{x}_{03}$.*

Proof. Denote by $\tilde{q}_1$, $\tilde{q}_2$, and $\tilde{q}_3$ the equilibria different from the desired equilibrium $\bar{q}$, and let $\tilde{C}_i = W(\tilde{q}_i, 0)$, $i = 1, 2, 3$. Define $\tilde{C}$ by $\tilde{C} = \min\{\tilde{C}_1, \tilde{C}_2, \tilde{C}_3\}$. Define the set $\mathcal{S}_{\tilde{C}} = \left\{ (q, \dot{q}) \in \mathcal{S} \mid W(q, \dot{q}) \leq \tilde{C} \right\}$. The set $\mathcal{S}_{\tilde{C}}$ is bounded by Lemma 21 and positively invariant by Lemma 17. Applying LaSalle's Invariance Theorem, all trajectories starting in $\mathcal{S}_{\tilde{C}}$ approaches $\bar{q}$ as $t \to \infty$. □

Note again that Remark 34 applies here.

3.5 Local tracking with measurement feedback

The stability of the controllers presented in the previous section makes possible to displace the load from an initial equilibrium $\bar{q}_I$ to a desired new one, denoted by $\bar{q}_F$, by simply changing the references of the measured variables and the input forces in the controller. However, doing so, the path followed by the load approaching the new equilibrium cannot be predicted, and undesired transient motions may occur before the stabilization. Such unpredictable transients are unacceptable if the crane operates in a congested environment.

Therefore, it would be preferable to influence the trajectory of the load between the two equilibria by assuring the tracking of a desired path. The problem of planning such trajectories has been undertaken in Section 3.3. The solution presented there allows to calculate a trajectory $q_c(t)$ of the configuration variables, its derivatives, and the corresponding motor forces T_{ci}, $i = 1, \ldots, d + s + 1$ ($d + s + 1$ gives the number of motors), such that $q_c(t_I) = q_I$ and $q_c(t_F) = \bar{q}_F$ with $t_I < t_F$. Because of the unavailability of measurements on the load position, the initial equilibrium $\bar{q}_F$ for the motion planning can be calculated using only the measured variables (positions of the motor axes) by supposing that the load is close to an equilibrium. Hence, there is a difference between the real initial configuration $q(t_I)$ and the initial configuration $\bar{q}_I$ used for the motion planning.

We investigate in this section the *closed loop* behavior of the 3D US Navy crane (see Example 11) using the same PD controller as for stabilization, but with time-varying references $q_c(t)$ and $T_{ci}(t)$, $i = 1, \ldots, 4$. For we replace in the controller the equilibrium references of the measured variables and the input forces by their trajectories connecting the two equilibria of the load.

To construct the *tracking PD controller*, define $\epsilon_q = q_c - q$ where q is given by (3.52) and let $\epsilon_\xi = \xi_c - \xi$ using (3.81). The tracking PD controller is given by

$$
\begin{aligned}
T_1 &= T_{1c} + k_{d1}\dot{\epsilon}_{L_1} + k_{p1}\epsilon_{L_1} \\
T_2 &= T_{2c} + k_{d2}\dot{\epsilon}_{L_2} + k_{p2}\epsilon_{L_2} \\
T_3 &= T_{3c} + k_{d3}\dot{\epsilon}_{L_3} + k_{p3}\epsilon_{L_3} \\
T_4 &= T_{4c} + k_{d4}\dot{\epsilon}_\xi + k_{p4}\epsilon_\xi.
\end{aligned}
\tag{3.88}
$$

Theorem 10. *Consider a reference trajectory $q_c(t)$ for the 3D US Navy crane connecting two equilibria: $q_c(t_I)$ and $q_c(t_F)$ with $-\infty < t_I < t_F < \infty$ and such that $W(q_c, \dot{q}_c) < \tilde{C}$ for all $t \in (t_I, t_F)$ ($\tilde{C}$ being defined in the proof of Theorem 9). Use the PD controller (3.88) to close the loop. For any such trajectory $q_c(t)$, there exists an open neighborhood V of $q_c(t_I)$ such that all trajectory in closed loop, emanating from V at time t_I, converge to $q_c(t_F)$ as $t \to \infty$.*

Proof. Note that for $t > t_F$, the PD controller coincides with the one given by Equation (3.82) with $\bar{q} = q_c(t_F)$ and $\bar{T}_i = T_{ci}(t_F)$, $i = 1, \ldots, 4$. By Theorem 9, $q_c(t_F)$ is stabilized in closed loop for $t > t_F$, provided that $W(q(t_F), \dot{q}(t_F)) < \tilde{C}$ with W defined by (3.84). Hence, we have to show that there exists an open neighborhood V of $q_c(t_I)$ such that $q(t_F) \in V$ implies that $W(q(t_F), \dot{q}(t_F)) < \tilde{C}$. Observe that $q_c(t_I) = q(t_I)$ implies that $q(t) = q_c(t)$ for all $t > t_I$ and thus $W(q(t), \dot{q}(t)) < \tilde{C}$ for all t, $t_I < t < t_F$, by the motion planning. Moreover, $\dot{q}$ and $\bar{q}$ remain bounded along the trajectory $q(t)$. Thus the neighborhood V exists by the continuity of the system equations in closed loop. $\square$

The theorem doesn't provide information about the local (or eventually global) stability of the trajectory itself, i.e. about the convergence of the error variables ϵ_q along the trajectory, i.e. during the interval $t \in [t_I, t_F]$. Note that the use of the energy function (3.84) in order to conclude about the stability applying LaSalle's Theorem is difficult since the derivatives of q_c and T_{ci}, $i = 1, \ldots, 4$, appear in the $\frac{dV}{dt}$, hence the energy function must be modified in a suitable but yet undiscovered way.

Theorem 10 states that the stability of the final equilibrium is preserved if the initial equilibrium used for the motion planning is known with a small error. Simulations show that the application of the time-varying reference connecting the two equilibria together with the tracking PD controller stabilizes the desired trajectory even if the initial position is known with a relatively high uncertainty. This allows to reduce the transients and oscillations around the final equilibrium and to follow a path avoiding obstacles.

As a conclusion to this section, let us compare the behavior of the stabilizing PD controller and the tracking PD controller for the 3D US Navy crane.

Comparison of the tracking and the stabilizing controllers by simulation (3D US Navy crane example)

Consider the reference trajectory starting from the equilibrium $x_{1I} = 14.2$, $x_{2I} = 1.5$, $x_{3I} = -5$ [cm][5] at $t_I = 0$ and finishing at the equilibrium $x_{1F} = 0.4$, $x_{2F} = 16$ and $x_{3F} = -5$ [cm] at

---

[5]The small distances are due to the fact that the controllers are experimented on the reduced size model of the US Navy crane and the simulator uses the physical parameters of this 1:80 model. Since precise measurements
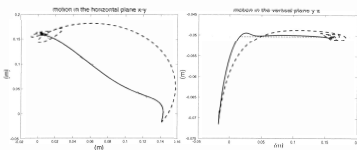
Figure 3.21: Closed-loop tracking behavior under PD control. Trajectories of the load in the horizontal and vertical planes: *i*) stabilizing equilibrium controller (hashed line); *ii*) tracking controller with motion planning; *iii*) reference to steer to equilibrium along a straight line (dotted).
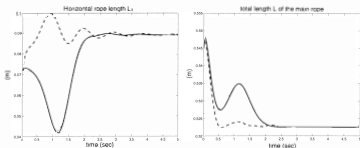

Figure 3.22: Closed-loop tracking behavior under PD control. Trajectory of the rope lengths: *i*) stabilizing equilibrium controller (hashed line); *ii*) tracking controller with motion planning; *iii*) reference to steer to equilibrium along a straight line (dotted).

$t_F = 2.5$ [s].

Figures 3.21-3.24 show the results of the simulation. The stabilizing controller shows a large error with respect to the reference trajectory and the load approximately stops at the end point after more than 3 periods of oscillations. On the contrary, the locally tracking controller shows a much smoother behaviour concerning both tracking and oscillations at the end point. With this tracking controller, the load needs less than 2 periods to get a comparable behavior. This is due to the fact that the reference trajectory arrives at the endpoint with vanishing derivatives up to order 6 and that the deviation with respect to this reference along the trajectory remains much smaller than the deviation with respect to the equilibrium. Thus, the feedback (3.88) yields smaller accelerations and consequently smaller oscillations, though the rate of decay of the energy is the same in both cases.

The settling time of the locally tracking controller is approximately 2.5 [s], almost the same
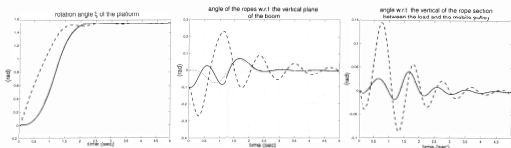
Figure 3.23:   Closed-loop tracking behavior under PD control. Trajectory of the angles: $\imath$)
stabilizing equilibrium controller (hashed line); $\imath\imath$) tracking controller with motion planning;
$\imath\imath\imath$) reference to steer to equilibrium along a straight line (dotted).
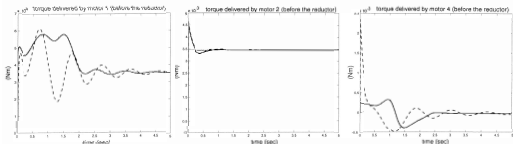
Figure 3.24: Closed-loop tracking behavior, motor torques: $\imath$) stabilizing equilibrium controller
(hashed line); $\imath\imath$) tracking controller with motion planning; $\imath\imath\imath$) reference to steer to equilibrium
along a straight line (dotted).

as the prescribed travelling duration $t_F - t_I$ of the reference trajectory, whereas the settling
time of the global stabilizing controller is about 5 [s] in the same conditions.

Chapter 4

Conclusions

The motion planning problem has been studied in this thesis for two classes of mechanical systems, namely hand-object structures and weight handling equipments (cranes). We have shown that simple solutions can be obtained when they enjoy flatness or Liouvillian properties, without restricting to quasi-static motion or to specific input signals.

In the case of cranes, we have also proved a global stabilization result of an arbitrary equilibrium point by measurement feedback PD controller and shown in simulations that it could be extended to track the reference trajectories computed by our motion planning algorithm.

The classification of HOSs w.r.t. the flatness and Liouvillian properties, however, is not complete. The extension of these properties to larger classes of HOSs, which would enlarge the applicability of the presented motion planning methods, remains an open problem.

It would be also interesting to analyze this problem in the setting of Lagrangian systems and to be able to detect the flatness or Liouvillian property directly on the Lagrangian as we have done for cranes. This could be also motivated by the fact that the flat and Liouvillian approaches are not affected by the presence of system drift which appears once the dynamics are considered in the model. This is not straightforward for methods exploiting the Lie algebraic structure of driftless systems [24, 39, 45, 53]. Note nevertheless that geometric constraints have the same structure for all cranes allowing to conclude that all these mechanisms are flat. For HOSs, the geometric and kinematic constraints depend on the surface geometry of the fingers and the object which makes general statements more difficult to obtain.

The closed loop control of HOSs allowing to stabilize the trajectories calculated by the proposed motion planning algorithms is not addressed in this work. Its study should be the subject of future research.

For the cranes studied in this thesis, the flatness property has been shown for all elements in a class, and the closed loop control, more precisely with measurement feedback, is addressed for some examples in the class. Though the stability results seem to be fairly general, their proof should be adapted in each case to cope with the specific geometry of each kind of crane.

A natural field of application of the motion planning for both classes of mechanical systems is teleoperation or remote control. The operator, supervising the scene thanks to cameras, gives the trajectory of the distant object, for HOSs, e.g. by manipulating a virtual object through a glove equipped with suitable sensors, or that of the distant load, for cranes, using for instance

a joystick or a gamepad.

Note that the motion planning problem studied in this thesis may be slightly adapted to include displacements between two points which are not necessarily equilibrium points — the operator may want to modify on-line the desired final state and the new trajectory must therefore start from the instantaneous transient position of the object or the load, with nonzero velocity, acceleration, and higher order derivatives, and possibly must respect additional constraints on the input variables. This requires additional measurements, for instance using image processing to take profit of the cameras, to obtain such information on-line.

Once the reference trajectories of the actuators and the measured variables are calculated, they are transmitted using a network connection (or eventually another type of telecommunication channel) to the local controller. (Local means here that the controller is located at the same termination of the communication link as the mechanical system.) The aim of the local controller is, as in this thesis, to stabilize the reference trajectory. Note that the visual information may be used as well by the distant operator for his visual feedback, for on-line motion planning and in the local feedback loop.

Such a remote control scheme fits well with the methods developed in this work and might be implemented on the reduced size model of the US Navy crane.

Conclusions

Le problème de la planification de trajectoires a été étudié dans cette thèse pour deux classes de systèmes mécaniques   structures mains-objets et engins de levage (grues). Nous avons obtenu des solutions simples pour les systèmes plats et Liouvilliens, sans se restreindre à des déplacements quasi-statiques ou à l'utilisation de signaux d'entrées particuliers.

Dans le cas des grues, nous avons aussi prouvé un résultat de stabilisation globale d'un point d'équilibre arbitraire par bouclage PD par retour de sortie et montré en simulation que l'on pouvait l'étendre au cas de la poursuite des trajectoires de référence obtenues par planification de trajectoire.

La classification des structures mains-objets selon leurs propriétés d'être plats ou Liouvilliens n'étant pas complète, l'extension de ces propriétés à une classe plus large de structures mains-objets reste ouverte. Cela pourrait également élargir le champ d'application des algorithmes de planification de trajectoires présentés.

Il serait en outre intéressant d'analyser ces propriétés dans le cadre des systèmes Lagrangiens, approche que nous avons utilisée pour les engins de levage. Une telle démarche peut être motivée par le fait que les algorithmes de planification de trajectoires présentés pour les systèmes plats ou Liouvilliens ne sont pas limités aux systèmes sans dérive et peuvent ainsi être utilisés pour les modèles avec dynamique. Cela est moins évident si on utilise les méthodes qui exploitent la structure d'algèbre de Lie des champs de vecteurs des systèmes sans dérive [39, 45, 53, 24]. Il faut cependant noter que les contraintes géométriques ont la même structure pour tous les engins de levage. Dans le cas des structures mains-objets, au contraire, les contraintes dépendent de la géométrie des surfaces des doigts et de l'objet, ce qui ne permet pas d'envisager facilement des résultats plus généraux.

Le problème de la commande en boucle fermée des mains de robots n'est pas abordé dans cette thèse et la stabilisation des trajectoires peut faire l'objet de futures recherches.

Concernant les engins de levage, la platitude a été montrée pour une classe étendue de mécanismes. La boucle fermée, ou plus précisément la commande par retour de sortie, a été étudiée sur quelques exemples de cette classe. Bien que les résultats de stabilité semblent être d'une porté relativement générale, leur preuve doit être adaptée dans chaque cas de grue pour tenir compte de sa géométrie spécifique.

Une application naturelle des algorithmes de planification de trajectoires présentés dans cette thèse est la téléopération ou la commande à distance. L'opérateur, surveillant la scène à l'aide de caméras, donne la trajectoire de l'objet distant, dans le cas de la manipulation, par exemple à l'aide d'un gant équipé de capteurs adaptés, ou de la charge distante, dans le cas de la commande des grues, en utilisant un "joystick" ou une "gamepad"

Une telle configuration pour la commande à distance pose un problème de planification de trajectoire légèrement différent de celui qui est abordé dans ce travail, pour des trajectoires entre deux points qui ne sont plus nécessairement des points d'équilibre. En effet, l'opérateur peut à tout instant vouloir modifier le point final à atteindre, et la nouvelle trajectoire, qui repart de la position actuelle, hors de l'équilibre, doit prendre en compte une vitesse, accélération, etc., initiales instantanées non nulles, et respecter d'éventuelles contraintes sur les entrées. Ce calcul en ligne nécessite des mesures supplémentaires, par exemple par traitement d'images pour tirer profit des caméras.

Les trajectoires de référence sont ensuite transmises au contrôleur local par un réseau ou par une ligne de communication différente. (Le mot local désigne ici l'emplacement physique du contrôleur dont on suppose qu'il se trouve au même nœud de connexion que le système à piloter.) Le but de ce contrôleur est, comme dans ce travail, de stabiliser la trajectoire de référence. Notons que l'information visuelle peut être utilisée aussi bien pour la boucle visuelle réalisée par l'opérateur, que pour la planification de trajectoire en-ligne, ou la boucle de rétroaction locale.

Un tel schéma de commande à distance peut être envisagé dans le cadre des méthodes que nous avons développées et devrait être testé sur la maquette de grue de la marine américaine.

Bibliography

[1] R. Abraham, J.E. Mardsen, and T. Ratiu. *Manifolds, Tensor Analysis, and Applications.* Applied Mathematical Sciences. Springer Verlag, 1988.

[2] P. Appell. *Traité de Mécanique Rationnelle.* Jacques Gabay, Sceaux, France, 6ième edition, 1991.

[3] S. Arimoto, P.T.A. Nguyen, H.Y. Han, and Z. Doulgeri. Dynamics and control of a set of dual fingers with soft tips. *Robotica,* 18:71–80, 2000.

[4] B. Armstrong-Hélouvry. *Control of Machines with Friction.* Kluwer Academic Publisher Boston/Dordrecht/London, 1991.

[5] A. Bicchi and A. Marigo. Rolling contacts and dextrous manipulation. In *Proceedings of the IEEE International Conference on Robotics and Automation,* pages 282–287, San Francisco, CA, April 2000.

[6] R.L. Bryant, S.S. Chern, R.B. Gardner, H.L. Goldschmidt, and P.A. Griffiths. *Exterior Differential Systems.* Springer-Verlag, 1991.

[7] T. Burg, D. Dawson, C. Rahn, and W. Rhodes. Nonlinear control of an overhead crane via the saturating control approach of Teel. In *Proceedings of the International Conference on Robotics and Automation,* pages 3155–3160, 1996.

[8] H. Butler, G. Honderd, and J. Van Amerongen. Model reference adaptive control of a gantry crane scale model. *IEEE Control System Magazine,* pages 57–62, January 1991.

[9] C.C. Cheah, S. Kawamura, H.Y. Han, and S. Arimoto. Grasping and position control of multi-fingered robot hands with uncertain jacobian matrices. In *Proc. of the IEEE Int. Conf. on Robotics and Automation,* pages 2403–2408, May 1998.

[10] A. Chelouah. Extensions of differential flat fields and Liouvillian systems. In *Proceedings of the IEEE Conference on Decision and Control,* pages 4268–4273, San Diego, CA. USA. December 1997

[11] M. Cherif and K.K. Gupta. Planning quasi-static motions for re-configuring object with a multi-fingered robotic hand. In *Proceedings of the IEEE International Conference on Robotics and Automation,* pages 986–991, Albuquerque, New Mexico, USA, April 1997

[12] A. A. Cole, J. E. Hauser, and S. S. Sastry. Kinematics and control of multifingered hands with rolling contact. *IEEE Transactions on Automatic Control,* 34(4):398–404, April 1989.

[13] A. A. Cole, P. Hsu, and S. S. Sastry. Dynamic control of sliding by robot hands for regrasping. *IEEE Transactions on Robotics and Automation*, 8(1):42–52, February 1992.

[14] J. Collado, R. Lozano, and I. Fantoni. Control of a convey-crane based on passivity. In *Proceedings of the American Control Conference*, pages 1260–1264, 2000.

[15] B. D'Andréa-Novel and J. Lévine. Modelling and nonlinear control of an overhead crane. In M.A. Kaashoek, J.H. Van Schuppen, and A.C.M. Ran, editors, *Robust Control of Linear Systems and Nonlinear Control*, pages 523–529. Birkhäuser, Boston, 1989.

[16] B. D'Andréa-Novel, P. Martin, and R. Sépulchre. Full linearization of a class of mechanical systems via dynamic state feedback. In H. Kimura and S. Kodama, editors, *Recent Advances in Mathematical Theory of Systems, Control, Networks and Signal Processing, II*, pages 327–332. Mita Press, Osaka, 1991.

[17] M. Fliess, J. Lévine, Ph. Martin, F. Ollivier, and P. Rouchon. Controlling nonlinear systems by flatness. In C.I. Byrnes, editor *Systems and Control in the Twenty-First Century*, pages 137–154, Boston, 1997

[18] M. Fliess, J. Lévine, Ph. Martin, and P. Rouchon. Sur les systèmes non linéaires différentiellement plats. *C.R. Acad. Sci. Paris*, I-315:619–629, 1992.

[19] M. Fliess, J. Lévine, Ph. Martin, and P. Rouchon. Linéarisation par bouclage dynamique et transformations de Lie-Bäcklund. *C.R. Acad. Sci. Paris*, I-317:981–986, 1993.

[20] M. Fliess, J. Lévine, Ph. Martin, and P. Rouchon. Flatness and defect of nonlinear systems: introductory theory and examples. *International Journal of Control*, 61(6):1327–1361 1995.

[21] M. Fliess, J. Lévine, Ph Martin, and P. Rouchon. Deux applications de la géométrie locale des diffiétés. *Ann. Inst. Henri Poincaré*, 66(3):275–292, 1997

[22] M. Fliess, J. Lévine, Ph. Martin, and P. Rouchon. A Lie-Bäcklund approach to equivalence and flatness of nonlinear systems. *IEEE Transactions on Automatic Control*, 38:700–716, 1999.

[23] D. Fragopoulos, M.P. Spathopoulos, and Y Zheng. A pendulation control system for offshore lifting operations. In *Proceedings of the 14th IFAC Triennal World Congress*, pages 465–470, Beijing, P.R. China, 1999.

[24] B. Goodwine. *Control of Stratified Systems with Robotic Applications*. PhD thesis. California Institute of Technology, 1998.

[25] D. T. Greenwood. *Classical Dynamics*. Prentice-Hall, Englewood Cliffs, N.J., 1977

[26] T. Gustafsson. On the design and implementation of a rotary crane controller. *European Journal of Control*, 2(3):166–175, March 1996.

[27] K.S Hong, J.H. Kim, and K.I Lee. Control of a container crane: Fast traversing, and residual sway control from the perspective of controlling an underactuated system. In *Proceedings of the American Control Conference*, pages 1294–1298, Philadelphia, PA, June 1998.

[28] J.B. Kerr. *An Analysis of Multifingered Hands*. PhD thesis, Dep. Mech. Eng. Stanford University, 1984.

[29] H. K. Khalil. *Nonlinear Systems*. Prentice-Hall, Englewood Cliffs, N.J., second edition, 1996.

[30] B Kiss and J. Lévine. On the control of a reduced scale model of the US Navy cranes. In *Proceedings of the IEEE International Conference on Intelligent Systems*, pages 127–132, Stará Lesná, Slovakia, November 1999.

[31] B. Kiss, J. Lévine, and B. Lantos. Trajectory planning for dextrous manipulation with rolling contacts. In *Proc. of the 38th IEEE Int. Conf. on Decision and Control*, pages 2118–2119, Phenix, Arizona, 1999.

[32] B. Kiss, J. Lévine, and B. Lantos. Trajectory planning for dextrous manipulation with special robotic hand structures. In *Proceedings of the IEEE International Conference on Intelligent Systems*, pages 133–138, Stará Lesná, Slovakia, November 1999.

[33] B. Kiss, J. Lévine, and B. Lantos. Object reconfiguration with rolling contacts using differentially flat robotic hand structures. In *Proceedings of the 6th International Conference on Control, Automation, Robotics and Vision*, pages on CD-ROM, ISBN981–04–2445–6, Singapore, 5-8 December 2000.

[34] B. Kiss, J. Lévine, and B. Lantos. On motion planning for robotic manipulation with rolling contacts. In *Proceedings of the 6th International IFAC Symposium on Robot Control*, pages 639–644, Vienna, Austria, 21-23 September 2000.

[35] B. Kiss, J. Lévine, and Ph. Mullhaupt. Modelling, flatness and simulation of a class of cranes. *Periodica Polytechnica*, 43(3):215–225, 1999.

[36] B. Kiss, J. Lévine, and Ph. Mullhaupt. Control of a reduced size model of US Navy crane using only motor position sensors. In A. Isidori, F. Lamnabhi-Lagarrigue, and W. Respondek, editors, *Nonlinear Control in the Year 2000*, volume 2, pages 1–12. Springer, 2000.

[37] B. Kiss, J. Lévine, and Ph. Mullhaupt. Modeling and motion planning for a class of weight handling equipments. In *Proceedings of the 14th International Conference on Systems Engineering*, Coventry, UK, September 2000.

[38] B Kiss, J. Lévine, and Ph. Mullhaupt. A simple output feedback PD controller for nonlinear cranes. In *Proceedings of the 39th Conference on Decision and Control*, Sydney, Australia, 12-15 December 2000.

[39] G. Lafferriere and H.J. Sussmann. Motion planning for controllable systems without drift. In *Proceedings of the IEEE International Conference on Robotics and Automation*, pages 1148–1153, Sacramento, CA, USA, 1991.

[40] B. Lantos. *Robot Control*. Hungarian Academic Press, Budapest, 1991

[41] B. Lantos, P. Klatsmányi, L. Ludvig, and F. Tél. Intelligent control system of a robot with dextrous hand. In *Proceedings of the IEEE INES'97*, pages 129–134, Budapest, 1997

[42] J. Lévine. Are there new industrial perspectives in the control of mechanical systems ? In Paul M. Frank, editor, *Advances in Control*, pages 195–226. Springer-Verlag, London, 1999.

[43] J. Lévine, P. Rouchon, G. Yuan, C. Grebogi, B.R. Hunt, E. Kostelich, E. Ott, and J. Yorke. On the control of US Navy cranes. In *Proceedings of the European Control Conference*, pages N–217, Brussels, Belgium, July 1997

[44] Z. Li, J. F. Canny, and S. S. Sastry. On motion planning for dextrous manipulation. In *Proceedings of the IEEE Conference on Robotics and Automation*, pages 775–780, 1989.

[45] A. Marigo and A. Bicchi. Rolling bodies with regular surface: Controllability theory and applications. *IEEE Transactions on Automatic Control*, 45(9):1586–1599, September 2000.

[46] Ph. Martin and P. Rouchon. Feedback linearization and driftless systems. *Mathematics of Control, Signals, and Systems*, 7(3):235–254, 1994.

[47] S.C. Martindale, D.M. Dawson, J. Zhu, and C. Rahn. Approximate nonlinear control for a two degree of freedom overhead crane: Theory and experimentation. In *Proceedings of the American Control Conference*, pages 301–305, 1995.

[48] M.T. Mason and J.K. Salisbury. *Robot Hands and the Mechanics of Manipulation*. MIT Press, 1985.

[49] D. Montana. The kinematics of contact and grasp. *International Journal of Robotics Research*, 7:17–31, 1988.

[50] K.A.F Moustafa. Reference trajectory tracking of overhead cranes. *Journal of Dynamic Systems, Measurement, and Control*, 123:139–141, March 2001

[51] Ph. Mullhaupt. *Analysis and Control of Underactuated Mechanical Nonminimum-Phase Systems*. PhD thesis, Ecole Polytechnique Fédérale de Lausanne, Lausanne, Suisse, 1999.

[52] R.M. Murray, Z. Li, and S.S. Sastry. *A Mathematical Introduction to Robotic Manipulation*. CRC Press, 1994.

[53] R.M. Murray and S.S. Sastry. Nonholonomic motion planning: steering using sinusoids. *IEEE Transactions on Automatic Control*, 38(5):700–716, May 1993.

[54] R. Muszyński and K. Tchoń. Singularities and mobility of nonholonomic systems: The ball rolling on a plane. In *Proceedings of the 6th IFAC Symposium on Robot Control*, pages 259–264, Vienna, Austria, September 2000.

[55] T. Naniwa, S. Arimoto, and K. Wada. A learning control method for coordination of multiple manipulators holding a geometrically constrained object. *Advanced Robotics*, 13(2):132–151, 1999.

[56] Ju.I. Neimark and N.A. Fufaev. *Dynamics of Nonholonomic Systems*. American Mathematical Society, Providence, Rhode Island, 1972.

[57] R.H. Overton. Anti-sway control system for cantilever cranes. United States Patent, June 1996. Patent No. 5,526,946.

[58] M.A. Peshkin and A.C. Sanderson. Minimization of energy in quasi-static manipulation. *IEEE Transactions on Robotics and Automation*, 5(1):53–60, 1989.

[59] Y. Sakawa and H. Sano. Nonlinear model and linear robust control of overhead travelling cranes. *Nonlinear Analysis*, 30(4):2197–2207 1997

[60] J.M. Selig. *Geometrical Methods in Robotics*. Springer, 1996.

[61] K.B. Shimoga. Robot grasp synthesis algorithms: A survey. *International Journal of Robotics Research*, 16(1):230–266, Feb 1997

[62] H. Sira-Ramírez. On the control of the variable length pendulum. In *Proceedings of the IEEE International Conference on Decision and Control*, pages 1188–1189, 1999.

[63] G. Vass, S. Payandeh, and B. Lantos. On controlled manipulation of objects within multiple dexterous agents. In *Proceedings of the 10th Congress on the Theory of Machines and Mechanisms*, Oulu, Finland, 1999.

[64] Weight handling equipment handbook. Available on the internet: http://ncc.navfac.navy.mil/ 1998. MIL-HDBK-1038.

[65] E.T Whittaker. *A Treatise on the Analytical Dynamics of Particles & Rigid Bodies*. Cambridge University Press, 1993.

[66] K. Yoshida and H. Kawabe. A design of saturating control with guaranteed cost and its application to the crane control system. *IEEE Transactions on Automatic Control*, 37(1):121–127, 1992.

[67] J. Yu, F.L. Lewis, and T Huang. Nonlinear feedback control of a gantry crane. In *Proceedings of the American Control Conference*, pages 4310–4315, 1995.

Appendix A

Some notions of analytical mechanics

For the reader's convenience, we recall here some basic notions, essentially (but not exclusively) used in Chapter 2. The reader can find a detailed presentation of the subject in recent books [52, 60] as well as in classical treatments such as [2, 65]. We focus our attention on two subjects: rigid body motions and nonholonomic mechanical systems.

Notations from differential geometry are used [1, 6]. We denote by TM the tangent bundle of a manifold M, and by T^*M its cotangent bundle. $d\varpi$ denotes the exterior derivative of the form ϖ on M, and $<,>$ stands for the duality product between TM and T^*M. The wedge product of two forms, ϖ_1 and ϖ_2, is denoted by $\varpi_1 \wedge \varpi_2$.

Rigid body motions

The motions of a rigid body in mechanics is described by the motions of a frame fixed to it. Thus we start with the definition of a rigid body and that of the frame fixed to it, and then we derive the relations on the velocities.

Definition 12 (rigid body with convex regular surface). *Let* $c : \mathbb{R}^3 \to \mathbb{R}$ *be a smooth function (i.e. of class C^∞). We say that $\mathcal{O}$ is a rigid body if*

1. $\mathcal{O} = \{P \in \mathbb{R}^3 | c(P) \leq 0\}$

2. c *is a convex function*

According to this definition, the surface $\partial\mathcal{O}$ of a rigid body is defined by the points such that the function $c : \mathbb{R}^3 \to \mathbb{R}$ vanish, namely $\partial\mathcal{O} = c^{-1}(0)$.

Throughout the text, the expression "rigid body" stands for "rigid body with convex regular surface".

A frame K^a in the Euclidean space $\mathbb{R}^3$ is given by

- a point A in $\mathbb{R}^3$ (origin of the frame)

- an ordered set of three orthogonal vectors $\{e_1^a, e_2^a, e_3^a\}$ with unit length such that $e_1^a \times e_2^a = e_3^a$, referred to as the basis of K^a

Here $\times$ stands for the usual cross product in $\mathbb{R}^3$ Consider a point P in $\mathbb{R}^3$ and a frame K^a One can write

$$\vec{AP} = x_P^a e_1^a + y_P^a e_2^a + z_P^a e_3^a,$$

and we say that the vector

$$p_P^a = (x_P^a, y_P^a, z_P^a)^T \tag{A.1}$$

is the position vector of the point P in the basis of K^a whose elements are the coordinates of the point P in K^a

One distinguishes a special frame, denoted by K^b and referred to as the inertial reference frame. For any frame K^a different from K^b we denote by p^a the position vector of its origin A in the basis of K^b

A frame K^a is said to be fixed to a rigid body at a point A (note that A is not necessarily a point of the body itself) if all points of the rigid body have fixed coordinates w.r.t. the base e_1^a, e_2^a, e_3^a and the point A coincides with the origin of K^a Hence, for all points P of the surface of the rigid body, the expression of the function c in the frame K^a denoted by c^a satisfies

$$c^a(x_P^a, y_P^a, z_P^a) = 0.$$

The expression of the function c is different for different frames fixed to the same rigid body.

Since the position of all points of the rigid body is fixed in the basis of K^a, their positions in the basis of K^b are known if the situation of K^a w.r.t. the basis of K^b is known. By the definition of the frame K^a, this relative situation is given by the coordinates of the vector p^a and by the vectors e_1^a, e_2^a, e_3^a, both expressed in the basis of K^b

Introduce the matrix Ω, called *orientation matrix*, defined by

$$\Omega = \begin{pmatrix} (e_1^a)^T \ e_1^b & (e_2^a)^T \ e_1^b & (e_3^a)^T \ e_1^b \\ (e_1^a)^T \ e_2^b & (e_2^a)^T \ e_2^b & (e_3^a)^T \ e_2^b \\ (e_1^a)^T \ e_3^b & (e_2^a)^T \ e_3^b & (e_3^a)^T \ e_3^b \end{pmatrix}$$

By construction, the matrix Ω satisfies $\Omega^T \Omega = \Omega \Omega^T = I$ and $\det \Omega = 1$ and thus is an element of the *special orientation Lie group* $SO(3)$. The word orientation comes from the fact that the scalar product $(e_i^a)^T \ e_j^b$ is equal to the cosine of the angle between the vectors e_i^a and e_j^b, for every $i, j = 1, 2, 3$.

Consider now a point P of the rigid body. Its coordinates are given by (A.1). The vector of coordinates of the same point, expressed in the basis of K^b are denoted by $p_P^b = (x_P^b, y_P^b, z_P^b)^T$ By construction of the matrix Ω and by the definition of p^a the following relation can be established for these two vectors:

$$p_P^b = p^a + \Omega \cdot p_P^a. \tag{A.2}$$

The vector p^a describes the *position* of the rigid body and Ω gives its *orientation* w.r.t. the inertial reference frame K^b. Therefore the possible positions and the orientations of a rigid body w.r.t. K^b form the set $\mathbb{R}^3 \times SO(3) = SE(3)$, referred to as the *special Euclidean group*,

which is also a Lie group. This manifold is six-dimensional and can be locally represented by six real scalar variables (p, ϕ) such that $p \in \mathbb{R}^3$ gives the position and $\phi \in \mathbb{R}^3$ gives the orientation of the rigid body.

Several local representations are used (in particular in robotics) for the $SO(3)$ group (see [60]). Examples are the Euler angles, RPY (Roll, Pitch, Yaw) angles, etc. For each choice, the elements of the vector ϕ correspond to three successive rotations allowing to make coincide the orientations of K^b and the frame fixed to the rigid body. For instance, the orientation matrix Ω_{RPY} corresponding to the RPY angles $\phi = (\varphi, \theta, \psi)$, is given by:

$$\Omega_{RPY}(\phi) = \begin{bmatrix} \cos \varphi \cos \theta & \cos \varphi \sin \theta \sin \psi - \sin \varphi \cos \psi & \cos \varphi \sin \theta \cos \psi + \sin \varphi \sin \psi \\ \sin \varphi \cos \theta & \sin \varphi \sin \theta \sin \psi + \cos \varphi \cos \psi & \sin \varphi \sin \theta \cos \psi - \cos \varphi \sin \psi \\ -\sin \theta & \cos \theta \sin \psi & \cos \theta \cos \psi \end{bmatrix}$$

(A.3)

Throughout the thesis, the RPY representation is used, thus the subscript RPY is omitted.

Rigid bodies evolve in time w.r.t. the inertial reference frame K^b and their motions can be instantaneously decomposed into a change of position and a change of orientation.

Consider a frame K^a fixed to a rigid body at a point A. Let the trajectory of the position and orientation of the frame given by the functions $p^a(t)$ and $\Omega^a(t) = \Omega(\phi^a(t))$, respectively. Observe that for any curve $\Omega^a(t)$ in $SO(3)$, the expression $\frac{d\Omega^a}{dt}(\Omega^a)^T$ is antisymmetric (this can be seen by differentiating $\Omega^a(t)\Omega^a(t)^T = I$) and introduce the following notation:

$$[\omega^a \times] = \begin{bmatrix} 0 & -\omega_z^a & \omega_y^a \\ \omega_z^a & 0 & -\omega_x^a \\ -\omega_y^a & \omega_x^a & 0 \end{bmatrix} = \frac{d\Omega^a}{dt}(\Omega^a)^T$$

(A.4)

This notation is motivated by the fact that for any vector a, the linear transformation $[\omega^a \times] a$ is equivalent to the standard cross product $\omega \times a$. Let us now define $v^a = \frac{d}{dt}p^a = \dot{p}^a$ the linear velocity and ω^a the angular velocity of the frame K^a.

Consider an arbitrary point P of the rigid body. By the definition of the frame K^a fixed to the rigid body we have that $\dot{p}_P^a = 0$. Differentiating (A.2) w.r.t. t, we get the instantaneous velocity of the point P expressed in K^b:

$$\frac{dp_P^b}{dt}(t) = \frac{dp^a}{dt}(t) + \frac{d\Omega^a}{dt}(t)p_P^a = \dot{p}^a(t) + \frac{d\Omega^a}{dt}(t)\Omega^a(t)^T\Omega^a(t)p_P^a = v^a + [\omega^a \times]\Omega^a(t)p_P^a$$

(A.5)

or

$$\dot{p}_P^b = v^a + [\omega^a \times](p_P^b - p^a).$$

Thus, to calculate the velocity of any point of the rigid body, it is enough to know the translational velocity v^a and the angular velocity ω^a of the frame fixed to it. Recall that v^a and ω^a are both expressed in K^b by definition.

Kinematic constraints and nonholonomy of mechanical systems

The mechanical state of a system composed by a collection of rigid bodies is determined by a finite number of variables, called generalized coordinates, denoted by the vector q. The admissible values of q define the configuration manifold M of the mechanical system.

Constraints on the configuration manifold of a mechanical system involving the general ized coordinates and their first order time derivatives (velocities) are referred to as kinematic constraints and assumed to be linear w.r.t. the velocities. They are given in the form:

$$A(q) \cdot \dot{q} = 0, \qquad (A.6)$$

where we suppose that the rows of $A(q)$ are linearly independent for all q. Roughly speaking, these constraints restrict the possible directions of motion at each configuration q of the mechanical system. The admissible motions are in the right null-space of the matrix $A(q)$.

Each row of the matrix $A(q)$ defines a one-form on the configuration manifold M

$$\alpha_i = \sum_j a_{ij}(q) dq_j,$$

where $a_{ij}(q)$ is the jth element of the ith row of the matrix $A(q)$. The one-forms α_i define a codistribution on M, denoted by Π. Let m be the dimension of the manifold M, and let p be the number of the rows of $A(q)$, assumed to be linearly independent, and let us denote by $\Lambda^1(M)$ the set of all one-forms on M

Theorem 11 (Frobenius). *A codistribution Π on a manifold M is integrable iff the exterior derivative of all one-forms ϖ in Π can be written as*

$$d\varpi = \alpha \wedge \beta \qquad \alpha \in \Pi, \quad \beta \in \Lambda^1(M).$$

If the codistribution Π is not integrable, one can look for the largest integrable codistribution contained in Π, denoted by Π^*. The construction of Π^* can be done according to the notion of the derived flag.

Definition 13 (derived flag). *The derived flag of the codistribution Π is given by the following sequence of codistributions:*

$$I^0 = \Pi \qquad I^{k+1} \stackrel{def}{=} \{\varpi \in I^k \cdot d\varpi = \alpha \wedge \beta \ with \ \alpha \in \Lambda^1(M), \beta \in I^k\}$$

This construction terminates at some N when $I^N = I^{N+1}$

By definition, the sequence of the codistributions $I^0, I^1, \dots, I^N$ is such that $I^k \supset I^{k+1}$ and by Frobenius' theorem, I^N gives the largest integrable codistribution contained in Π.

Definition 14 (holonomic and fully nonholonomic mechanical system). *Consider a mechanical system evolving on a manifold M of dimension m. Let the kinematic constraints be given by a set of independent one-forms $\varpi_1, \dots, \varpi_p$ on M with $p < m$, spanning the codistribution Π. Calculate the derived flag of Π using Definition 13 and denote by r the dimension of I^N The mechanical system is said to be holonomic if $r = p$ and fully nonholonomic if $r = 0$.*

We say that a distribution Δ is the annihilator of the codistribution Π on the manifold M if for all points q of M, for all covectors $\nu \in \Pi$, and for all vectors $v \in \Delta$ we have $<\nu, v> = 0$. This is also denoted by $< \Pi, \Delta >= 0$.

Note that if the system is holonomic then there exists an $m - p$ dimensional submanifold N of M such that $\Delta = TN$. This implies that kinematic constraints involving velocities of the configuration variables can be transformed into p geometric constraints defining precisely the submanifold N of M

Definition 15 (associated driftless system). *Consider the kinematics given by Equation* (A.6). *Define* $\Delta = span\{g_1, \quad, g_k\}$. $k = m - p$ *as the largest annihilator of* Π. *Then the driftless system associated to the kinematics* (A.6) *is given by*

$$\dot{q} = \sum_{i=1}^{k} g_i(q) u_i \tag{A.7}$$

where u_i, $i = 1, \quad, k$ *are the control inputs.*

For nonholonomic mechanical systems, the inputs u_i of (A.7) are referred to as generalized velocities.

Controllability properties of (A.7) can be analyzed using the Lie-algebra generated by the vector fields g_i, or by the derived flag of the codistribution Π. Note that by Definition 14, the controllability of the driftless system (A.7) is equivalent to the full nonholonomy of the kinematic constraints (A.6) (see e.g. [46]).